THE
PHYSICAL REVIEW
A journal of experimental and theoretical physics established by E. L. Nichols in 1893

SECOND SERIES, VOL. 67, NOS. 1 AND 2, JANUARY 1 AND 15, 1945

Threshold Measurements on the Nuclear Photo-Effect

GEORGE C. BALDWIN* AND H. W. KOCH
Department of Physics, University of Illinois, Urbana, Illinois
(Received March 27, 1944)

The high voltage x-radiation from the betatron has been employed to produce (γ, n) reactions in several elements of atomic number up to 47, the reaction observed by detection of induced radioactivity. The peak x-ray energy was controlled by integrating the voltage on the main coils with an RC circuit, which actuated the orbit expander at a predetermined electron energy. Upon irradiating samples at sequences of energies, measuring their activity with beta-counters, and plotting activities against peak energy, smooth curves were obtained from which thresholds were estimated. The accuracy of the method is limited by low activity in almost all cases and by uncertainties in energy output. The following thresholds in Mev have been measured: C^{11}, 18.7 to 19.4; N^{13}, 11.1±0.5; O^{15}, 16.3±0.4; Fe^{52}, 14.2±0.4; Cu^{62}, 10.9±0.3; Zn^{63}, 11.6±0.4; $Se^{79 \text{ or } 81}$, 9.8±0.5 for the lower, short period isomer; $Mo^{91 \text{ or } 93}$, 13.5±0.4; Ag^{105}, 9.3±0.5; Ag^{106}, 9.5. The first three are in fair agreement with other data, but because of exceptionally weak activities are not sufficiently reliable to afford a test of the method. Rough measurements on the uranium photo-fission threshold are also reported. Since the radiation from the betatron is continuous and its spectral distribution is unknown, the excitation curves are not susceptible to interpretation, and cross sections for the above reactions cannot be estimated at present.

INTRODUCTION

WITH the high energy x-rays now available from the betatron, it is energetically possible to photo-disintegrate nearly all nuclei. In all cases so far observed, photo-disintegration of a target nucleus of charge Z and mass number A leads to an isotope of the target with mass number $A-1$, upon ejection of a neutron from the target nucleus. The process may be detected by direct observation of the ejected neutron; however, frequently the product nucleus is radioactive and the reaction is then most conveniently detected by observation of the induced activity in an irradiated sample—this method having the added advantage of definitely identifying the particular isotopes of the target element involved in the reaction.

To produce the photo-effect it is necessary that the energy of the incident quantum exceed the binding energy of the particle to be ejected. The following reaction is typical:

$$N^{14}+h\nu \rightarrow N^{13}+n^1,$$
$$N^{13} \rightarrow C^{13}+e^+ +e^- +\eta+Q.$$

Conservation of energy requires that

$$h\nu \geq M({}_6C^{13})+M({}_0n^1)+2mc^2+Q-M({}_7N^{14}),$$

where M denotes the atomic mass. Substitution of numerical values[1,2] for the masses of N^{14} and

*Now at General Electric Research Laboratory, Schenectady, New York.

[1] R. T. Birge, Rev. Mod. Phys. 13, 233 (1941).
[2] J. J. Livingood and G. T. Seaborg, Rev. Mod. Phys. 12, 30 (1940).

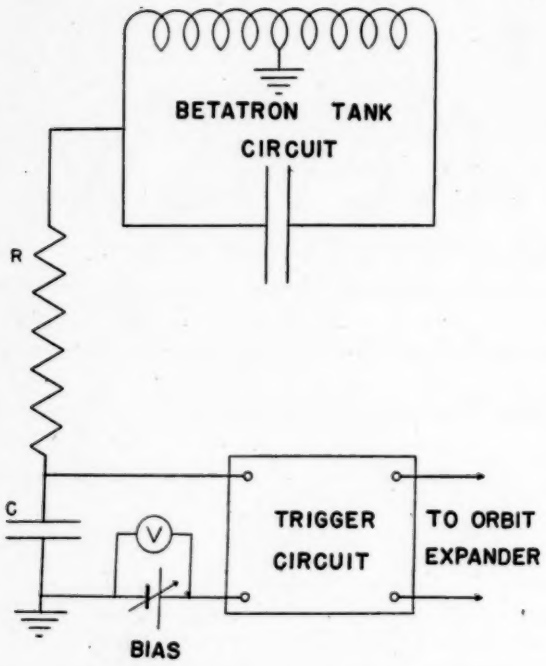

FIG. 1. Circuit scheme for control of peak x-ray energy.

C^{13} and for Q leads to

$$h\nu = 10.65 \pm 0.15 \text{ Mev}$$

for the threshold of the photo-effect in N^{14}. Similar calculations give thresholds of 15.6 ± 0.6 for O^{16} and 18.7 ± 0.3 for C^{12}. Calculation of the threshold is possible only in several cases, however. Since a knowledge of the binding energies of particles in nuclei is of considerable theoretical interest, we have undertaken measurements of photo-effect thresholds in a sequence of nuclei from $Z=6$ to $Z=43$. This work has been reported elsewhere.[3]

Previous work on the photo-effect, except in the cases of beryllium and deuterium, has been limited by the unavailability of x-rays of sufficiently high energy. For heavier nuclei at least 8 Mev are required; in all cases reported herein, considerably higher energies are necessary. Gamma-rays from proton bombardment of lithium and boron have been the chief photo-disintegrative agents employed in past work. Bothe and Gentner[4] have measured the cross section for the reaction $Cu^{63}(\gamma, n)Cu^{62}$ with lithium and boron gamma-rays, and have compared the yields induced by both radiations in other elements. Inhomogeneity of the boron radiation, together with low yields of activity, makes interpretation of their results uncertain. Thresholds could not be estimated in this sort of measurement.

[3] G. C. Baldwin and H. W. Koch, Phys. Rev. **63**, 59A and 426A (1943).

[4] W. Bothe and W. Gentner, Zeits. f. Physik **112**, 45 (1939).

METHOD

The threshold measurements reported in this paper were made by irradiating samples at a sequence of energies, the energy being raised in small steps until the process was observed to occur, as evidenced by radioactivity induced in the sample. The yield of activity was plotted as a function of peak x-ray energy, giving a curve from which the threshold was obtained by inspection. This method involved the problems of (1) accurate control of peak energy, (2) monitoring of x-ray intensity, and (3) detection of the reaction.

For energy control, use was made of the fact that the energy acquired by electrons during acceleration in the betatron is proportional to the magnetic flux linking their orbit, which is in turn proportional to the flux linking the main coils.[5] A resistor and capacitor were placed in series across one of the main coils, the time constant large compared with the period of the alternating flux. The condenser voltage, proportional to the integral of the applied voltage, was proportional to the flux linkage and hence to the energy. This voltage was applied in series with an adjustable bias to a trigger circuit to actuate the orbit expander at a chosen critical input voltage read on the bias voltmeter. The block diagram of Fig. 1 illustrates the circuit scheme. With the constants employed ($R=10^6$ ohms, $C=10^{-7}$ farad) a voltage of 88.5 v on the integrating condenser corresponded to an electron energy of 20 Mev. The trigger point, reproducible to within 0.2 v, showed negligible drift after adequate warm-up. All voltages were electronically stabilized.

This circuit was calibrated by a search coil in the orbit plane. It was known that the magnet flux is an accurate sine wave, the third harmonic amounting to only 0.07 percent at the highest amplitude. The flux within the search coil could thus be readily determined by a voltage measure-

[5] D. W. Kerst, Phys. Rev. **60**, 47 (1941); Rev. Sci. Inst. **13**, 387 (1942).

ment and simultaneously compared with the voltage integrator response and with the magnet voltage read on a 2-turn coil about the magnet yoke. The latter reading was made a permanent substandard to which each setting was referred by determining the magnet voltage at which the integrator circuit would cause orbit expansion at peak flux. From these calibration data the Hr value at which the electrons struck the target could be computed. The probable error of this calibration was 1.5 percent; in actual energy settings further error arose. The total error in most cases did not exceed 2 percent.

Samples were irradiated at a standard position in the x-ray beam, 46 cm from the target, ordinarily to half-saturation. Irregularities in the resulting activity could be largely accounted for by variations in x-ray intensity from run to run. The intensity, monitored by an ionization chamber, was recorded in roentgens per minute at 1 meter from the target. The method of correction to standard intensity will be evident from a consideration of the process of radioactive growth under decay. During an infinitesimal time interval dt, the number of active nuclei N will change by

$$dN = kIdt - Ndt/\tau \qquad (1)$$

where k is a constant, I the x-ray intensity, and τ the mean life of the expected activity. This gives for the number of active nuclei produced between

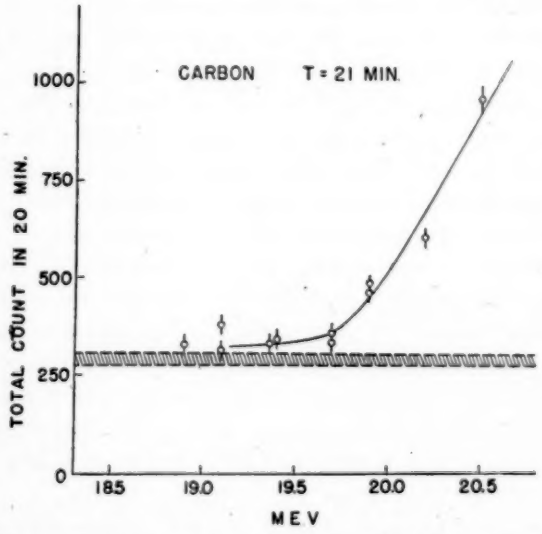

FIG. 2. Excitation curve for production of C^{11} by x-rays. The cross-hatched area represents the statistical spread in natural background of the Geiger-Müller counter.

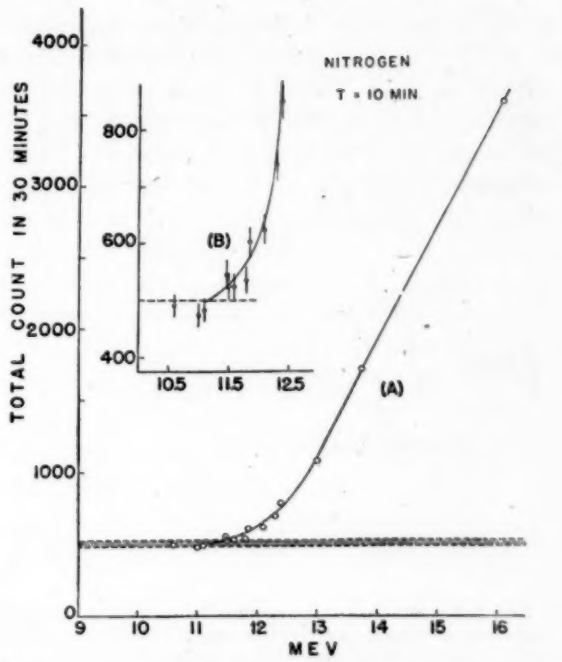

FIG. 3. Excitation curve for N^{13}: (*A*) Corrected for intensity variations; (*B*) Uncorrected points near threshold.

$t=0$ and $t=T$

$$N = k \exp(-T/\tau) \int_0^T I(t) \exp(t/\tau) dt = kR. \qquad (2)$$

In practice the integral was replaced by a weighted sum; the monitor was read at regular intervals during irradiation, each reading multiplied by the weighting factor, $\exp(t/\tau) \cdot \exp(-T/\tau)$, and the results added. The resulting sum R is called the "irradiation."

To reduce as far as possible the effect of intensity fluctuations all points were then corrected to the irradiation which the sample ordinarily received near threshold. This did not change points near threshold, where the effects were small or doubtful, but smoothed the curves somewhat and thereby facilitated threshold estimation.

The resulting smoothed curves are not susceptible to ready interpretation. It is not yet possible to determine from them the trend of the cross section for the process. That portion of the x-ray spectrum which is responsible for the reaction is responsible for only a small portion of the monitor response. If the cross section of the process be given by $\sigma(E)$ and the unknown spectral distribution by $N(E)$, the yield at some peak

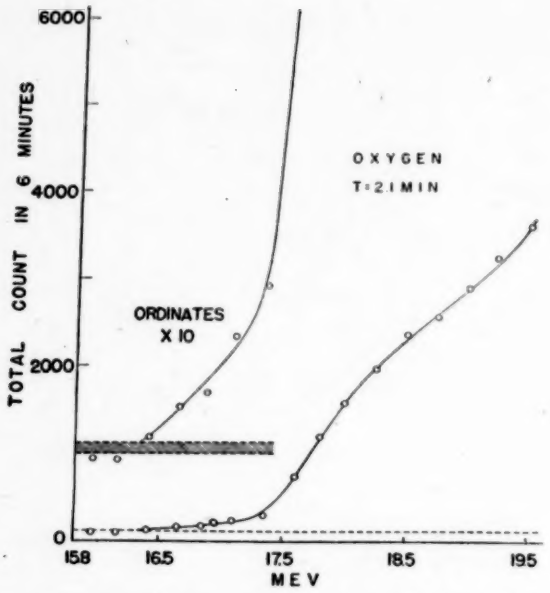

FIG. 4. Excitation curve for O^{15}. Points near threshold are replotted to larger scale in the inset. The first two points are below background because of the shielding effect of the water sample in which the counter was immersed.

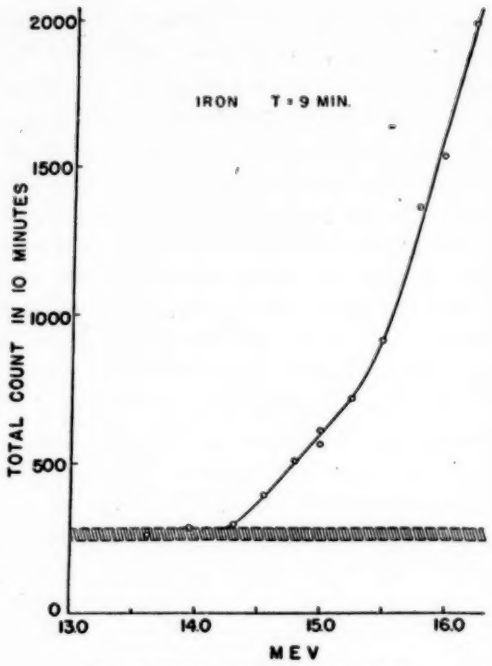

FIG. 5. Excitation curve for Fe^{53}.

energy E_{max} is proportional to

$$\int_{E_0}^{E_{max}} N(E)\sigma(E)dE,$$

where E_0 is the threshold for the reaction. The monitor response is given by a similar expression, but the lower limit and the energy-dependence of the integrand are entirely different. There is thus no simple correlation between activities observed at two different values of E_{max}, even though both were produced by the same total irradiation.

Activity, usually rather weak, was detected with β-ray counters. The counter walls were silvered glass 7 cm long, 16 mm in diameter, and about 0.2 mm thick. They were filled with 9:1 argon-alcohol to 9-cm pressure. The counter was coupled to a Neher-Harper circuit followed by a scale-of-16 counter circuit. Background of about 35 min.$^{-1}$ was reduced to 15 min.$^{-1}$ by enclosure in a lead shield 10 cm thick. Still further reduction of background is desirable. Samples were usually thick cylinders which fitted snugly over the counters.

RESULTS

For the first three of the following elements it was possible to predict the threshold from mass and beta-decay data. These reactions would provide a check on the accuracy of the method, except that the resulting activities are the weakest of all those studied. All other elements give higher yields and sharper thresholds, but reliable mass and beta-decay data are not available for comparison.

CARBON

This reaction should appear above 18.75±0.3 Mev,[6] hence, it has not been produced with natural sources of gamma-radiation.

Cylinders of graphite 7.5 cm long, 2.5 cm in diameter, and 2 mm thick were irradiated at 21 Mev for 20 minutes and gave an initial activity of 200 counts per minute with a half-life of 20±3 minutes. At lower energies the yields became so small that it was uncertain whether the activity was actually 21-minute C^{11}—almost any other substance, such as adsorbed air, becomes active at considerably lower energy. The total counts obtained at various energies, reduced to irradiations of 50R, are shown in Fig. 2. The cross-hatched area is the statistical spread of counter

[6] F. W. Aston, *Mass Spectra and Isotopes* (Longmans, Green and Company, New York, 1942); Delsasso, White, Barkas, and Creutz, Phys. Rev. **58**, 586 (1940); S. K. Allison, Phys. Rev. **55**, 624 (1939); L. P. Smith, Phys. Rev. **56**, 548 (1939).

background. The threshold of such a curve is taken as the energy below which points consistently fall within the background spread. The points below 19.4 Mev may or may not be genuine carbon activity. The threshold is probably below 19.4 and above 18.7 Mev, in fair agreement with the predicted value—a high result naturally being observed with such a weak activity. More accurate work with carbon must await the production of higher intensity x-radiation than has yet been obtained with the betatron.

NITROGEN

As with carbon, yields from nitrogen[7,8] are extremely weak, but there is less danger of contamination of samples, as the threshold is low. At 16-Mev peak energy the observed activity was only 600 counts per minute. Samples of NaN_3, irradiated for 10-minute periods, were held for counting between concentric aluminum cylinders. The inner cylinder, 0.8 mm thick, was perforated with 600 evenly-spaced 2-mm holes, which were covered by 0.001″ aluminum foil. This was placed over the counter. The annular section of NaN_3 thus employed was 4.5 mm thick.

Figure 3, curve *A*, shows 30-minute counting totals corrected to an irradiation of 25R. Uncorrected counts in the vicinity of threshold are plotted to larger scale in the inset, curve *B*. The difficulty of estimating a threshold is apparent, but no activity is observable below 11.1 Mev, while the sample is definitely active at 11.5 Mev. We have therefore placed the threshold for the reaction $N^{14}(\gamma, n)N^{13}$ at 11.1 ± 0.5 Mev. The stated uncertainty includes estimated uncertainties both in energy settings and in determination of the intercept of the excitation curve. This result is to be compared with the value predicted in the introduction, above.

OXYGEN

The 2.1-minute positron activity of O^{15} should have a threshold of 15.6 ± 0.6 Mev.[1,9] It has been weakly produced with lithium gamma-rays.[4,8,10]

Preliminary measurements[3] indicated a higher threshold, between 16.3 and 16.7 Mev. These measurements were repeated with improved technique, using water samples and an immersion counter of the same dimensions as the other counters used in this work. The volume of each water sample was 130 cm³, which surrounded the counter to a thickness of 1 cm.

Samples were irradiated for 4 minutes to a total irradiation of 50R; counting was begun 30 seconds after irradiation and continued for three half-lives to give optimum measure of activity.

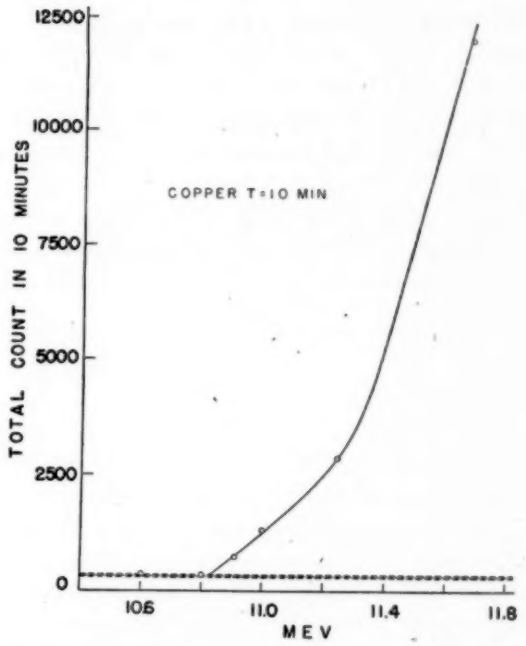

FIG. 6. Excitation curve for Cu^{62}. The energy values should be increased by about 0.1 Mev, as explained in the text.

Figure 4 shows the resulting excitation curve up to 19.5 Mev, with points near threshold replotted to larger scale. The threshold is 16.3 ± 0.4 Mev.

IRON

Iron gave a moderately strong 9-minute activity, which has been assigned to Fe^{53}.[2,8] Bothe and Gentner[4,7] did not report this activity; Carlson and Henderson[11] failed to obtain it with higher intensity lithium gamma-rays. Huber *et al.*[8] recently obtained it with 17-Mev gamma-

[7] W. Bothe and W. Gentner, Zeits. f. Physik **106**, 236 (1937).
[8] O. Huber, P. Scherrer, O Lienhard, and H. Waffler, Helv. Phys. Acta **XV**, 312 (1942).
[9] W. A. Fowler, L. A. Delsasso, and C. C. Lauritsen, Phys. Rev. **49**, 561 (1936).
[10] W. Chang, M. Goldhaber, and R. Sagane, Nature **139**, 962 (1937).
[11] P. R. Carlson and J. E. Henderson, Phys. Rev. **58**, 193A (1940).

rays and reported a yield of 38 percent that observed with copper, based on the original isotope Fe^{54}. It is surprising that it was completely missed in previous work—the yields obtained with the betatron were quite strong. Flat iron plates, 10×8×1 cm, were irradiated for 10 minutes to 29R. For detection they were placed 5 mm from an unshielded counter. The initial counting rate at 1 Mev above threshold was three times the background of 26 min.$^{-1}$ From Fig. 5 the threshold is 14.2±0.4 Mev.

COPPER

The 10-minute Cu^{62} is the strongest activity observed in a (γ, n) reaction,[7,8] and its threshold is quite sharp. Bothe and Gentner[4] measured the cross section for lithium gamma-rays as 5×10^{-26} cm^2, and with boron gamma-rays to be 2.3 times smaller.

Copper tubes 7.5 cm long, 1 mm thick, and 2.5 cm in diameter were used as samples. Irradiation was for 10-minute periods. The data are shown in Fig. 6, reduced to an irradiation of 15R. There is a slight systematic error in energy-values here because of phase-shift in the integrating unit, which is appreciable only when expansion occurs well below peak flux. The correction to be applied in this case was found to be not more than 0.1 Mev. The threshold has accordingly been taken as 10.9±0.3 Mev. This is considerably lower than measurements of the $(n, 2n)$ threshold have indicated.[12]

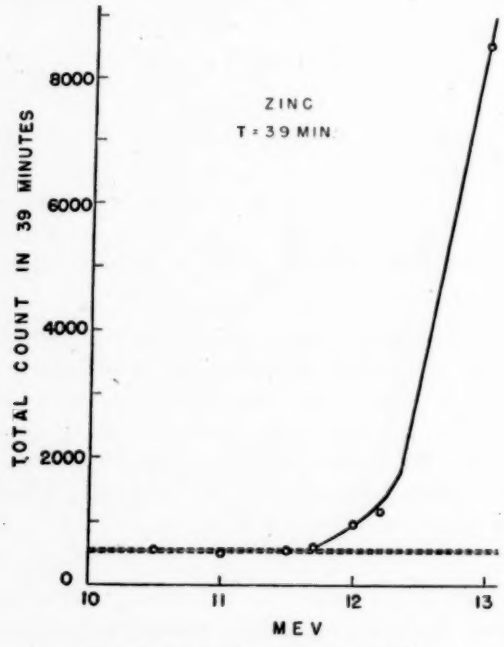

FIG. 7. Excitation curve for Zn^{63}.

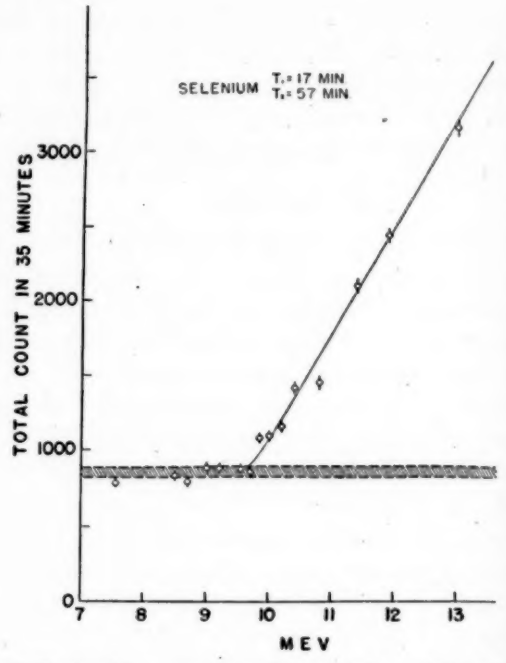

FIG. 8. Excitation curve for total activity in selenium. The observed count is owing to two isomeric activities.

ZINC

Cylinders of zinc 6 cm long, 2.5 cm in diameter, of 3-mm wall-thickness were irradiated for 25 minutes. Strong yields of Zn^{63} were obtained.[2,8] The counts for irradiations of 50R are shown in Fig. 7. The threshold is 11.6±0.4 Mev.

SELENIUM

X-rays induce two activities in this element, one of about 17-minute half-life (also reported as 19-minute),[2] the other about an hour. Bothe and Gentner[4] obtained both by 1-hour irradiation of selenium with 17-Mev gamma-rays and also produced them with slow neutrons. Langsdorf and Segrè[13] showed that they are isomers of either Se^{79} or Se^{81}. These isomers were separated by chemical methods, and it was established that the 57-minute selenium decays into the 17-minute

[12] R. Sagane, Phys. Rev. **53**, 492 (1938).
[13] A. Langsdorf and E. Segrè, Phys. Rev. **57**, 105 (1939).

isomer, emitting a 98-kev gamma-ray; the lower isomer decays by emission of a 1.5-Mev beta-particle. There is no evidence that the upper state decays directly by beta-emission.

Plates of pure selenium, 7.5×5×1 cm, were irradiated for 15-minute periods, then placed 1 mm from the counter surface. Total activity in 35-minute counting periods, reduced to irradiation of 15R (computed on the basis of a 17-minute half-life), is plotted in Fig. 8. No activity results below 9.8±0.5 Mev (there was an uncertainty of as high as 3 percent in the energy settings in this experiment). If the short period

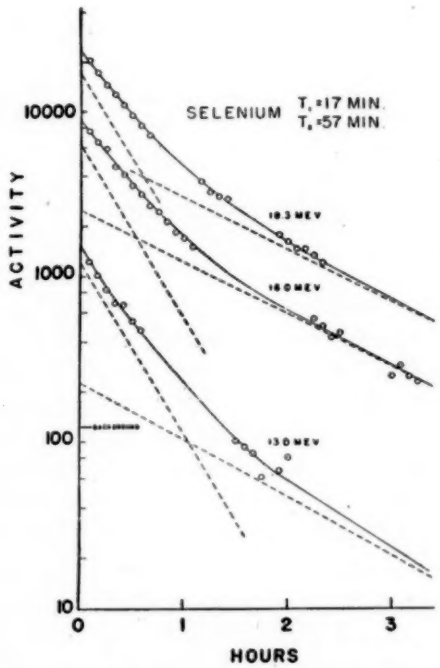

FIG. 9. Decay of selenium activity, $Se^{79 \text{ or } 81}$.

is the lower isomer, this threshold should be that of the 17-minute period. Analysis of decay curves indicates that this is probably true.

Designating the upper state by the subscript γ and the lower by β, the differential equations for production are

$$-\dot{N}_\gamma=\frac{N_\gamma}{\tau_\gamma}-k_\gamma I, \tag{3}$$

$$-\dot{N}_\beta=\frac{N_\beta}{\tau_\beta}-\frac{N_\gamma}{\tau_\gamma}-k_\beta I, \tag{4}$$

the lower isomer being produced by decay of the upper state as well as by the (γ, n) process. These equations could be solved for the initial populations of the two states and for the ratio of initial activities which should be observed if the constants k_β and k_γ were given. The beta-decay exhibits both half-lives. Since the beta-ray counter employed in the experiment had very low efficiency for gamma-rays, we need not consider the gamma-activity. With the simplifying assumption that the x-ray intensity is constant, it can be shown that

$$\frac{k_\beta}{k_\gamma}=r\left[\frac{1-\exp(-T/\tau_\gamma)}{1-\exp(-T/\tau_\beta)}\right]\left[\frac{\tau_\gamma}{\tau_\gamma-\tau_\beta}\right]+\frac{\tau_\beta}{\tau_\gamma-\tau_\beta}, \tag{5}$$

where

$$r=\frac{\text{initial activity decaying with lifetime } \tau_\beta}{\text{initial activity decaying with lifetime } \tau_\gamma}.$$

Note that in the absence of direct photoelectric production of the lower isomer (i.e., for $k_\beta=0$), r would be negative, indicating that growth, rather than decay, should be initially observed for the activity with lifetime τ_β.

From decay curves (Fig. 9) it is evident that r is always positive and tends to increase at lower energies. Near threshold the curves become difficult to analyze because of large relative statistical fluctuations, but it is still possible to estimate upper and lower limits for the 57-minute activity. These estimates indicate that k_γ/k_β decreases with decreasing energy, hence that the 57-minute threshold is probably higher than the 17-minute. This trend is shown in Fig. 10; as the energy is increased, k_γ/k_β appears to attain a limiting value of about 0.6. In making any deductions from this trend, it should be borne in mind that the activity observed at a given peak energy is the integrated effect of all x-ray quanta above threshold energy. This treatment must be regarded as essentially qualitative as it was not possible to make a reliable analysis of decay curves near threshold, but it clearly indicates the trend. A chemical separation would be out of the question with the weak activities obtained with this reaction.

MOLYBDENUM

The 17-minute isotope of this element is the only one of convenient lifetime for the present

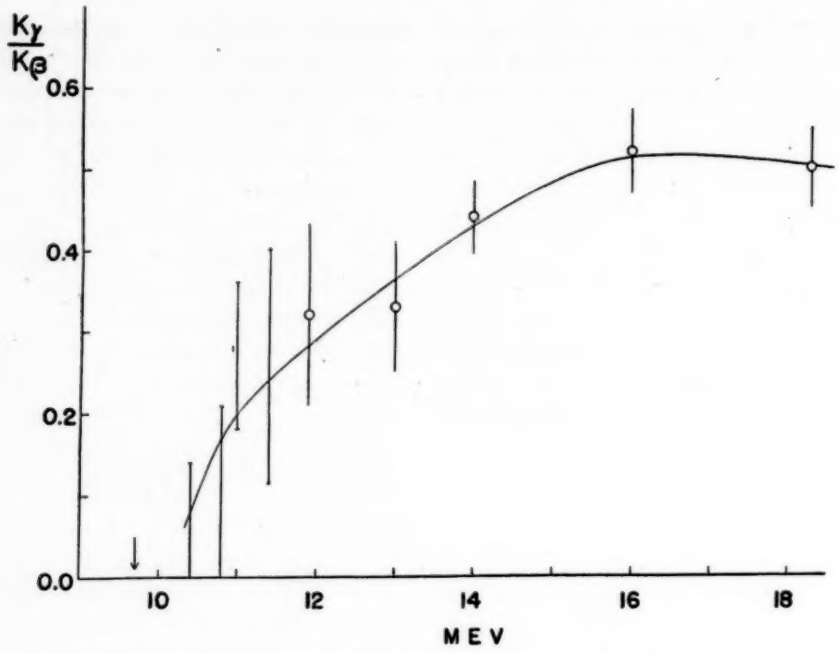

FIG. 10. Ratio of rate of production for upper isomer to that for lower isomer of $Se^{79 \text{ or } 81}$.

experiments.[2] Activities were moderately strong. A shorter period of about 1-minute half-life was observed above 14 Mev; it was allowed to decay for 5 minutes before counting was begun on the 17-minute activity, and did not interfere with determination of the latter threshold. Analysis of the molybdenum samples revealed no impurity other than a slight trace of tungsten. No attempt has yet been made to identify this period.

Samples of rolled sheet molybdenum, approximately 0.8 mm thick, measuring 6 cm ×7 cm, were irradiated for 10-minute periods. The counts plotted in Fig. 11 have been corrected to an irradiation of 30R. The threshold is 13.5±0.4 Mev.

SILVER

Two activities are induced in silver by photodisintegration.[2,7] Ag^{106} is positron-active with a 24.5-minute half-life (the isomeric 8.2-day period is too long to be observed in the present study); Ag^{108} emits electrons with a half-life of 2.3 minutes. To determine a threshold for each, it is necessary to separate their effects. This was done by analyzing the decay curves by somewhat the same procedure as that used for selenium.

A silver plate 7×6.5 cm, 1 mm thick, was rolled into a cylinder which fit snugly over the counter. This was allowed to decay completely between successive runs. A series of 25-minute runs gave the decay curves shown in Fig. 12. From this and from Fig. 13*A* it is evident that the short period predominates at lower energies. Below 10 Mev it is difficult to estimate the longer activity, but an

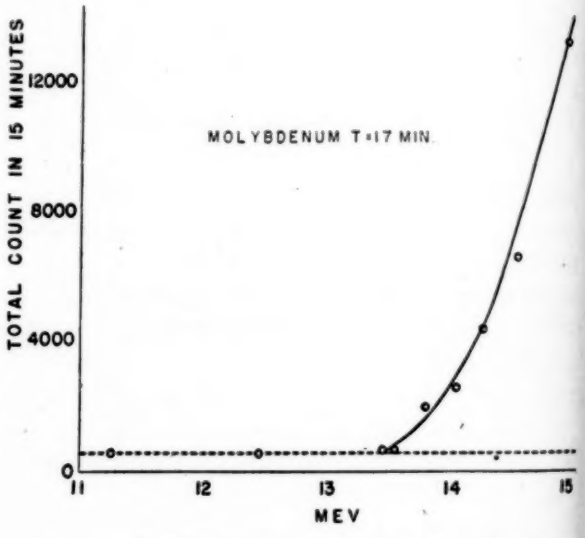

FIG. 11. Excitation curve for 17-min Mo activity.

upper limit for it can be set as in the case of selenium. Part *B* of Fig. 13 gives totals in a series of 3-minute runs to irradiations of 3.2R, indicating a threshold of 9.3±0.5 Mev for the 2.3-minute period.

Since each isotope is produced independently of the other, growth under irradiation follows Eq. (1). The ratio of the constants k_{106} and k_{108} is

$$\frac{k_{106}}{k_{108}}=r\left[\frac{24.5}{2.3}\right]\left[\frac{R_{108}}{R_{106}}\right],$$

where the R's are the weighted irradiations for each isotope and

$$r=\frac{\text{initial 24.5-minute activity}}{\text{initial 2.3-minute activity}}.$$

Were each isotope irradiated to saturation at the same x-ray intensity, k_{106}/k_{108} would be the ratio of activities observed. Values of this ratio computed from decay-curve data are plotted in Fig. 14. At and below 9.5 Mev the 24.5-minute activity is not produced. It is therefore concluded that the 2.3-minute threshold lies below the 24.5-minute threshold by at least 0.25 Mev.

TABLE I. Threshold energy values for nuclear photo-effects.

Z	Target element	Active isotope	Half-life (minutes)	Threshold (Mev)
6	Carbon	C^{11}	21	18.7 to 19.4
7	Nitrogen	N^{13}	10	11.1±0.5
8	Oxygen	O^{16}	2.1	16.3±0.4
26	Iron	Fe^{53}	9	14.2±0.4
29	Copper	Cu^{62}	10.3	10.9±0.3
30	Zinc	Zn^{63}	39	11.6±0.4
34	Selenium	$Se^{79 \text{ or } 81}$	17	9.8±0.5
		$Se^{79 \text{ or } 81}$	57	higher
42	Molybdenum	$Mo^{91 \text{ or } 93}$	17	13.5±0.4
47	Silver	Ag^{108}	2.3	9.3±0.5
		Ag^{106}	24.5	above 9.5

CONCLUSIONS

Thresholds which have been measured so far are tabulated in Table I. Probable errors listed include uncertainties both in energy settings and in determination of threshold from inspection of the excitation curve. The chief difficulty in the latter arises from statistical fluctuation in counter background. A threshold determination is limited by the sensitivity of the means of detecting the effect. Since the effects are comparable with

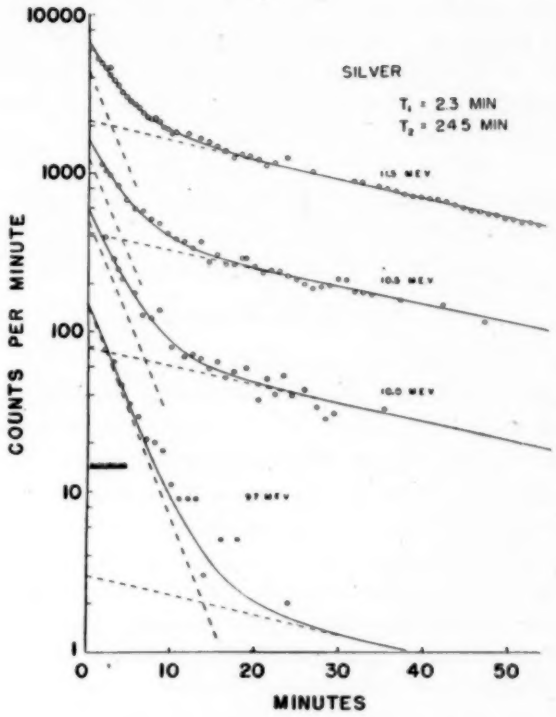

FIG. 12. Decay of silver activity at various irradiation energies.

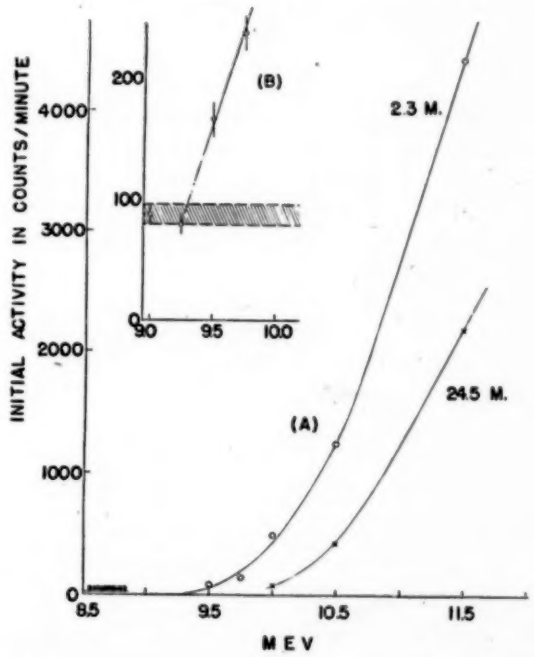

FIG. 13. (*A*) Initial activities of Ag^{106} and Ag^{108} vs. irradiation energy. (*B*) Excitation curve for silver with short irradiation period.

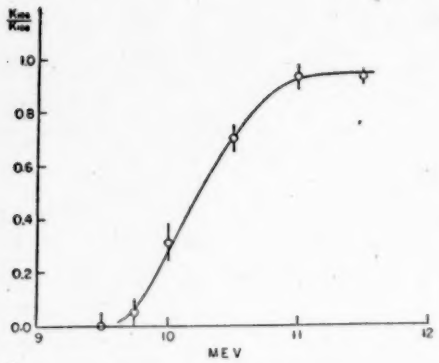

FIG. 14. Ratio of production rates for Ag^{106} and Ag^{108}.

background fluctuations in several cases, one cannot be completely satisfied that the true threshold may not lie considerably below the point where the effect first becomes detectable. The first three elements, yielding weak activities, gave thresholds consistently higher than predicted values. This may indicate that the true thresholds are below those read from the curves. It should be pointed out, however, that emission of gamma-rays after the beta-decay would make the calculated threshold seem too low. This might be the case for oxygen.

In other elements, the relatively better data warrant confidence that the true thresholds do not differ from those listed by more than the errors given.

No interpretation of the shapes of the excitation curves has been attempted. The spectral distribution of the radiation employed, which arises from a target of intermediate, variable thickness, must be known before actual cross sections and true excitation curves can be found. There is a general similarity of shape in all the curves.

All the measured thresholds are appreciably above the mean binding energy per particle, which is under 8 Mev in all cases studied. The trend is toward lower values in the heavier elements, but the list is not yet large enough to warrant generalizations from the data. An extension of the list to heavier elements is contemplated, together with a thorough rechecking of the present list. Present conditions make it unlikely that this work can be completed in the near future, however.

PHOTO-FISSION

Photo-fission of uranium was also investigated by collecting fission recoils on a paper catcher and measuring the collected activity. Uranium oxide was coated on a cylindrical form. A cylinder of paper was slipped over this sample and held by

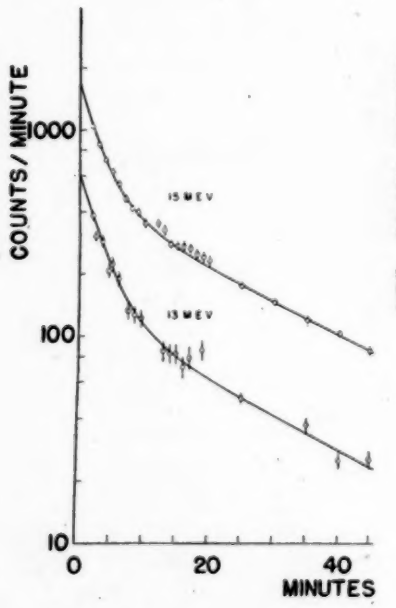

FIG. 15. Decay curves for photo-fission of uranium, observed by collection of fission recoils.

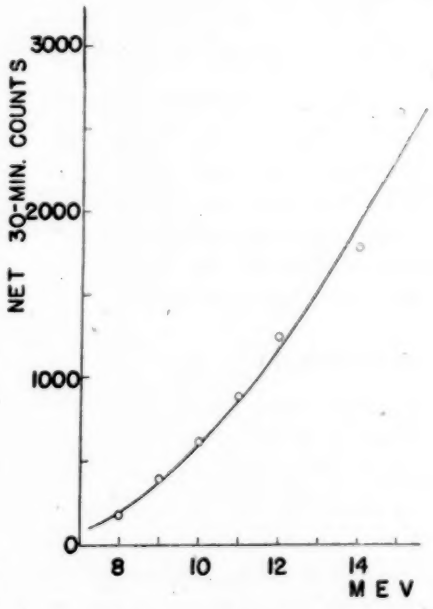

FIG. 16. Excitation curve for photo-fission of uranium from measured activity of collected recoils.

spacers 1 mm from the uranium. This was irradiated for 10-minute intervals at various energies, and the activity was measured with a counter. Blank tests on ordinary bond paper showed no activity below the oxygen threshold at 16.3 Mev.

Decay of the collected fission fragments was followed for 45 minutes after runs at 13 and 15 Mev. The points shown in Fig. 15 were fitted by a double exponential of half-lives 2.2 and 18 minutes, though the full decay scheme is much more complex. The activity is not strong enough to permit resolving the various activities present.

Net 30-minute counting totals (background of 500 subtracted out), corrected to an x-ray intensity of 1R per minute at one meter (or an irradiation of 10R, if no allowance be made for decay), are plotted in Fig. 16. Below 8 Mev the collected activity becomes too weak to follow. The threshold is apparently below 7 Mev, however.

Attempts to observe photo-fission in lead by this method were unsuccessful at energies up to 16 Mev, where the collector became active.

ACKNOWLEDGMENT

The writers wish to express their appreciation to Professor Donald W. Kerst for his direction of this research, and to Dr. Philip Morrison for many helpful discussions and suggestions.

PHYSICAL REVIEW VOLUME 67, NUMBERS 1 AND 2 JANUARY 1 AND 15, 1945

Expansion of Positive Energy Coulomb Wave Functions in Powers of the Energy*

J. G. BECKERLEY
Pupin Physics Laboratories, Columbia University, New York, New York

(Received September 16, 1944)

The non-relativistic wave function (in spherical polar coordinates) for a charged particle in a Coulomb field is expressed in a form suitable for problems in which the particle has a small positive energy. This formulation amounts to expanding the radial part of the wave function in powers of the energy E and is achieved by simple algebraic manipulation of power series and recurrence formulas. The coefficients of the expansion are functions of the radial coordinate and are identified with Bessel functions of integral order.

FUNDAMENTAL EQUATIONS

A PARTICLE of mass m and charge[1] $Z'e$ is moving in the Coulomb field of a nucleus with charge Ze. If the energy of the particle is $E(\geq 0)$ and if it is described in terms of spherical polar coordinates, r, θ, ϕ (origin at Ze), then a suitable wave function for the particle is:[2]

$$\psi_{klm}(r,\theta,\phi)=Ne^{im\phi}P_l^{|m|}(\cos\theta)L_{k,l}(r),$$

$$L_{k,l}(r)=e^{-\pi\beta l/(2k)}\left[\left|\Gamma\left(l+1+i\frac{\beta}{k}\right)\right|/\Gamma(2l+2)\right] \tag{1}$$

$$\times(2kr)^l e^{ikr}\,{}_1F_1\left(i\frac{\beta}{k}+l+1,\ 2l+2,\ -2ikr\right),$$

$$\beta=ZZ'me^2/\hbar^2;\quad k^2=2mE/\hbar^2$$

in which the constant factors in $L_{k,l}(r)$ have been chosen so that asymptotically

$$L_{k,l}\sim(kr)^{-1}\sin\left[kr-l\frac{\pi}{2}+\arg\Gamma\left(l+1+i\frac{\beta}{k}\right)-\frac{\beta}{k}\ln 2kr\right].$$

The confluent hypergeometric function ${}_1F_1$ is defined[3] as

$${}_1F_1(a,b,z)=1+\frac{a}{b}z+\frac{a(a+1)}{b(b+1)}\frac{z^2}{2!}+\cdots. \tag{2}$$

To simplify the analysis consider, instead of $L_{k,l}(r)$, the function [essentially $r^{-1}L_{k,l}(r)$]

$$u_{k,l}(r)=e^{ikr}\,{}_1F_1\left(i\frac{\beta}{k}+l+1,\ 2l+2,\ -2ikr\right), \tag{3}$$

---

* Publication assisted by the Ernest Kempton Adams Fund for Physical Research of Columbia University.

[1] e is positive throughout, so that, e.g., $Z'=-1$ for an electron or $+2$ for an alpha-particle.

[2] N. F. Mott and H. S. W. Massey, *Theory of Atomic Collisions* (Oxford University Press, 1933), p. 39.

[3] E. T. Whittaker and G. N. Watson, *Modern Analysis* (Cambridge University Press, 1927), p. 338.

which is real and satisfies the differential equation $ru''+(2l+2)u'+(k^2r-2\beta)u=0$. The power series solution (regular at $r=0$) of this differential equation is:

$$u_{k,l}(r)=\sum_{n=0}^{\infty} b_n(k^2, l)r^n/n!,$$
$$b_0=1,$$
$$(n+3+2l)b_{n+2}-2\beta b_{n+1}+(n+1)k^2b_n=0. \quad (4)$$

The condition $b_0=1$ follows from the definitions (2) and (3). b_n has been written as a function of k^2 since, as is apparent from the recurrence formula, only the square of k is involved.

In calculating numerically the radial part of $\psi(r, \theta, \phi)$ one can use Eq. (4) with a reasonable amount of labor (provided r is not too large). When k^2 is small, however, it is possible to simplify the calculation and to derive an expression for u of the form:

$$u_{k,l}(r)=\sum_{\mu=0}^{\infty} u_{0,l}^{\mu}(r)\cdot k^{2\mu}. \quad (5)$$

The purpose of this paper is to develop formulas for the functions $u_{0,l}^{\mu}(r)$, using the properties of the expansion coefficients $b_n(k^2, l)$.

COEFFICIENTS b_n EXPANDED IN POWERS OF k^2

From Eq. (4) it follows that

$$b_n=[2\beta/(n+1+2l)]b_{n-1}+k^2[(1-n)/(n+1+2l)]b_{n-2}.$$

If b_{n-1} is replaced by the value of b_{n-1} obtained from the same recurrence formula, that is,

$$b_{n-1}=[2\beta/(n+2l)]b_{n-2}+k^2[(2-n)/(n+2l)]b_{n-3},$$

and terms in k^2 are collected, the result is:

$$b_n=\frac{(2\beta)^2}{(n+2l+1)(n+2l)}b_{n-2}+k^2\left[\frac{(1-n)}{(n+2l+1)}b_{n-2}+\frac{2\beta}{(n+2l+1)}\frac{(2-n)}{(n+2l)}b_{n-3}\right].$$

Now repeat this procedure, substituting for the first b_{n-2} on the right the expression $b_{n-2}=\cdots b_{n-3}+k^2\cdots b_{n-4}$. Again collect terms in k^2 and obtain $b_n=\cdots b_{n-3}+k^2(\cdots b_{n-2}+\cdots b_{n-3}+\cdots b_{n-4})$. Finally repeat this $n-3$ times until the first term has the factor b_0 (which $=1$). The general theorem thus derived is:

$$b_n(k^2, l)=\frac{(2\beta)^n(2l+1)!}{(n+2l+1)!}-k^2\sum_{\nu=1}^{n-1}\frac{\nu(\nu+2l+1)!}{(n+2l+1)!}(2\beta)^{n-\nu-1}b_{\nu-1}(k^2, l). \quad (6)$$

From this formula it is possible to develop an expansion of b_n in powers of k^2. The coefficient of the zeroth power of k^2 is just the first term on the right side of the equation. The coefficient of k^2 is obtained by substituting the zeroth power coefficient into the finite sum. Coefficients of higher powers are obtained in a similar manner. In each case the only difficulty is the evaluation of the finite sum over ν. In terms of the finite sums the result of this process is an expansion of the b_n in powers of k^2:

$$b_n(k^2, l)=\sum_{\mu=0}^{\infty} b_n^{\mu}(0, l)\cdot k^{2\mu}.$$
$$b_n^{\mu}(0, l)=(-1)^{\mu}[(2l+1)!/(n+2l+1)!]\times(2\beta)^{n-2\mu}S_n^{\mu}, \quad (7)$$
$$S_n^0=1; \quad S_n^{\mu}=\sum_{\nu=1}^{n-1}\nu(\nu+2l+1)S_{\nu-1}^{\mu-1} \text{ for } \mu\geq 1.$$

Now substitute this expansion into Eq. (4) and compare the result with Eq. (5). It is immediately apparent that the functions $u_{0,l}^{\mu}(r)$ are just

$$u_{0,l}^{\mu}(r)=\sum_{n=0}^{\infty} b_n^{\mu}(0, l)r^n/n!$$
$$=(-1)^{\mu}(2\beta)^{-2\mu}\sum_{n=0}^{\infty}[(2l+1)!/(n+2l+1)!](2\beta r)^n\frac{S_n^{\mu}}{n!}. \quad (8)$$

The power series of (8) is to be compared to the expansion of the Bessel function $\Lambda_p[2(-2\beta r)^{\frac{1}{2}}]$ defined[4] as

$$\Lambda_p[2(-2\beta r)^{\frac{1}{2}}]=p!(-2\beta r)^{-p/2}J_p[2(-2\beta r)^{\frac{1}{2}}]$$
$$=\sum_{n=0}^{\infty}[p!/(n+p)!](2\beta r)^n\frac{1}{n!}. \quad (9)$$

The comparison shows that if the S_n^{μ} are not

[4] E. Jahnke and F. Emde, *Tables of Functions* (B. G. Teubner, 1938), p. 128.

too complicated, it should be possible to reduce the $u^{\mu}_{0,l}(r)$ to a finite sum of Λ_p's.

Inspection of the definition of S_n^{μ}, Eq. (7), shows that the S_n^{μ} are polynomials in n of degree 3μ. In evaluating S_n^{μ} it is convenient to express these polynomials as a sum of terms each with the general form

$$\alpha n(n-1)(n-2)\cdots(n-\lambda)(n+2l+1)\times(n+2l)\cdots(n+2l+1-\lambda'),$$

where $\lambda, \lambda' \geq 0$ (and $\lambda+\lambda'+2 \leq 3\mu$ since the highest power of n must be $n^{3\mu}$). This form is chosen so that when it is substituted in place of S_n^{μ} in Eq. (8), the resulting series in n can be compared to Eq. (9) and immediately identified as

$$\alpha(-4\beta^2)^{-\mu}(2\beta r)^{\lambda+1}[(2l+1)!/(2l+1+\lambda-\lambda')!]\times\Lambda_{2l+1+\lambda-\lambda'}[2(-2\beta r)^{\frac{1}{2}}].$$

EVALUATION OF THE FINITE SUMS

Instead of the definition of S_n^{μ}, Eq. (7), it is more convenient to consider the difference equation satisfied by S_n^{μ}:

$$\Delta S_n^{\mu} = S_{n+1}^{\mu} - S_n^{\mu} = n(n+2l+1)S_n^{\mu-1}; \quad (10)$$
$$S_n^0 = 1.$$

By solving this equation [or Eq. (7)] for the special cases $\mu=1$ and $\mu=2$, one is led to surmise that the general solution which has the desired form is:

$$S_n^{\mu} = [n!/(3^{\mu}\mu!(n-2\mu)!)] \times \sum_{\nu=0}^{\mu} \alpha_{\mu\nu}[(n+2l+1)!/(n+2l+1-\mu+\nu)!]. \quad (11)$$

It is apparent that this is of the appropriate degree (3μ) in n, but that it has the necessary number of arbitrary constants [to be determined by Eq. (10)] is not immediately apparent.

The validity of (11) is readily established by substituting it into Eq. (10), expanding both sides in powers of n, and comparing coefficients. The result is a series of $\mu+1$ equations defining each $\alpha_{\mu\nu}$ in terms of $\alpha_{\mu,\lambda-1}$ and $\alpha_{\mu-1,\lambda}$ for $\lambda \leq \nu$. Starting with $\nu=0$ and then considering $\nu=1, 2, \cdots\mu$, each successive equation for the $\alpha_{\mu\nu}$ is a linear equation in one unknown (assuming the $\alpha_{\mu-1,\nu}$ to be previously determined):

$$\alpha_{\mu,0} = \alpha_{\mu-1,0} = 1,$$

$$\alpha_{\mu\nu} = \frac{1}{(3\mu-\nu)}\left\{3\mu\alpha_{\mu-1,\nu} - \sum_{\lambda=0}^{\nu-1}(\beta_{\mu\lambda}^{\mu-\nu}\alpha_{\mu\lambda} + \gamma_{\mu\lambda}^{\mu-\nu}\alpha_{\mu-1,\lambda})\right\}, \quad (12a)$$

$$\alpha_{\mu\nu} = 0 \text{ for } \nu > \mu,$$

with

$$[n(3\mu-\lambda)+4\mu(l+1)+(\mu-\lambda)(1-2\mu)] \times \frac{(n+2l+1)!}{(n+2l+2-\mu+\lambda)!} = \sum_{\nu'=0}^{\mu-\lambda}\beta_{\mu\lambda}^{\nu'}n^{\nu'},$$

$$-3\mu[(n+2l+1)!/(n+2l+1-\mu+\lambda)!] = \sum_{\nu'=0}^{\mu-\lambda}\gamma_{\mu\lambda}^{\nu'}n^{\nu'}.$$

The β's and γ's can be expressed explicitly in terms of μ, λ, l, and substituted in the $\alpha_{\mu\nu}$ recurrence formula above. Then taking $\nu=1$, the sum over λ reduces to one term, $\lambda=0$, and since $\alpha_{\mu 0} = \alpha_{\mu-1,0} = 1$, a simple relation between $\alpha_{\mu 1}$ and $\alpha_{\mu-1,1}$ is obtained. This can be solved in terms of μ and l, yielding $\alpha_{\mu 1} = \mu l - (\mu/5)(\mu-1)$. In principle it is possible to continue this process finding $\alpha_{\mu 2}$, $\alpha_{\mu 3}$, etc., as explicit functions of μ and l. However, the algebra becomes tedious mainly through the occurrence of polynomials in l, so that in practice it is easier to calculate an extensive table of $\alpha_{\mu\nu}$ when some particular numerical value of l is used.

The values of $\alpha_{\mu\nu}$ for $\mu=0, 1, 2, 3$ are:

$$\mu=0: \quad \alpha_{00}=1$$

$$\mu=1: \quad \alpha_{10}=1, \quad \alpha_{11}=l$$

$$\mu=2: \quad \alpha_{20}=1, \quad \alpha_{21}=(2/5)(5l-1), \quad \alpha_{22}=(l/5)(5l-1) \quad (12b)$$

$$\mu=3: \quad \alpha_{30}=1, \quad \alpha_{31}=(3/5)(5l-2), \quad \alpha_{32}=(3/35)(35l^2-21l+4), \quad \alpha_{33}=(l/35)(35l^2-21l+4).$$

EXPANSION OF ψ IN POWERS OF k^2

Substitution of (11) into Eq. (8) yields a general formula for the functions $u^{\mu}_{0,l}$ in terms of sums[5] of μ Bessel functions of integral order:

$$u^{\mu}_{0,l}(r)=\frac{(-1)^{\mu}(2l+1)!}{3^{\mu}\mu!}(r)^{2\mu}\sum_{\nu=0}^{\mu}\frac{\alpha_{\mu\nu}}{(2l+1+\mu+\nu)!}\times\Lambda_{2l+1+\mu+\nu}[2(-2\beta r)^{\frac{1}{2}}], \quad (13)$$

with

$$\Lambda_{2l+1+\mu+\nu}[2(-2\beta r)^{\frac{1}{2}}]=(2l+1+\mu+\nu)!\times(-2\beta r)^{-(2l+1+\mu+\nu)/2}J_{2l+1+\mu+\nu}[2(-2\beta r)^{\frac{1}{2}}].$$

For repulsive fields β is positive so the Bessel functions have an imaginary argument; in (13) Λ_p is to be taken as $p!(2\beta r)^{-p/2}i^{-p}J_p[2i(2\beta r)^{\frac{1}{2}}]$. β is negative for attractive fields so the Bessel functions have a real argument. (For $\beta>0$ the Bessel functions are monotonically increasing functions and for $\beta<0$ they are oscillatory functions with decreasing amplitude.)

Thus the wave function [asymptotically $Ne^{im\phi}P_l^{|m|}(\cos\theta)\sin(kr\cdots)/(kr)$] for a particle with charge $Z'e$ in the Coulomb field of Ze is:

$$\psi_{klm}(r,\theta,\phi)=Ne^{im\phi}P_l^{|m|}(\cos\theta)e^{-\pi\beta/(2k)}\times\left|\Gamma\left(l+1+i\frac{\beta}{k}\right)\right|(2kr)^l\sum_{\mu=0}^{\infty}[(-1)^{\mu}/(3^{\mu}\mu!)](kr)^{2\mu}\times\sum_{\nu=0}^{\mu}\frac{\alpha_{\mu\nu}\Lambda_{2l+1+\mu+\nu}[2(-2\beta r)^{\frac{1}{2}}]}{(2l+1+\mu+\nu)!}. \quad (14)$$

As long as k is finite the radial part of ψ_{klm} is asymptotically (for $r\gg 1/k$) $\sim\sin(kr\cdots)/(kr)$. For $k\equiv 0$ the radial function behaves at large distances like $\Lambda_{2l+1}[2(-2\beta r)^{\frac{1}{2}}]$.

In (14) the factor $(-1)^{\mu}(kr)^{2\mu}$ appears. This means that the expansion is an alternating series in powers of $(kr)^2$; consequently the convergence will be rapid only when $kr\ll 1$. For $kr\gg 1$ the asymptotic $\sin(kr\cdots)/(kr)$ is valid, while for $kr\sim 1$ (and $\beta/k\gg 1$) it is necessary to derive an asymptotic formula for the ${}_1F_1$ of Eq. (3) valid when the first parameter is large and imaginary.

CONCLUSION

As formula (14) is most useful when kr is small enough to make only the first few terms important, these terms are explicitly presented here:

$$\psi_{klm}(r,\theta,\phi)=Ne^{im\phi}P_l^{|m|}(\cos\theta)e^{-\pi\beta/(2k)}\times\left[\left|\Gamma\left(l+1+i\frac{\beta}{k}\right)\right|/\Gamma(2l+2)\right](2kr)^l\times\left\{\Lambda_{2l+1}-\frac{(kr)^2}{3(2l+2)}\left(\Lambda_{2l+2}+\frac{l\Lambda_{2l+3}}{(2l+3)}\right)+\frac{(kr)^4}{18(2l+2)(2l+3)}\left(\Lambda_{2l+3}+\frac{2}{5}(5l-1)\frac{\Lambda_{2l+4}}{(2l+4)}+\frac{l}{5}(5l+1)\frac{\Lambda_{2l+5}}{(2l+4)(2l+5)}\right)-\cdots\right\} \quad (15)$$

where $\Lambda_p=\Lambda_p[2(-2\beta r)^{\frac{1}{2}}]$.

The above expansion[6] of $\psi_{klm}(r,\theta,\phi)$ in powers of $(ikr)^2$ is particularly useful in calculating matrix integrals involving slow positive energy electrons in a Coulomb field provided the interaction is such that the most important region of integration is near $r=0$. In this case the convergence of the series, Eq. (14), is so rapid that only the first few terms are needed in the calculation.

A special case of the theorem, Eq. (15), has been used by the author in his Ph.D. dissertation (unpublished) submitted to Stanford University, California.

[5] The number of terms in each of the sums may be reduced to two terms by repeated application of the recurrence formula for Λ_p or J_p:

$$\Lambda_{p+1}(x)=[4p(p+1)/x^2][\Lambda_p(x)-\Lambda_{p-1}(x)]$$

or

$$J_{p+1}(x)=(2p/x)\cdot J_p(x)-J_{p-1}(x).$$

[6] This same expansion can no doubt be derived by transformation of the integral representation for the function $u_{kl}(r)$ instead of by the algebraic methods of the present derivation.

Effect of Nuclear Electric Quadrupole Moment on the Energy Levels of a Diatomic Molecule in a Magnetic Field*†

Part I. Heteronuclear Molecules

BERNARD T. FELD AND WILLIS E. LAMB, JR.
Pupin Physics Laboratories, Columbia University, New York, New York

(Received September 28, 1944)

The energy levels of a diatomic molecule—in which one nucleus has electric quadrupole moment and the second zero spin—are derived in "weak" and "strong" magnetic fields, and for intermediate fields in the special case of nuclear spin 1. The calculations are made for large molecular rotational quantum number. The transitions which would be induced in a molecular beam resonance experiment are discussed: Formulae are given for the energy differences involved in these transitions, and the shape of the molecular beam resonance spectrum, corresponding to the various transitions, is considered in detail. It is shown that the presence of nuclear electric quadrupole moment introduces subsidiary minima into the spectrum; from the energy differences between these minima, one can derive the value of the constant e^2qQ (e is the electronic charge, Q is the nuclear electric quadrupole moment, and q is a constant, depending on the charge distribution of the rest of the molecule, which must be independently evaluated in each case). The possibility of experimental application of these results is discussed. From heretofore unpublished data, we obtain a value for e^2qQ of Li^7 in LiF of $1.0\pm0.5\times10^{-21}$ erg. This may be compared with 0.3×10^{-21} erg for D in HD and D_2.

I. INTRODUCTION

THE existence of a nuclear electric quadrupole moment was first inferred from spectroscopic measurements of hyperfine structure. Thus, the departure of the hyperfine energy differences of europium[1,2] from the interval rule was explained on this basis. The molecular beam "zero-moment" technique was first applied to the measurement of the nuclear quadrupole moments of In^{115} [3] and $Ga^{69,71}$ [4] at the suggestion of I. I. Rabi. One of the early applications of the "molecular beam resonance method" was the determination by Kellogg, Rabi, Ramsey, and Zacharias[5] of the quadrupole moment of the deuteron from measurements of the hyperfine structure of HD and D_2 in a magnetic field. The molecular beam resonance method has been discussed in a number of papers.[6,7] However, a short review of the highlights will probably not be amiss.

A beam of well-collimated molecules, at low pressure, is passed successively through three magnetic fields. The first and third are inhomogeneous fields, equal in magnitude and direction but with gradients oppositely directed. Between these, there is a homogeneous magnetic field.

Because of its magnetic moment, the molecule is deflected in the inhomogeneous field. If no change in the magnetic moment of the molecule takes place, while it goes through the homogeneous field, the deflection in the two inhomogeneous fields will be equal and opposite; as a result, the fields will have no effect on the intensity of the beam, as measured by a suitable detector placed at the end of its path. However, should the orientation or magnitude of the magnetic moment change between fields, the deflections will not compensate; there will then be a decrease in beam intensity.

Changes in orientation are brought about by the application of a small, oscillating magnetic field perpendicular to and in the region of the

* Submitted by Bernard T. Feld in partial fulfillment of the requirements for the degree of Doctor of Philosophy in the Faculty of Pure Science, Columbia University, New York, New York.

† Publication assisted by the Ernest Kempton Adams Fund for Physical Research of Columbia University.

[1] H. Schüler and T. Schmidt, Zeits. f. Physik **94**, 457 (1935).

[2] H. B. G. Casimir, Physica **II**, 719 (1935).

[3] D. R. Hamilton, Phys. Rev. **56**, 30 (1939).

[4] N. A. Renzetti, Phys. Rev. **57**, 753 (1940).

[5] J. M. P. Kellogg, I. I. Rabi, N. F. Ramsey, Jr., and J. R. Zacharias, Phys. Rev. **57**, 677 (1940).

[6] I. I. Rabi, S. Millman, P. Kusch, and J. R. Zacharias, Phys. Rev. **55**, 526 (1939).

[7] P. Kusch, S. Millman, and I. I. Rabi, Phys. Rev. **57**, 765 (1940).

homogeneous field. In the homogeneous field, the quantum mechanical system (molecule) will tend to orient itself in such a way that its spin satisfies the stationary state quantum conditions for a magnetic moment in a magnetic field; the component of the angular momentum in the direction of the field must be an integral or half-integral multiple of $h/2\pi$.

In general, corresponding to different orientations of the magnetic moment in the magnetic field, the system has different energies. When h times the frequency ν of the oscillating field is very close or (better) equal to the difference in energy W between two states of the system and when the quantum mechanical conditions allow a transition between these states, there will occur a reorientation within the system, leading to a change of the resultant magnetic moment of the molecule. Thus, for values of the frequency of

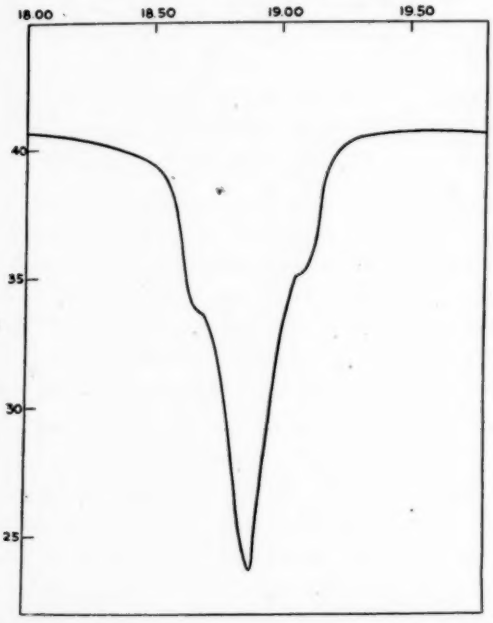

FIG. 1. Li^7 resonance in LiF. The ordinates are arbitrary, while the abscissa numbers are galvanometer readings, proportional to the strength of the homogeneous magnetic field. The perturbing oscillating field frequency was held constant. This is one of a number of heretofore unpublished curves, for which we are indebted to Drs. Kusch and Millman.

oscillating field such that

$$h\nu = W, \qquad \text{I (1)}$$

there will be a decrease of beam intensity at the detector. Measurement of the resonance frequencies and corresponding values of the homogeneous field at the resonance minima may lead to valuable information concerning such properties as gyromagnetic ratio, hyperfine splitting, electric quadrupole moment, etc.

An important application of this method has been the measurement of nuclear magnetic moments in molecules having zero electronic angular momentum.[6, 8–10] In one of these investigations,[8] it was found that the resonance minima for Na^{23} and K^{39} (in the molecules Na_2 and K_2) are accompanied by subsidiary minima. Furthermore, these subsidiary minima (for a particular nucleus) appear always to be separated by a constant energy difference, independent of the value of frequency and magnetic field at which the resonance occurs. This seems to imply the existence of a constant interaction between the nucleus and the rest of the molecule. In addition, the investigators[8] have shown that the effect is at least of an order of magnitude too great to be explained as magnetic dipole interaction between the two nuclei or between the nuclei and the rotational magnetic moment of the molecule. To quote the authors: "It appears likely to us that these large effects may be due, in part, to the presence of a quadrupole electrical moment in the nucleus which interacts electrostatically with the rest of the molecule."

Very similar effects have been observed by Kusch and Millman[11] in a number of heteronuclear molecules. In Fig. 1 is plotted one of their upublished curves for a resonance involving a reorientation of the nucleus of Li^7 in LiF. The subsidiary unresolved minima have been observed always to appear in the curve under a variety of conditions. The figure is an example of resonance in a molecule of the type to which the calculations of this paper pertain.

We have, in fact, calculated the energy levels and spectrum for heteronuclear molecules in a magnetic field when one member has electric quadrupole moment. The calculation has been

[8] P. Kusch, S. Millman, and I. I. Rabi, Phys. Rev. **55**, 1176 (1939).
[9] S. Millman, P. Kusch, and I. I. Rabi, Phys. Rev. **56**, 165 (1939).
[10] J. M. B. Kellogg, I. I. Rabi, N. F. Ramsey, Jr., and J. R. Zacharias, Phys. Rev. **56**, 728 (1939).
[11] We are greatly indebted to Drs. Millman and Kusch for having allowed us access to a large amount of unpublished data.

made for fields ranging from "weak" to "strong," for nuclear spins from 1 to 9/2, and large rotational quantum number J. A "weak" field is one in which the energy of interaction between the field and the magnetic moment of the molecule is

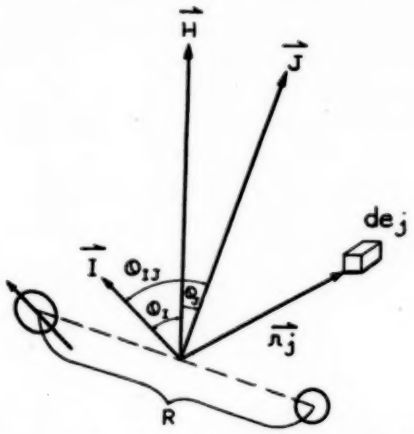

FIG. 2. Diatomic molecule with rotational spin J, and one nucleus having spin I and electric quadrupole moment. The second nucleus has zero spin. The molecule is in a magnetic field H.

small compared to the electric quadrupole interaction energy of the molecule; thus, the magnetic interaction terms can be treated as perturbations on the energy of the system. In "strong" fields, the electric quadrupole interaction is small compared to the magnetic interaction. A calculation of this type has already been made for the molecule HD,[5] and differs from our calculation in that the rotational quantum number J is quite small in HD. Although the condition of large J introduces many quantum states into the problem, it results in a simplification insofar as **J** can now be treated as a classical angular momentum vector, and the magnitude of the nuclear spin I can be neglected as compared to that of J.

For the purpose of simplification, we have made the assumption that the spin of the second nucleus comprising the molecule is zero. As long as the electric quadrupole interaction is large compared to the magnetic interaction between nuclei, and between nucleus and the field caused by molecular rotation,[12] this assumption may be made without detracting from the generality of our treatment. For it is evident that, if the afore-mentioned considerations hold, the energy of the molecule (because of quadrupole interaction) depends only on the orientation of the quadrupole nucleus with respect to the rotational angular momentum. The energy of the molecule in a magnetic field consists then of two completely separate parts, pertaining to the two nuclei; so that the effects of the quadrupole moment of one nucleus are independent of the state of the second, and energy changes caused by the reorientation of one nucleus are not affected by the state of the other.

A diatomic molecule of this type may be pictured diagrammatically as in Fig. 2. The nuclei are rotating about the direction **J**; de_j represents a small element of electronic charge. The rest of the charge, which is distributed in a suitable fashion throughout the molecule, is not shown. The externally applied magnetic field is represented by the vector **H**.

The part of the Hamiltonian for this molecule in an external magnetic field **H**, which is of interest in our problem, may be written as

$$\mathcal{H}=\mu_0 g_I \mathbf{H}\cdot\mathbf{I}+\mu_0 g_J \mathbf{H}\cdot\mathbf{J}+\mathcal{H}(Q), \qquad \text{I (2)}$$

where μ_0 is the nuclear magneton, g_I and g_J are the Landé g factors for the nuclear and rotational spin, respectively, and $\mathcal{H}(Q)$ is the Hamiltonian for the interaction of the electric quadrupole moment of the nucleus with the rest of the charges in the molecule.

II. STRONG MAGNETIC FIELDS; PASCHEN-BACK EFFECT

(1) Semiclassical Treatment

In sufficiently strong magnetic field, nuclear spin and molecular rotation may be considered as uncoupled. One can adopt a semiclassical approach. Allowing the subscript i to represent the nucleus with spin and quadrupole moment, and j the remainder of the molecule, we write as the quadrupole term in the energy expansion

[12] If the nuclear magnetic moment is μ_n and the distance between nuclei R, then the magnitudes of both the nuclear spin-spin and spin-orbit energies are of order μ_n^2/R^3. For a nuclear magnetic moment of one nuclear magneton and R of 10^{-8} cm, this energy turns out to be of order 10^{-22} erg. The quadrupole interaction has order of magnitude e^2qQ, where e is the electronic charge, q is a factor depending on the electronic charge distribution, of order $1/R^3$, and Q is the value of the electric quadrupole moment. For values of Q of order 10^{-25} cm^2 (magnitude of the Q's observed spectroscopically) $e^2qQ \approx 10^{-20}$ erg. In the case of HD, the quadrupole moment of the deuteron having been determined to be $\approx 10^{-27}$ cm^2, $e^2qQ \approx 10^{-22}$ and the magnetic effects could not be neglected.

for our system

$$E(Q)=\frac{eQN}{4}\int_j \frac{de_j(3\cos^2\theta_{ij}-1)}{r_j^3}. \qquad \text{II (1)}$$

In this expression, the quadrupole moment Q is defined by the integral over the nucleus

$$eQ=\int_i de_i r_i^2(3\cos^2\theta_{Ii}-1), \qquad \text{II (2)}$$

and N is a normalization factor, to be discussed. The angle θ_{Ii} is measured between the direction of nuclear spin and an element of nuclear charge de_i. Likewise, θ_{Ij} is the angle between the nuclear spin direction and the element of charge de_j (Fig. 2).

Introducing the direction of molecular rotation **J**, we apply the addition theorem of spherical harmonics.[13] Thus, we may write

$$(3\cos^2\theta_{Ij}-1)=\tfrac{1}{2}(3\cos^2\theta_{Jj}-1)(3\cos^2\theta_{IJ}-1)$$
$$+\text{terms with } \exp(i\varphi_{Jj})\exp(i\varphi_{IJ}). \qquad \text{II (3)}$$

Performing the integration II (1) over the molecule, we find the terms $\exp(i\varphi_{Jj})$ average out to zero, giving

$$E(Q)=\frac{e^2qQN}{8}(3\cos^2\theta_{IJ}-1), \qquad \text{II (4)}$$

where

$$eq=\int_j \frac{de_j(3\cos^2\theta_{Jj}-1)}{r_j^3}. \qquad \text{II (5)}$$

Taking advantage of the fact that **I** and **J**, for strong fields, may be considered to precess independently about the direction of the field **H** (Fig. 2), we write

$$(3\cos^2\theta_{IJ}-1)=\tfrac{1}{2}(3\cos^2\theta_I-1)(3\cos^2\theta_J-1)$$
$$+\text{terms with } \exp(i\varphi_I)\exp(i\varphi_J). \qquad \text{II (6)}$$

Averaging over all directions about **H**, we obtain

$$E(Q)=\frac{e^2qQN}{16}(3\cos^2\theta_J-1)(3\cos^2\theta_I-1). \qquad \text{II (7)}$$

Since J is large, the molecular rotation may be considered from a classical point of view. Hence, $\cos\theta_J=m_J/J$ ranges continuously from -1 to $+1$.

[13] E. U. Condon and G. H. Shortley, *Theory of Atomic Spectra* (Cambridge University Press, 1935), p. 53 (henceforth referred to as Condon and Shortley).

The nuclear spin I, being small, must be treated quantum mechanically. Thus, only certain orientations of **I** with respect to **H**, characterized by integral or half-integral m_I ($\cos\theta_I=m_I/|I|$) are permitted. In addition, there is the relationship $\mathbf{I}^2=I(I+1)$.

In the definition of quadrupole moment by Eqs. II (1) and II (2), there is introduced a normalization factor N. This factor is evaluated by incorporating into the definition of quadrupole moment the condition that when $m_I=I$, the factor $eQN\frac{1}{2}(3\cos^2\theta_I-1)$ becomes equal to eQ.[14] From this and the relationships introduced in the last paragraph, we have

$$N=\frac{2I(I+1)}{3I^2-I(I+1)}. \qquad \text{II (8)}$$

Thus, we arrive at an expression for the quadrupole term in the electrostatic energy of the molecule:

$$E(Q)=\frac{e^2qQ}{8}\left(3\frac{m_J^2}{J^2}-1\right)\frac{[3m_I^2-I(I+1)]}{I(2I-1)}. \qquad \text{II (9)}$$

The quadrupole energy is seen to be proportional to the product qQ. Thus, knowledge of the quadrupole energy alone will not suffice to determine the quadrupole moment Q.

The quantity q depends on the electronic configuration of the molecule and can be evaluated if this distribution is known.[15] Although no attempt shall be made in this work to calculate q, it should be stressed that before the results of our calculations can be utilized for the determination of nuclear electric quadrupole moments, an independent evaluation of q is required.

(2) Quantum Mechanical Treatment

(a) *Energy Values*

In strong magnetic field, the Hamiltonian for our system may be written as the sum of two terms. The first

$$\mathcal{H}_0=\mu_0 g_I H m_I+\mu_0 g_J H m_J, \qquad \text{II (10)}$$

[14] H. B. G. Casimir, "On the interaction between atomic nuclei and electrons," prize essay published by Teyler's Tweede Genootschap (1936). Also published in the *Archives du Musee Teyler* [III], **VIII**, 201 (1936) (henceforth referred to as Casimir).

[15] A. Nordsieck, Phys. Rev. **58**, 310 (1940); E. Teller, Phys. Rev. **57**, 556A (1940).

in which the symbols are used as defined in the preceding section, expresses the interaction between the magnetic moments associated with **I** and **J** and the external magnetic field. This term is diagonal in a representation characterized by the quantum numbers m_I, m_J.

The perturbation term of the Hamiltonian results from the electric quadrupole interaction between nucleus and the rest of the molecule, and is given by the expression[14]

$$\mathcal{H}=\frac{e^2qQ}{2J(2J-1)I(2I-1)}\{3(\mathbf{I}\cdot\mathbf{J})^2+\tfrac{3}{2}(\mathbf{I}\cdot\mathbf{J}) -I(I+1)J(J+1)\}. \quad \text{II (11)}$$

Referring to the operator in brackets as F, we have for its matrix elements in the m_I, m_J representation:[5]

$$\begin{aligned}
&(m_J, m_I|F|m_J, m_I)=\tfrac{1}{2}[3m_I^2-I(I+1)][3m_J^2-J(J+1)],\\
&(m_J, m_I|F|m_J-1, m_I+1)=\tfrac{3}{4}(2m_J-1)(2m_I+1)[(J+m_J)(J-m_J+1)(I-m_I)(I+m_I+1)]^{\frac{1}{2}},\\
&(m_J, m_I|F|m_J+1, m_I-1)=\tfrac{3}{4}(2m_J+1)(2m_I-1)[(J-m_J)(J+m_J+1)(I+m_I)(I-m_I+1)]^{\frac{1}{2}},\\
&(m_J, m_I|F|m_J-2, m_I+2)=\tfrac{3}{4}[(J+m_J)(J+m_J-1)(J-m_J+1)(J-m_J+2)\\
&\qquad\times(I-m_I)(I-m_I-1)(I+m_I+1)(I+m_I+2)]^{\frac{1}{2}},\\
&(m_J, m_I|F|m_J+2, m_I-2)=\tfrac{3}{4}[(J-m_J)(J-m_J-1)(J+m_J+1)(J+m_J+2)\\
&\qquad\times(I+m_I)(I+m_I-1)(I-m_I+1)(I-m_I+2)]^{\frac{1}{2}}.
\end{aligned} \quad \text{(II 12)}$$

In the case $\mathcal{H}\ll\mathcal{H}_0$, first-order perturbation theory gives for the quadrupole energy,

$$E^{(1)}(Q)=\frac{e^2qQ}{4J(2J-1)I(2I-1)} \times[3m_J^2-J(J+1)][3m_I^2-I(I+1)], \quad \text{II (13)}$$

which, for large J, reduces to

$$E^{(1)}(Q)=\frac{e^2qQ}{8}\left[\frac{3m_J^2}{J^2}-1\right]\frac{[3m_I^2-I(I+1)]}{I(2I-1)}. \quad \text{II (14)}$$

This is, of course, identical with the result obtained in the previous section.

From the value of the Hamiltonian and the above matrix elements, it is possible to calculate, by the use of perturbation theory,[16] the energy level system of the molecule for different values of I. The case $I=\frac{1}{2}$ is of no interest to us, because the charge density of the nucleus in this state is spherically symmetrical and, hence, $Q=0$.

For the systems under consideration, there are $(2J+1)(2I+1)$ different states. However, since J is large, we shall calculate only the $2I+1$ states of different m_I, retaining m_J/J (which can be considered as varying continuously) as a parameter.

The energy values, including second-order perturbation terms, for the case $I=1$, are: (The expressions for $I\geqslant\frac{3}{2}$ have the same form, although differing in detail.)

$$\begin{aligned}
E(m_I=1)&=\mu_0g_IH+\mu_0g_JHm_J+\frac{e^2qQ}{8}(3z^2-1)\\
&\quad+\tfrac{1}{2}(\tfrac{3}{8}e^2qQ)^2\frac{(3z^2+1)(1-z^2)}{\mu_0g_IH-\mu_0g_JH},\\
E(m_I=0)&=\mu_0g_JHm_J-\frac{e^2qQ}{4}(3z^2-1), \quad \text{II (15)}^{17}\\
E(m_I=-1)&=-\mu_0g_IH+\mu_0g_JHm_J\\
&\quad+\frac{e^2qQ}{8}(3z^2-1)\\
&\quad-\tfrac{1}{2}(\tfrac{3}{8}e^2qQ)^2\frac{(3z^2+1)(1-z^2)}{\mu_0g_IH-\mu_0g_JH}.
\end{aligned}$$

In the above expressions, we have substituted the continuously varying parameter z for m_J/J.

(b) *The Spectrum*

Transitions between states of our system are caused by a small perturbation in the form of a weak, oscillating magnetic field $\mathbf{H}'$, whose contribution to the Hamiltonian (too small to effect the energies of the system) may be ex-

[16] Reference 13, p. 30.

[17] $\mu_J=\mu_0g_JJ$; $\mu_I=\mu_0g_II$. We know from experimental evidence that $\mu_I\approx\mu_J$. Hence $g_I/g_J\approx J/I$; $g_I\gg g_J$. We shall, in all further computations write $g_J=\epsilon g_I$, where ϵ is a small number.

pressed as

$$\mathcal{H}' = \mu_0 g_I \mathbf{H}' \cdot \mathbf{I} + \mu_0 g_J \mathbf{H}' \cdot \mathbf{J}. \qquad \text{II (16)}$$

In general,

$$\mathbf{H}' = (H_x'\mathbf{i} + H_y'\mathbf{j} + H_z'\mathbf{k}) \cos(\omega t + \delta). \qquad \text{II (17)}$$

In the approximation for which m_I and m_J are the appropriate quantum numbers, **I** and **J** may be pictured as precessing independently about the direction of the homogeneous magnetic field. The matrix elements for such angular momenta are given in Condon and Shortley:[18]

$$\begin{aligned} &(m|\mathbf{I}|m) = m\mathbf{k}, \\ &(m|\mathbf{I}|m+1) = \tfrac{1}{2}[(I-m)(I+m+1)]^{\frac{1}{2}}(\mathbf{i}+i\mathbf{j}), \\ &(m|\mathbf{I}|m-1) = \tfrac{1}{2}[(I+m)(I-m+1)]^{\frac{1}{2}}(\mathbf{i}-i\mathbf{j}). \end{aligned} \qquad \text{II (18)}$$

In effect, we are dealing with a resonance process[19] for which transitions between states occur at values of the frequency of oscillating field equal to the energy difference divided by h. The probability of a transition is, in general, a function of the matrix elements between states, as well as of the velocity distribution in the molecular beam and the length of the oscillating field. Assuming a monoenergetic beam subject to a small perturbation (such that only a small fraction of the molecules capable of undergoing a transition are effected) we may take the transition probability P to be proportional to the square of the corresponding matrix element.[20]

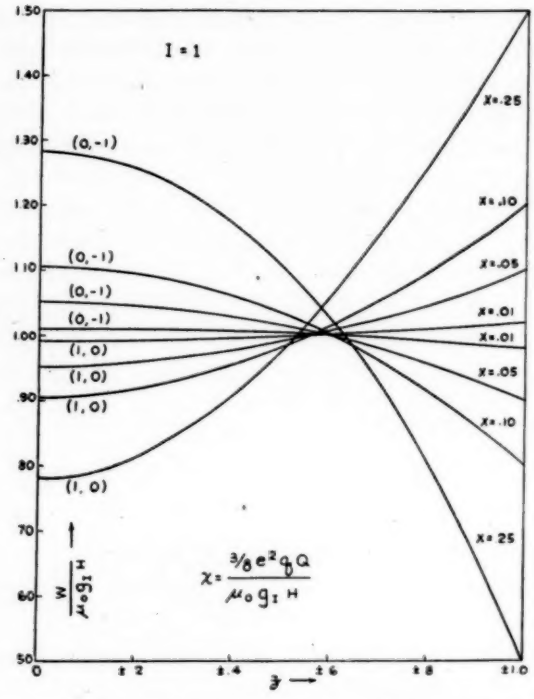

FIG. 3. Energy of transition for $I=1$ in strong magnetic fields as a function of $z=m_J/J$, for different values of the perturbation x. The two sets of curves are for the transition $m_I=0 \rightarrow m_I=-1$ and $m_I=1 \rightarrow m_I=0$, respectively. ($\Delta m_J=0$ in both cases.)

In considering a transition, then, two factors must be taken into account: (1) the energy differences W are in general functions of the parameter $z=m_J/J\,[W=f(z)]$. This parameter varies continuously from -1 to $+1$, each value having equal probability of occurrence. For an interval ΔW there corresponds an interval $\Delta z=\Delta W \cdot dz/dW$. Since the number of values of z in the interval ΔW, and hence the number of transitions within this interval, is proportional to Δz, we may define a "density of transitions" D, given by

$$D(z) = \Delta z/\Delta W = 1/f'(z). \qquad \text{II (19)}$$

The reciprocal of the slope of the W *vs.* z curve (Fig. 3) will thus be proportional to the number of states involved in transitions having a given energy difference; hence, the depth of the resonance minimum will vary with this quantity. (2) The product of $D(z)$ by the transition probability $P(z)$ is a measure of the relative strength of the transition, as a function of the parameter z. $D(z)P(z)$ will henceforth be called the "shape function" for a transition.

[18] Reference 13, pp. 47–49.

[19] The resonance process has been discussed in the following references: I. I. Rabi, Phys. Rev. **51**, 652 (1937); J. Schwinger, Phys. Rev. **51**, 648 (1937); F. Block and A. Siegert, Phys. Rev. **57**, 522 (1940); A. F. Stevenson, Phys. Rev. **58**, 1061 (1940); H. C. Torrey, Phys. Rev. **59**, 293 (1941).

[20] The transition probability between two states p and q, if we assume no interference from other transitions, is

$$P_{pq} = \frac{\sin^2 \pi t[b_{pq}^2 + (\nu - \nu_{pq})^2]^{\frac{1}{2}}}{b_{pq}^2 + (\nu - \nu_{pq})^2} \cdot b_{pq}^2$$

where b_{pq} is the matrix element of the perturbation $(p|\mathcal{H}'|q)$ divided by h, t is the time spent in the perturbing field, and ν_{pq} is the frequency at which the resonance takes place ($h\nu_{pq}=W_{pq}$). At resonance, and for small b_{pq}, $P_{pq}=\pi^2 t^2 b_{pq}^2$. The natural width of a line is most simply obtained from the uncertainty principle $\Delta E \Delta t \approx h$. For molecules (assumed molecular wt. $\simeq$50 and temp. $\simeq$1000° Abs.) in an oscillating field of length 5 cm. $\Delta E \sim 5\times 10^{-22}$ erg. Since this is considerably less than the energies involved in the quadrupole interaction (see footnote 12) we shall henceforth neglect natural widths in our discussion of line shapes.

The selection rules corresponding to a perturbation of the type II (13) are[18] $\Delta m_I=0, \pm 1$, $\Delta m_J=0, \pm 1$. Since transitions of the type $\Delta m_J=\pm 1$ result in very small energy changes, and therefore correspond to very low oscillating field frequencies, they are of comparatively little interest. We, therefore, confine our attention to the resonance spectrum corresponding to the transitions $\Delta m_I=\pm 1$.

Returning, now, to the case $I=1$, for which we have already calculated the energy values, we write for the energy differences corresponding to the selection rules $\Delta m_I=\pm 1$, $\Delta m_J=0$.

$$W(1,0)=\mu_0 g_I H+\tfrac{3}{8}e^2qQ(3z^2-1)+\tfrac{1}{2}(\tfrac{3}{8}e^2qQ)^2\frac{(3z^2+1)(1-z^2)}{\mu_0 g_I H(1-\epsilon)},$$
$$W(0,-1)=\mu_0 g_I H-\tfrac{3}{8}e^2qQ(3z^2-1)+\tfrac{1}{2}(\tfrac{3}{8}e^2qQ)^2\frac{(3z^2+1)(1-z^2)}{\mu_0 g_I H(1-\epsilon)}. \qquad \text{II (20)}$$

In Fig. 3 is plotted $W/\mu_0 g_I H$ as a function of z for different values of the (small) variable $x=\frac{3}{8}e^2qQ/\mu_0 g_I H$ and for $\epsilon=0$.

Calculation of the shape function for the spectrum requires the transition probabilities, which we obtain directly from the matrix elements II (18), and the condition $\mathbf{H}'=H_z'\mathbf{i}$.

$$P(1,0)=(1,m_J|\mathcal{H}'|0,m_J)^2=\tfrac{1}{2}\mu_0^2 g_I^2 H_z'^2,$$
$$P(0,-1)=(0,m_J|\mathcal{H}'|-1,m_J)^2=\tfrac{1}{2}\mu_0^2 g_I^2 H_z'^2. \qquad \text{II (21)}$$

The fact that P is independent of z is caused, of course, only by the fact that we are considering transitions for which $\Delta m_J=0$. Thus, the shape function for this transition depends on z only through the factor $D(z)$.

Considering the value of $W(z)$ up to first-order perturbation terms, we have $f(z)=k(3z^2-1)$. Hence, $D(z)=k/6z$. In Fig. 4 we have plotted the strength of the line (in arbitrary units) as a function of the transition energy in units of $W/\mu_0 g_I H$. To do this, we note that z is proportional (up to terms of first order in x) to the square root of the energy, measured from the value for $z=0$. This enables us to write for the shape function of $m_I=1\rightarrow m_I=0$.

$$D=\frac{k}{6}\frac{1}{\left[\dfrac{W-\mu_0 g_I H}{\frac{3}{8}e^2qQ}+1\right]^{\frac{1}{2}}} \qquad \text{II (22)}$$

in which the value of W varies from $\mu_0 g_I H-\frac{3}{8}e^2qQ$ to $\mu_0 g_I H+2\times\frac{3}{8}e^2qQ$. The value of D for the transition $m_I=0\rightarrow m_I=-1$ differs from the above only by the sign of the term 1 in the denominator. The final line shape is determined by superposing the shape functions of both transitions.

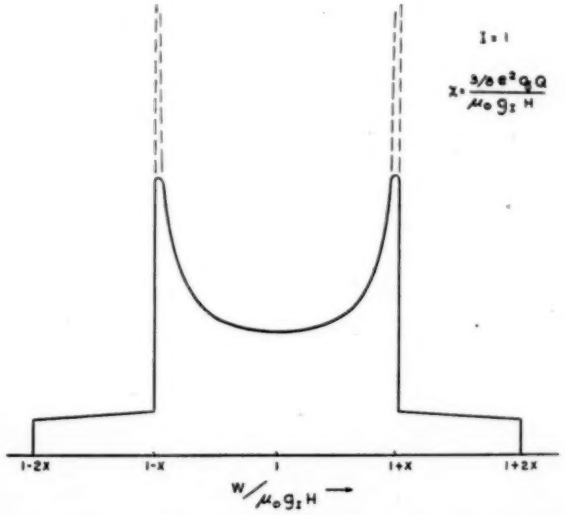

FIG. 4. Shape of the resonance line for $I=1$, corresponding to the transitions $\Delta m_I=\pm 1$, $\Delta m_J=0$, in strong magnetic fields, as a function of the transition energy. The ordinate unit is arbitrary, as is the height at which the line is cut off. The calculation of shape includes only first order perturbation terms. The figure corresponds to a molecular beam experiment in which the field is held constant while the oscillating frequency is varied through the resonance.

The idealized line shape shown in Fig. 4 has certain striking features. For values of W corresponding to $z=0$, the denominator of the shape function vanishes and the line strength becomes infinite. It is also to be noted that the outsides of the lines are very sharp, while, on the inside, the lines merge into one another. Observed molecular beam spectra may be expected to differ from this idealized shape mainly because, as discussed in footnote 20, a transition has natural breadth, the magnitude of which increases with increased oscillating field. The effect of the natural breadth will be to broaden the lines and to "wash out" the sharpness of the line shape. The height at which we have cut off the line strength is completely arbitrary; in an

actual case, this height will depend on the strength of the perturbation, on the value of J, as well as on other experimental factors. In addition, the effect of second-order perturbation terms—which were disregarded in our discussion of line shapes—will be to distort the shape of the line and to shift the positions of the minima—without, however, changing the distance between them—towards higher energies by an amount equal to $\frac{1}{2}x^2$.

The case $I=\frac{3}{2}$ differs from $I=1$ only in that there is a third transition of energy difference intermediate between the other two, and whose energy is—to first-order perturbation theory—independent of z. The energy differences, including terms of second-order perturbation, are:

$$W(\tfrac{3}{2},\tfrac{1}{2})=\mu_0 g_I H+\frac{e^2qQ}{4}(3z^2-1)+6\left(\frac{e^2qQ}{4}\right)^2\frac{z^2(1-z^2)}{\mu_0 g_I H(1-\epsilon)},$$

$$W(\tfrac{1}{2},-\tfrac{1}{2})=\mu_0 g_I H-\tfrac{3}{4}\left(\frac{e^2qQ}{4}\right)^2\frac{(1-z^2)(9z^2-1)}{\mu_0 g_I H(1-\epsilon)} \qquad \text{II (23)}$$

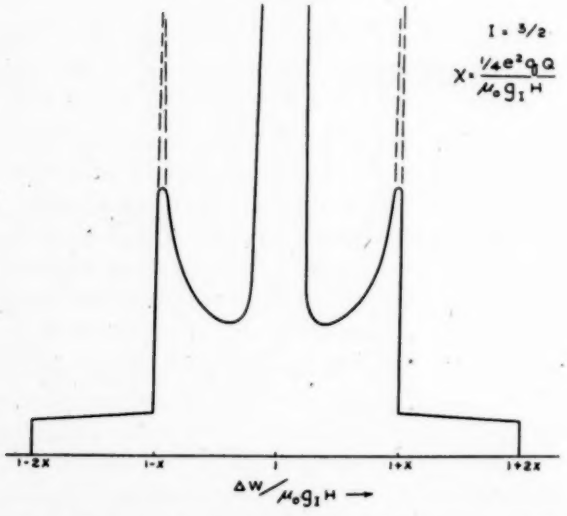

FIG. 5. Shape of the resonance line for $I=\frac{3}{2}$, corresponding to the transition $\Delta m_I=\pm 1$, $\Delta m_J=0$, in strong magnetic fields, as a function of the transition energy. The ordinate unit is arbitrary, as is the height at which the wings are cut off. The central minimum rises to a height approximately four times that of the wings. The shape function includes only first-order perturbation terms. The figure corresponds to a molecular beam experiment in which the field is held constant while the oscillating frequency is varied through the resonance.

$$W(-\tfrac{1}{2},-\tfrac{3}{2})=\mu_0 g_I H-\frac{e^2qQ}{4}(3z^2-1)+6\left(\frac{e^2qQ}{4}\right)^2\frac{z^2(1-z^2)}{\mu_0 g_I H(1-\epsilon)}.$$

Corresponding to these differences, the transition probabilities are:

$$P(\tfrac{3}{2},\tfrac{1}{2})=\tfrac{3}{4}\mu_0^2 g_I^2 H_x'^2,$$
$$P(\tfrac{1}{2},-\tfrac{1}{2})=\mu_0^2 g_I^2 H_x'^2, \qquad \text{II (24)}$$
$$P(-\tfrac{1}{2},-\tfrac{3}{2})=\tfrac{3}{4}\mu_0^2 g_I^2 H_x'^2.$$

The shape functions for the transitions $(\frac{3}{2},\frac{1}{2})$ and $(-\frac{1}{2},-\frac{3}{2})$ have the same form as those calculated for the $I=1$ transitions—provided only the terms of first-order perturbation are taken into account. In addition, in this approximation, the central minimum is independent of z and hence the breadth of the central minimum will be determined only by the natural width and can be made quite small compared to the breadth of the wings. The total probability of the central line (and, hence, the area underneath) is greater by a factor of 4/3 than for each of the other two lines.

In Fig. 5 the shape functions of the various transitions are superposed to show the shape of the spectrum for $I=\frac{3}{2}$. The width of the central minimum and the height at which the others cut off are arbitrary. As was the case for $I=1$, finite transition widths will cause a general broadening of the lines as well as a loss of sharpness of the contours.

In this case, second-order perturbation, besides broadening the lines, will cause the central minimum to shift towards higher energies by $\frac{3}{4}x^2$; the wings, on the other hand, suffer only a distortion of shape unaccompanied by a shifting of the position of the minimum.

The idealized spectral line shapes for the cases $I=2$ through 9/2 are shown in Fig. 6. As I increases, the structure of the wings becomes increasingly complicated. However, in an experiment of finite resolving power, it is not to be expected that this structure will be resolved. Instead, most structure will probably be run together, so that the patterns will be similar to those shown for $I=1$ or $I=\frac{3}{2}$.

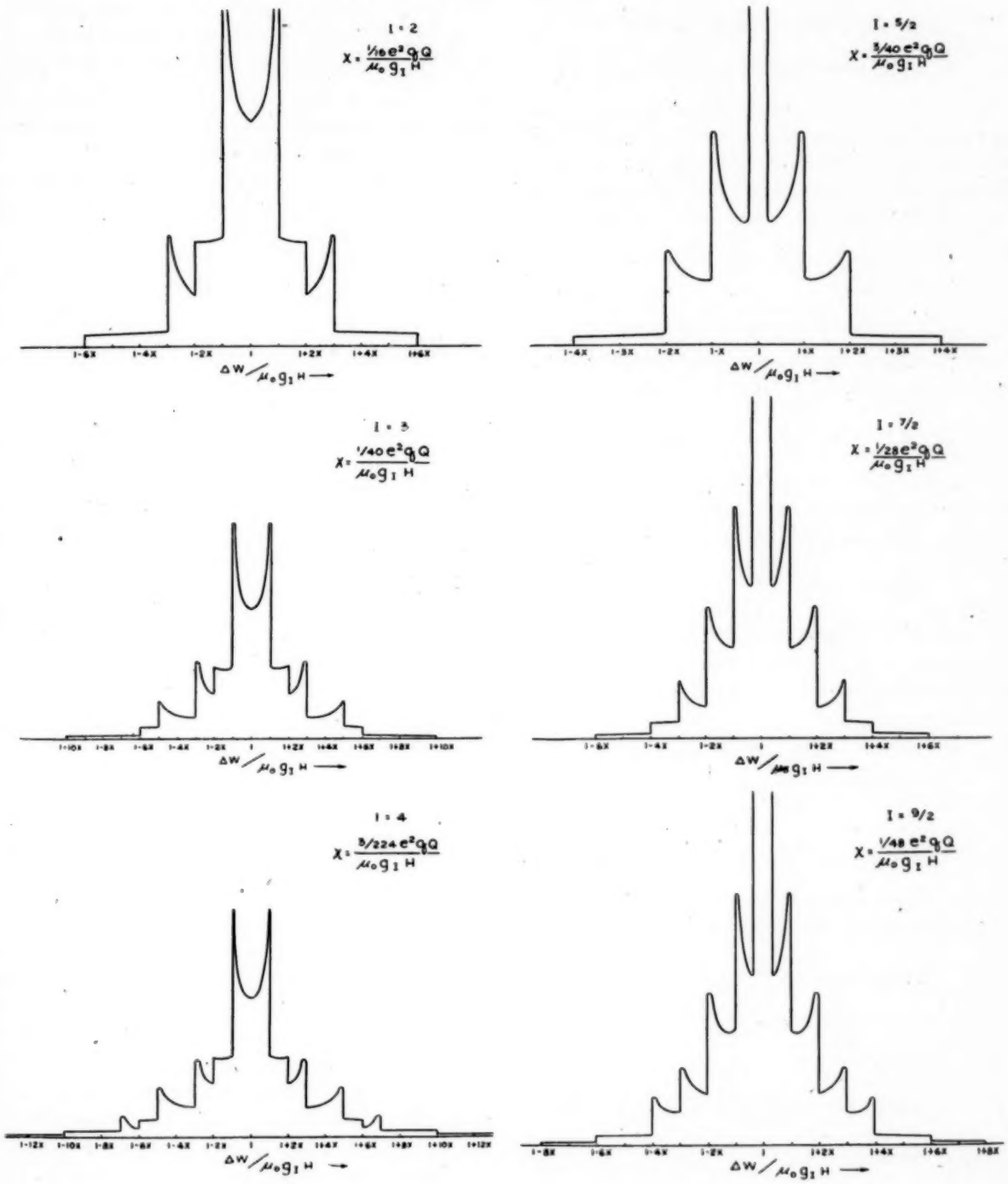
I = 2
$X = \frac{1/16\, e^2qQ}{\mu_0 g_1 H}$
$\Delta W / \mu_0 g_1 H \longrightarrow$
I = 5/2
$X = \frac{3/40\, e^2qQ}{\mu_0 g_1 H}$
$\Delta W / \mu_0 g_1 H \longrightarrow$
I = 3
$X = \frac{1/40\, e^2qQ}{\mu_0 g_1 H}$
$\Delta W / \mu_0 g_1 H \longrightarrow$
I = 7/2
$X = \frac{1/28\, e^2qQ}{\mu_0 g_1 H}$
$\Delta W / \mu_0 g_1 H \longrightarrow$
I = 4
$X = \frac{3/224\, e^2qQ}{\mu_0 g_1 H}$
$\Delta W / \mu_0 g_1 H \longrightarrow$
I = 9/2
$X = \frac{1/48\, e^2qQ}{\mu_0 g_1 H}$
$\Delta W / \mu_0 g_1 H \longrightarrow$

FIG. 6. Idealized shape of the resonance lines for $I=2$ through 9/2, corresponding to the transitions $\Delta m_I = \pm 1$, $\Delta m_J = 0$, in strong magnetic fields, as a function of the transition energy. The ordinate unit is completely arbitrary, as is the height at which the central lines and wings are cut off. The shape function includes only first-order perturbation terms. The figures correspond to molecular beam experiments in which the field is held constant while the perturbing oscillating frequency is varied through the resonance.

III. WEAK MAGNETIC FIELDS; ZEEMAN EFFECT

A. Zero Field Energy Levels

(1) *Semiclassical Derivation*

In zero field, the coupling between nuclear spin and molecular rotation is strong; we may adopt the Russell-Saunders approximation. In this scheme, we define a total angular momentum $\mathbf{F}=\mathbf{I}+\mathbf{J}$, where $\mathbf{F}$ may assume the values

$$F=J+I,\ J+I-1,\ \cdots,\ J-I,\quad F=J+i. \qquad \text{III (1)}$$

For large J, since $\mathbf{J}$ and $\mathbf{F}$ so nearly coincide, we may consider $\mathbf{I}$ to be precessing about $\mathbf{J}$, with angle between $\mathbf{I}$ and $\mathbf{J}$ (Fig. 2) given by

$$\cos\theta_{IJ}=i/|I|. \qquad \text{III (2)}$$

Adopting the same method, as in Section II (1), for the calculation of the quadrupole term in the energy expansion, one arrives again at Eq. II (4)

$$E(Q)=\tfrac{1}{4}e^2qQN(\tfrac{3}{2}\cos^2\theta_{IJ}-\tfrac{1}{2}). \qquad \text{III (3)}$$

As a result of the quantum mechanical nature of the vector $\mathbf{I}$, it is again necessary to introduce the normalization factor $2I(I+1)/3I^2-I(I+1)$. Hence

$$E(Q)=\frac{e^2qQ}{2}\frac{[3i^2-I(I+1)]}{2I(2I-1)}. \qquad \text{III (4)}$$

(2) *Quantum Mechanical Solution*

The quantum mechanical expression for the quadrupole energy is given by Casimir[14]

$$E(Q)=\frac{e^2qQ[\frac{3}{8}K(K+1)-\frac{1}{2}I(I+1)J(J+1)]}{I(2I-1)J(2J-1)}, \qquad \text{III (5)}$$

where

$$K=F(F+1)-I(I+1)-J(J+1). \qquad \text{III (6)}$$

Using the relationships $F=J+i$; $J\gg i, I$, we have

$$E(Q)=\frac{e^2qQ}{2}\frac{[3i^2-I(I+1)]}{2I(2I-1)}, \qquad \text{III (7)}$$

a result identical with that deduced by semiclassical methods.

Since $E(Q)$ only involves i as i^2, there are in zero field, for given J,

$I+1$ levels—for I an even multiple of $\frac{1}{2}$,
$I+\frac{1}{2}$ levels—for I an odd multiple of $\frac{1}{2}$,

independent of the value of J (provided J is large). For transitions with the selection rule $\Delta i=\pm1$,[21] the energy differences are

$$W(i,i-1)=\frac{e^2qQ}{4I(2I-1)}3(2i-1). \qquad \text{III (8)}$$

Thus, for $I=1$

$$W(\pm1,0)=\frac{3e^2qQ}{4} \qquad \text{III (9)}$$

and for $I=\frac{3}{2}$

$$W(\tfrac{3}{2},\tfrac{1}{2})=W(-\tfrac{1}{2},-\tfrac{3}{2})=\frac{e^2qQ}{2}, \qquad \text{III (10)}$$

etc.

From the above considerations it may be seen that a measurement of the zero-field molecular beam spectrum of a diatomic molecule in which one nucleus has electric quadrupole moment, can yield considerable information. The value of the quadrupole moment—or, at least, of qQ—can be determined directly, by a measurement of the frequency of the lowest (or any other) transition. In addition, the nuclear spin can be obtained by counting the number of transition lines appearing in the spectrum. A mere counting is not, however, unambiguous, since even nuclear spin and odd nuclear spin $\frac{1}{2}$ integer greater yield the same number of transitions. If in addition to counting transitions, one measures the ratios of the energy differences [see III (8)] involved, one then has an unambiguous determination of nuclear spin.

Molecular beam resonance transitions, however, cannot be observed in zero magnetic field. The necessity for a field arises from the fact, as explained in Section I, that in order to detect changes in magnetic moment, the molecules must pass through inhomogeneous fields before and after their passage through the homogeneous field. If the strength of the central, homogeneous field is very much different from that of the neighboring inhomogeneous fields, there will be

[21] In the section to follow, it will be shown that the selection rule for Russell-Saunders coupling is $\Delta F=0,\ \pm1$. For given J, in the zero-field approximation, this is equivalent to $\Delta i=0,\ \pm1$. However, $\Delta i=0$ does not lead to appreciable energy differences and does not interest us. Thus, we consider the selection rules for transitions in zero field $\Delta i=\pm1$.

induced "non-adiabatic transitions" by the sudden field changes. To avoid this, the magnitudes of all fields must be made approximately equal—; thus, the homogeneous field cannot easily be reduced to zero.

The introduction of a small magnetic field into the problem results in a perturbation and splitting of the energy levels. This problem (the Zeeman effect) is treated in the following sections.

B. Weak Field Energy Levels and Transitions

In weak fields, the Hamiltonian for our system contains, in addition to the field-independent electric quadrupole term already discussed, a perturbation of the form, $\mu_0 g_I H I_z + \mu_0 g_J H J_z$. In the F, m_F[22] representation, the quadrupole term is diagonal with elements given by Eq. III (4). The matrix elements for **I** and **J** in this representation[23] have the following form:

$$(F, m|\mathbf{I}|F+1, m+1)$$
$$=-\frac{1}{2}\left\{\frac{(F+1-I+J)(F+1+I-J)(I+J+2+F)(I+J-F)(F+m+1)(F+m+2)}{4(F+1)^2(2F+1)(2F+3)}\right\}^{\frac{1}{2}}(\mathbf{i}+i\mathbf{j}),$$

$$(F, m|\mathbf{I}|F+1, m)=\left\{\frac{(F+1-I+J)(F+1+I-J)(I+J+2+F)(I+J-F)[(F+1)^2-m^2]}{4(F+1)^2(2F+1)(2F+3)}\right\}^{\frac{1}{2}}\mathbf{k},$$

$$(F, m|\mathbf{I}|F+1, m-1)$$
$$=+\frac{1}{2}\left\{\frac{(F+1-I+J)(F+1+I-J)(I+J+2+F)(I+J-F)(F-m+1)(F-m+2)}{4(F+1)^2(2F+1)(2F+3)}\right\}^{\frac{1}{2}}(\mathbf{i}-i\mathbf{j}),$$

$$(F, m|\mathbf{I}|F, m+1)=\frac{I(I+1)-J(J+1)+F(F+1)}{2F(F+1)}\cdot\tfrac{1}{2}\{(F-m)(F+m+1)\}^{\frac{1}{2}}(\mathbf{i}+i\mathbf{j}),$$

$$(F, m|\mathbf{I}|F, m)=\frac{I(I+1)-J(J+1)+F(F+1)}{2F(F+1)}m\mathbf{k}, \qquad \text{III (11)}$$

$$(F, m|\mathbf{I}|F, m-1)=\frac{I(I+1)-J(J+1)+F(F+1)}{2F(F+1)}\cdot\tfrac{1}{2}\{(F+m)(F-m+1)\}^{\frac{1}{2}}(\mathbf{i}-i\mathbf{j}),$$

$$(F, m|\mathbf{I}|F-1, m+1)$$
$$=+\frac{1}{2}\left\{\frac{(F-I+J)(F+I-J)(I+J+1+F)(I+J+1-F)(F-m)(F-m-1)}{4F^2(2F-1)(2F+1)}\right\}^{\frac{1}{2}}(\mathbf{i}+i\mathbf{j}),$$

$$(F, m|\mathbf{I}|F-1, m)=\left\{\frac{(F-I+J)(F+I-J)(I+J+1+F)(I+J+1-F)(F^2-m^2)}{4F^2(2F-1)(2F+1)}\right\}^{\frac{1}{2}}\mathbf{k},$$

$$(F, m|\mathbf{I}|F-1, m-1)$$
$$=-\frac{1}{2}\left\{\frac{(F-I+J)(F+I-J)(I+J+1+F)(I+J+1-F)(F+m)(F+m-1)}{4F^2(2F-1)(2F+1)}\right\}^{\frac{1}{2}}(\mathbf{i}-i\mathbf{j}).$$

The matrix elements for **J** are obtained as follows: for $\Delta F=0$; interchange J and I in the matrix elements for **I**. For $\Delta F=\pm 1$; the matrix elements for $\mathbf{J}=-$the corresponding matrix elements for **I**.

The matrix elements, in the F, m representation, for the small oscillating perturbation $\mu_0 g_I H_x' I_x + \mu_0 g_J H_x' J_x$ are obtained from the above. The selection rules for this perturbation are seen to be $\Delta F=0, \pm 1, \Delta m=\pm 1$. However, we shall not consider the transitions $\Delta F=0$. For these only involve changes in m; and since the

[22] Henceforth m_F shall always be referred to as m.
[23] Reference 13, pp. 63, 64, 67.

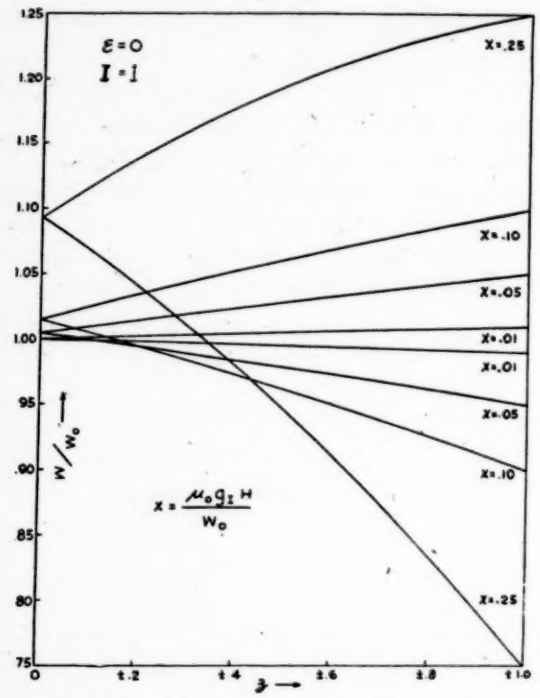

FIG. 7. Energy of transition for $I=1$ in weak magnetic fields as a function of $z=m/J$, for different values of the perturbation x. The two sets of curves correspond to the transitions $F=J+1\rightarrow F=J$ and $F=J-1\rightarrow F=J$. The four transitions of Eqs. III (14) reduce to two because of the condition $\epsilon=0$.

main (electric quadrupole) term in the energy is independent of m, these transitions will not involve the quadrupole moment. In addition, since $\Delta F=0$ transitions are concerned with differences between small perturbation terms, the energy differences will be very small compared to transitions for which $\Delta F=\pm 1$.

In a fashion completely similar to that described in the preceding sections, we may calculate energies, energy differences, transition probabilities, and line shapes for the system in weak fields.

(1) $I=1$

(a) Using perturbation theory including terms of second order, we find the energy values are:

$$E(J+1,m)=\frac{e^2qQ}{4}+\mu_0 g_J Hm+(\mu_0 g_I H-\mu_0 g_J H)z+\frac{\frac{1}{2}(\mu_0 g_I H-\mu_0 g_J H)^2}{\frac{3}{4}e^2qQ}(1-z^2),$$

$$E(J,m)=\frac{-e^2qQ}{2}+\mu_0 g_J Hm-\frac{(\mu_0 g_I H-\mu_0 g_J H)^2}{\frac{3}{4}e^2qQ}(1-z^2), \quad \text{III (12)}$$

$$E(J-1,m)=\frac{e^2qQ}{4}+\mu_0 g_J Hm-(\mu_0 g_I H-\mu_0 g_J H)z+\frac{\frac{1}{2}(\mu_0 g_I H-\mu_0 g_J H)^2}{\frac{3}{4}e^2qQ}(1-z^2).$$

The continuously varying parameter z is used for the quantity m/J. The variable expressing the strength of the perturbation we denote by

$$x=\mu_0 g_I H/\tfrac{3}{4}e^2qQ=\mu_0 g_I H/W_0. \quad \text{III (13)}$$

We have seen that[17] $g_I \gg g_J$. We write $g_J=\epsilon g_I$. Although we retain terms of order ϵ in all of the following expressions, most of the calculations shall be made for $\epsilon=0$.

(b) From the expressions for the energy values and the definitions given above, the energy differences for the selection rules $\Delta F=\pm 1$,

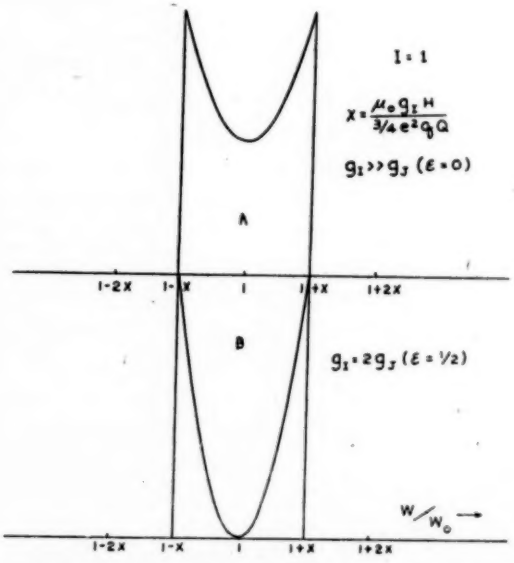

FIG. 8. Shape of the resonance lines for $I=1$, corresponding to the transitions $\Delta F=\pm 1$, $\Delta m=\pm 1$, in weak magnetic fields, as a function of the transition energy. The shape function is calculated to terms including only first-order perturbation. 8 (a) is the shape function for $\epsilon=0$, and 8 (b), for $\epsilon=\frac{1}{2}$. The figures correspond to molecular beam experiments in which the magnetic field is held constant while the oscillating field frequency is varied through the resonance.

$\Delta m=\pm 1$ follow:

$$\frac{W(J+1,m;J,m+1)}{W_0}=1+[(1-\epsilon)z-\epsilon]x+\tfrac{3}{2}(1-z^2)(1-\epsilon)^2x^2,$$

$$\frac{W(J+1,m;J,m-1)}{W_0}=1+[(1-\epsilon)z+\epsilon]x+\tfrac{3}{2}(1-z^2)(1-\epsilon)^2x^2,$$

$$\frac{W(J-1,m;J,m+1)}{W_0}=1-[(1-\epsilon)z+\epsilon]x+\tfrac{3}{2}(1-z^2)(1-\epsilon)^2x^2,$$

$$\frac{W(J-1,m;J,m-1)}{W_0}=1-[(1-\epsilon)z-\epsilon]x+\tfrac{3}{2}(1-z^2)(1-\epsilon)^2x^2. \qquad \text{III (14)}$$

In Fig. 7 are plotted the energy differences as a function of z, for $\epsilon=0$. The energy differences are shown for different values of the perturbation x—which is varied from 0.01 to 0.25.

(c) Corresponding to the energy differences, are the transition probabilities:

$$P(J+1,m;J,m+1)=(J+1,m|\mathfrak{IC}'|J,m+1)^2=\tfrac{1}{8}\mu_0^2g_I^2(1-\epsilon)^2H_z'^2(1-z)^2,$$

$$P(J+1,m;J,m-1)=\tfrac{1}{8}\mu_0^2g_I^2(1-\epsilon)^2H_z'^2(1+z)^2,$$

$$P(J-1,m;J,m+1)=\tfrac{1}{8}\mu_0^2g_I^2(1-\epsilon)^2H_z'^2(1+z)^2,$$

$$P(J-1,m;J,m-1)=\tfrac{1}{8}\mu_0^2g_I^2(1-\epsilon)^2H_z'^2(1-z)^2. \qquad \text{III (15)}$$

The shape of the spectrum is obtained by taking the products of P by $D=1/(dW/dz)$. If we consider first-order perturbation terms only, we see that W depends linearly upon z; the factor D is, then, independent of z. Hence, the shape function is simply proportional to P. In Figs. 8(a) and 8(b) are plotted the shape of the spectral lines for the transition $\Delta F=\pm 1$, $\Delta m=\pm 1$. Figure 8(a) represents the case $g_I \gg g_J$; 8(b) has $g_I=2g_J$. The shape of the spectrum for a value of ϵ between 0 and $\frac{1}{2}$ will be intermediate between these extremes.

In an experimental measurement of the spectrum, the observed shapes will differ considerably from the idealizations shown. Deviations will

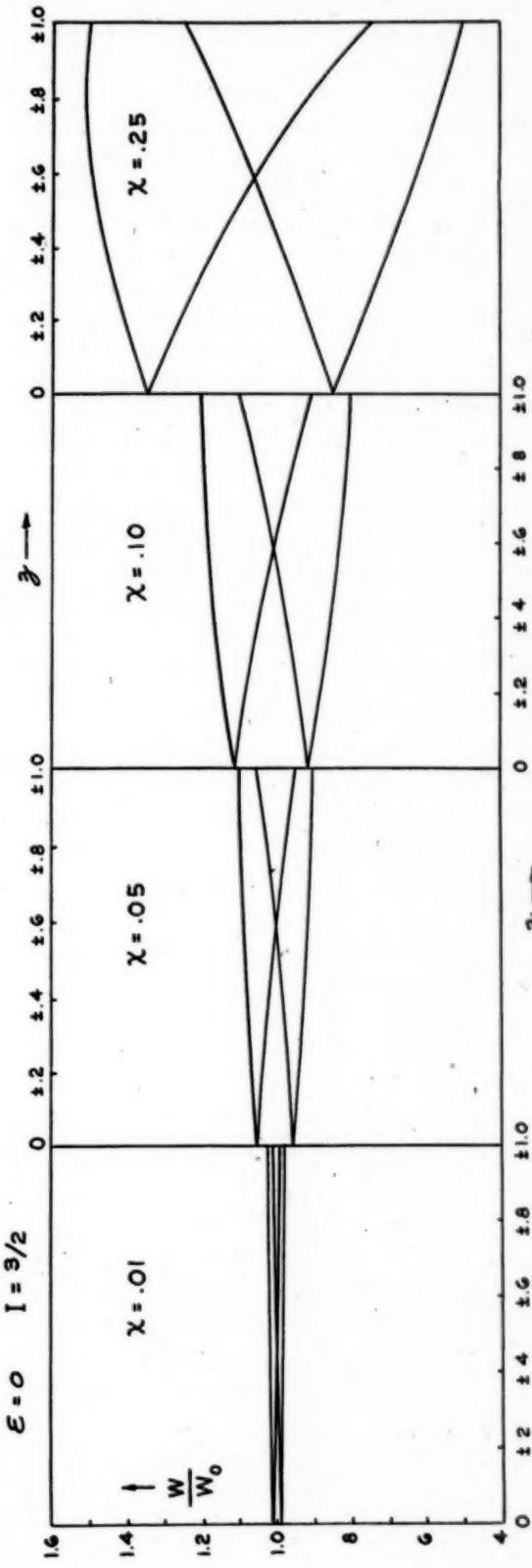

FIG. 9. Energy of transition for $I=\frac{3}{2}$ in weak magnetic fields as a function of $z=m/J$, for different values of the perturbation x. The eight transitions of Eq. III (19) reduce, for $\epsilon=0$, to the four shown.

result from failure to satisfy the assumptions upon which the calculations are based; the perturbation caused by the homogeneous magnetic field may, for instance, be so large that it is no longer sufficient to consider only the first-order term in determining line shapes. In this case, introduction of second and higher order perturbation terms will cause the line shape to be a more complicated function of z, and of energy; in general, lines will be somewhat broadened and distorted by this effect. Increase in the magnitude of the oscillating field will also introduce complications in the values for the transition probabilities P,[20] and similarly, result in a distortion and broadening of the spectral lines. In addition, the velocity distribution in the molecular beam will add to the broadening and diffusion of the shape of the line, since a spread in the times spent in the oscillating magnetic field introduces a corresponding spread in the transition probabilities for molecules in the beam. As a result of these factors, the observed spectral line will probably be rather flat and broad, with width about $2\mu_0 g_I H$.

(2) $I=\frac{3}{2}$

(a) Energy values. Calculation of the energy values for $I=\frac{3}{2}$ by perturbation theory is complicated by the fact that the unperturbed (zero field) energy levels are degenerate [see Eq. III (4)]. More important, there exist non-vanishing matrix elements between the degenerate states $F=J+\frac{1}{2}$ and $F=J-\frac{1}{2}$. Hence, it is necessary to apply degenerate perturbation theory to the problem.[24] To do this, we define two new states characterized by the wave functions Ψ_+ and Ψ_-; these are linear combinations of the original $\Psi_{J+\frac{1}{2}}$ and $\Psi_{J-\frac{1}{2}}$, chosen to satisfy the requirement that the matrix element $(\Psi_+|\mathcal{H}|\Psi_-)$[25] vanish. The combinations

$$\begin{aligned}\Psi_+&=\sin\theta\Psi_{J+\frac{1}{2}}+\cos\theta\Psi_{J-\frac{1}{2}},\\ \Psi_-&=-\cos\theta\Psi_{J+\frac{1}{2}}+\sin\theta\Psi_{J-\frac{1}{2}},\end{aligned}\qquad \text{III (16)}$$

where

$$\tan 2\theta=\frac{-2(\Psi_{J+\frac{1}{2}}|\mathcal{H}|\Psi_{J-\frac{1}{2}})}{(\Psi_{J+\frac{1}{2}}|\mathcal{H}|\Psi_{J+\frac{1}{2}})-(\Psi_{J-\frac{1}{2}}|\mathcal{H}|\Psi_{J-\frac{1}{2}})}\qquad \text{III (17)}$$

satisfy this requirement, as well as the normalization and orthoganality conditions. We may apply second-order perturbation theory to these new states, together with the original $J+\frac{3}{2}$ and $J-\frac{3}{2}$ states, and obtain the following energies:

$$\begin{aligned}E(J+\tfrac{3}{2},m)&=\frac{e^2qQ}{4}+\mu_0 g_J Hm+\tfrac{3}{2}\mu_0 g_I H(1-\epsilon)z+\tfrac{3}{4}\frac{\mu_0^2 g_I^2 H^2(1-\epsilon)^2(1-z^2)}{\frac{1}{2}e^2qQ},\\ E(+,m)&=\frac{-e^2qQ}{4}+\mu_0 g_J Hm+\mu_0 g_I H(1-\epsilon)(1-\tfrac{3}{4}z^2)^{\frac{1}{2}}-\tfrac{3}{4}\frac{\mu_0^2 g_I^2 H^2(1-\epsilon)^2(1-z^2)}{\frac{1}{2}e^2qQ},\\ E(-,m)&=\frac{-e^2qQ}{4}+\mu_0 g_J Hm-\mu_0 g_I H(1-\epsilon)(1-\tfrac{3}{4}z^2)^{\frac{1}{2}}-\tfrac{3}{4}\frac{\mu_0^2 g_I^2 H^2(1-\epsilon)^2(1-z^2)}{\frac{1}{2}e^2qQ},\\ E(J-\tfrac{3}{2},m)&=\frac{e^2qQ}{4}+\mu_0 g_I Hm-\tfrac{3}{2}\mu_0 g_I H(1-\epsilon)z+\tfrac{3}{4}\frac{\mu_0^2 g_I^2 H^2(1-\epsilon)^2(1-z^2)}{\frac{1}{2}e^2qQ}.\end{aligned}\qquad \text{III (18)}$$

(b) Energy differences: Adopting the selection rule $\Delta F=\pm1$, $\Delta m=\pm1$, there are eight possible transitions (involving the quadrupole term), with energy differences:

$$\begin{aligned}\frac{W(J+\frac{3}{2},m;+,m+1)}{W_0}&=1+[(1-\epsilon)\{\tfrac{3}{2}z-(1-\tfrac{3}{4}z^2)^{\frac{1}{2}}\}-\epsilon]x+\tfrac{3}{2}(1-\epsilon)^2(1-z^2)x^2,\\ \frac{W(J+\frac{3}{2},m;+,m-1)}{W_0}&=1+[(1-\epsilon)\{\tfrac{3}{2}z-(1-\tfrac{3}{4}z^2)^{\frac{1}{2}}\}+\epsilon]x+\tfrac{3}{2}(1-\epsilon)^2(1-z^2)x^2,\end{aligned}$$

[24] Reference 13, pp. 30–24.
[25] $\mathcal{H}=\mu_0 g_I HI_z+\mu_0 g_J HJ_z$.

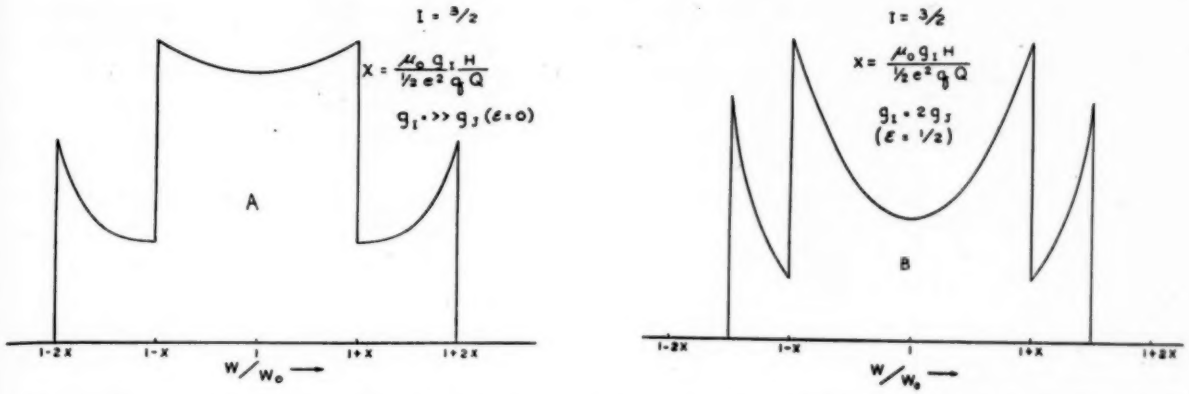

FIG. 10. Shape of the resonance lines for $I=\frac{3}{2}$ corresponding to transitions $\Delta F=\pm1$, $\Delta m=\pm1$, in weak magnetic fields, as a function of the transition energy. The shape functions include only first-order perturbation terms. 10 (a) is for $\epsilon=0$, while 10 (b) is for $\epsilon=\frac{1}{2}$.

$$\frac{W(J+\frac{3}{2},m;-,m+1)}{W_0}=1+[(1-\epsilon)\{\tfrac{3}{2}z+(1-\tfrac{3}{4}z^2)^{\frac{1}{2}}\}-\epsilon]x+\tfrac{3}{2}(1-\epsilon)^2(1-z^2)x^2,$$

$$\frac{W(J+\frac{3}{2},m;-,m-1)}{W_0}=1+[(1-\epsilon)\{\tfrac{3}{2}z+(1-\tfrac{3}{4}z^2)^{\frac{1}{2}}\}+\epsilon]x+\tfrac{3}{2}(1-\epsilon)^2(1-z^2)x^2,$$

$$\frac{W(J-\frac{3}{2},m;+,m+1)}{W_0}=1-[(1-\epsilon)\{\tfrac{3}{2}z+(1-\tfrac{3}{4}z^2)^{\frac{1}{2}}\}+\epsilon]x+\tfrac{3}{2}(1-\epsilon)^2(1-z^2)x^2, \qquad \text{III (19)}$$

$$\frac{W(J-\frac{3}{2},m;+,m-1)}{W_0}=1-[(1-\epsilon)\{\tfrac{3}{2}z+(1-\tfrac{3}{4}z^2)^{\frac{1}{2}}\}-\epsilon]x+\tfrac{3}{2}(1-\epsilon)^2(1-z^2)x^2,$$

$$\frac{W(J-\frac{3}{2},m;-,m+1)}{W_0}=1-[(1-\epsilon)\{\tfrac{3}{2}z-(1-\tfrac{3}{4}z^2)^{\frac{1}{2}}\}+\epsilon]x+\tfrac{3}{2}(1-\epsilon)^2(1-z^2)x^2,$$

$$\frac{W(J-\frac{3}{2},m;-,m-1)}{W_0}=1-[(1-\epsilon)\{\tfrac{3}{2}z-(1-\tfrac{3}{4}z^2)^{\frac{1}{2}}\}-\epsilon]x+\tfrac{3}{2}(1-\epsilon)^2(1-z^2)x^2,$$

where

$$W_0=\tfrac{1}{2}e^2qQ,\quad x=\frac{\mu_0 g_I H}{\tfrac{1}{2}e^2qQ},\quad \epsilon=g_J/g_I,\quad z=m/J. \qquad \text{III (20)}$$

These energy differences are plotted in Fig. 9 as a function of z, for $\epsilon=0$, and for different values of the perturbation parameter x.

(c) The transition probabilities corresponding to the above energy differences are:

$$P(J+\tfrac{3}{2},m;+,m\pm1)=\tfrac{3}{32}\mu_0^2g_I^2H_x'^2(1-\epsilon)^2(1\mp z)^2\left[1+\frac{z}{2(1-\frac{3}{4}z^2)^{\frac{1}{2}}}\right],$$

$$P(J+\tfrac{3}{2},m;-,m\pm1)=\tfrac{3}{32}\mu_0^2g_I^2H_x'^2(1-\epsilon)^2(1\mp z)^2\left[1-\frac{z}{2(1-\frac{3}{4}z^2)^{\frac{1}{2}}}\right],$$

$$P(J-\tfrac{3}{2},m;+,m\pm1)=\tfrac{3}{32}\mu_0^2g_I^2H_x'^2(1-\epsilon)^2(1\pm z)^2\left[1-\frac{z}{2(1-\frac{3}{4}z^2)^{\frac{1}{2}}}\right], \qquad \text{III (21)}$$

$$P(J-\tfrac{3}{2},m;-,m\pm1)=\tfrac{3}{32}\mu_0^2g_I^2H_x'^2(1-\epsilon)^2(1\pm z)^2\left[1+\frac{z}{2(1-\frac{3}{4}z^2)^{\frac{1}{2}}}\right].$$

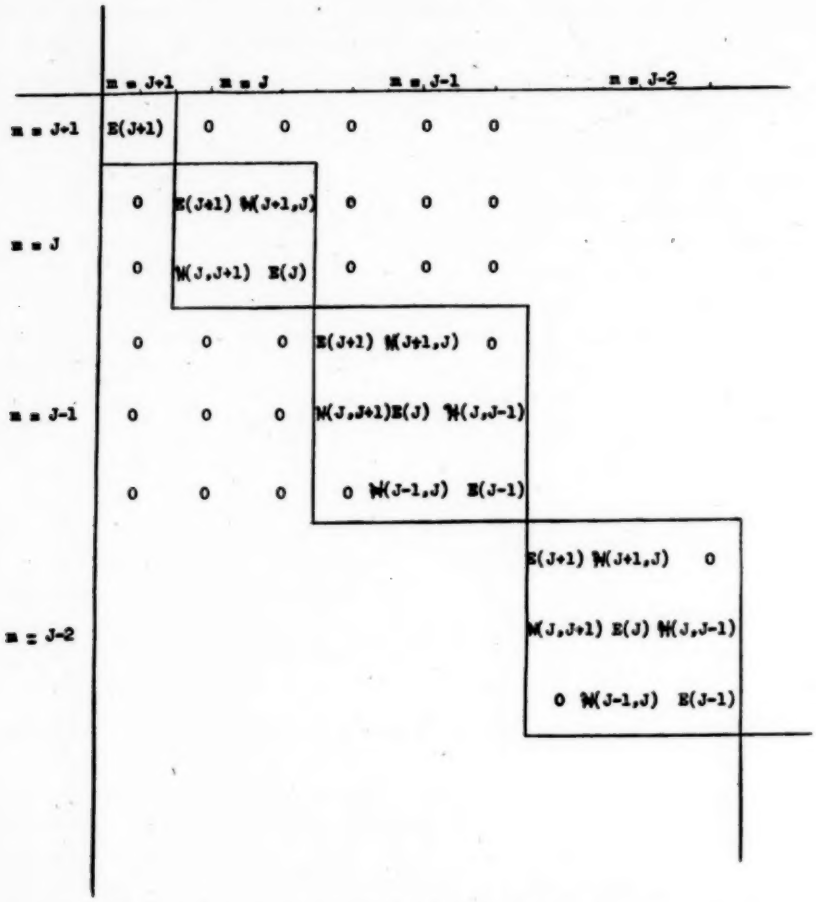

FIG. 11. Complete energy matrix for $I=1$ in the F, m representation.

The product $D\times P$ (considering only first-order perturbation terms) turns out to be particularly simple in this case. In fact, the shape function may be obtained from the transition probability by dropping the last factor. Thus, $D\times P(J+\frac{3}{2}, m; +, m+1)=k(1-z)^2$, etc.

In Figs. 10(a) and 10(b) are plotted the line shapes for $\epsilon=0$ and $\epsilon=\frac{1}{2}$, respectively. Again, we have assumed monoenergetic molecules and small perturbation. The same factors as have been discussed for the case $I=1$ will again come into play in this case to distort the line shape.

The shapes of the spectra, for the cases $I=2$ through $I=9/2$, have been investigated. Corresponding to each line in the zero-field spectrum, there is a group of transitions. For integral values of I, the shapes of the spectral lines are identical (except for second-order effects) with those shown in Fig. 8. Half-integral values of I involve two types of spectral lines. For transitions not involving the degenerate states ($F\neq J\pm\frac{1}{2}$), the shape of the spectrum will again be as shown in Fig. 8. For transitions involving the degenerate states, the shape will—in general—be considerably more complicated (even than Fig. 10), although the general nature of the spectral group is like that shown in Fig. 10. However, in an experimental observation of the spectrum the more complicated structure will probably remain unresolved. Hence, we shall omit a more detailed discussion of these transitions.

IV. INTERMEDIATE FIELDS; $I=1$, EXACT SOLUTION

A. Energy Values

In the representation of our system for which F and m are the appropriate quantum numbers, the quadrupole term in the Hamiltonian is diagonal. The only off-diagonal terms in the

energy matrix arise, for constant m, from the matrix elements of I_z and J_z in this representation. The complete energy matrix takes the form shown in Fig. 11 where the diagonal terms are represented by E and the off-diagonal terms by $\mathcal{H}$.

Thus, the matrix divides up into a series of three-row, three-column submatrices (except the ends). Since there are no connecting elements between different submatrices, each one of these may be diagonalized separately. Hence, the secular equation for our problem takes the general form:

$$\begin{vmatrix} \beta+b-E & c & 0 \\ c & \alpha-E & c \\ 0 & c & \beta-b-E \end{vmatrix}=0, \quad \text{IV (1)}$$

where

$$\beta=\frac{e^2qQ}{4}+\mu_0 g_J H m,$$

$$\alpha=\frac{-e^2qQ}{2}+\mu_0 g_J H m, \quad \text{IV (2)}$$

$$b=\mu_0 g_I H(1-\epsilon)z,$$

$$c=\mu_0 g_I H(1-\epsilon)\{\tfrac{1}{2}(1-z^2)\}^{\frac{1}{2}}.$$

This determinant reduces to a cubic equation having, in general, three different, real roots. These may be found by a straightforward algebraic process. The general results are rather complicated, and will be omitted here.

In special cases, the solution takes on a rather simplified form.

(1) $m \approx J$

For this condition, $c=0$; upon expansion of the general expressions for the energies, we obtain for the roots:

$$E_I=\alpha,$$

$$E_{II}=\beta-b, \quad \text{IV (3)}$$

$$E_{III}=\beta+b.$$

Since, for $c=0$, the energy matrix is diagonal for all values of the field [Eq. IV (1)], we are enabled to identify the roots with the F, m quantum numbers. This simple comparison of roots gives

$$E_I=E(J, m),$$

$$E_{II}=E(J-1, m), \quad \text{IV (4)}$$

$$E_{III}=E(J+1, m).$$

(2) *Weak Fields*

For small field perturbation, $[b,\ c \ll (\beta-\alpha)]$, the solutions reduce to:

$$E(J+1, m)=E_{III}=\frac{e^2qQ}{4}+\mu_0 g_J H m+\mu_0 g_I H(1-\epsilon)z+\tfrac{1}{2}\frac{\mu_0^2 g_I^2 H^2(1-\epsilon)^2}{\frac{3}{4}e^2qQ}(1-z^2)$$

$$+\tfrac{1}{8}(1/z-6z+5z^3)\frac{\mu_0^3 g_I^3 H^3(1-\epsilon)^3}{(\frac{3}{4}e^2qQ)^2},$$

$$E(J, m)=E_I=\frac{-e^2qQ}{2}+\mu_0 g_J H m-\frac{\mu_0^2 g_I^2 H^2(1-\epsilon)^2}{\frac{3}{4}e^2qQ}(1-z^2), \quad \text{IV (5)}$$

$$E(J-1, m)=E_{II}=\frac{e^2qQ}{4}+\mu_0 g_J H m-\mu_0 g_I H(1-\epsilon)z+\tfrac{1}{2}\frac{\mu_0^2 g_I^2 H^2(1-\epsilon)^2}{\frac{3}{4}e^2qQ}(1-z^2)$$

$$-\tfrac{1}{8}(1/z-6z+5z^3)\frac{\mu_0^3 g_I^3 H^3(1-\epsilon)^3}{(\frac{3}{4}e^2qQ)^2}.$$

These results are seen to agree with the energies obtained from second-order perturbation theory, in Section III.

It is interesting to note that for $m=0$ $(z=0)$, the third-order term in the weak field expansion diverges. Furthermore, the third-order term in the perturbation theory expression for the energy is also found to exibit the same property. The

reason for this behavior becomes clear when we consider that we are dealing with a degenerate system. Even though there are no matrix elements connecting states of equal unperturbed energy, it is not permissible to apply perturbation theory, *unless the degeneracy is removed by the first or second-order perturbation.*[26] That this condition does not hold for $m=0$ may be observed, if we consider the energy matrix for $b=0$ [IV (1)]. However, for the case $b=0$, it is easy to solve the secular equation exactly.

(3) $m=0$

Solution of the equation gives

$$E(J+1,0)=\frac{-e^2qQ}{8}+\mu_0 g_J Hm-\tfrac{1}{2}\{(\tfrac{3}{4}e^2qQ)^2+4\mu_0^2 g_I^2 H^2(1-\epsilon)^2(1-z^2)\}^{\frac{1}{2}},$$

$$E(J,0)=\frac{e^2qQ}{4}+\mu_0 g_J Hm, \qquad \text{IV (6)}$$

$$E(J-1,0)=\frac{-e^2qQ}{8}+\mu_0 g_J Hm+\tfrac{1}{2}\{(\tfrac{3}{4}e^2qQ)^2+4\mu_0^2 g_I^2 H^2(1-\epsilon)^2(1-z^2)\}^{\frac{1}{2}}.$$

(4) *Strong Fields*

For this approximation, we may consider the quadrupole interaction small compared to the magnetic interaction. Thus, $b, c \gg (\beta-\alpha)$. Expanding the exact solution, we arrive at the following energy values:

$$E(J+1,m)=-\mu_0 g_I H+\mu_0 g_J H(m+1)-\tfrac{1}{8}e^2qQ(1-3z^2)-\frac{(\frac{3}{8}e^2qQ)^2}{\mu_0 g_I H(1-\epsilon)}\cdot(1-z^2)(1+3z^2)$$
$$-4z^4(1-z^2)\frac{(\frac{3}{8}e^2qQ)^3}{\mu_0^2 g_I^2 H^2(1-\epsilon)^2},$$

$$E(J,m)=\mu_0 g_J Hm+\tfrac{1}{4}e^2qQ(1-3z^2)+8z^4(1-z^2)\frac{(\frac{3}{8}e^2qQ)^3}{\mu_0^2 g_I^2 H^2(1-\epsilon)^2}, \qquad \text{IV (7)}$$

$$E(J-1,m)=\mu_0 g_I H+\mu_0 g_J H(m-1)-\tfrac{1}{8}e^2qQ(1-3z^2)+\frac{(\frac{3}{8}e^2qQ)^2}{\mu_0 g_I H(1-\epsilon)}(1-z^2)(1+3z^2)$$
$$-4z^4(1-z^2)\frac{(\frac{3}{8}e^2qQ)^3}{\mu_0^2 g_I^2 H^2(1-\epsilon)^2}.$$

The representation in which it is convenient to discuss the Paschen-Back effect has as quantum numbers m_I and m_J. To achieve the transition between representations, we recall that our matrix elements have been calculated for constant m. Thus

$$m=m_I+m_J=\text{constant}. \qquad \text{IV (8)}$$

Hence, if $m_I=1$, $m_J=m-1$; likewise for $m_I=0$, $m_J=m$; and for $m_I=-1$, $m_J=m+1$. These relationships provide the connection between representations, and we get

$$E(J+1,m)=E(-1,m_J),$$
$$E(J,m)=E(0,m_J), \qquad \text{IV (9)}$$
$$E(J-1,m)=E(1,m_J).$$

[26] Reference 13, first paragraph, p. 34.

With these identifications, we see that the energy values calculated above agree exactly with those obtained in Section II, by perturbation theory.

B. Eigenfunctions

The wave functions Ψ_i of our system in uniform magnetic field may be expressed in terms of the set of wave functions $\Phi_{F,m}$ for which the quadrupole term is diagonal.

$$\Psi_i=a_i\Phi_{J+1,m}+b_i\Phi_{J,m}+c_i\Phi_{J-1,m}. \qquad \text{IV (10)}$$

These obey the wave equation

$$\mathcal{H}\Psi_i=E_i\Psi_i, \quad i=1,2,3 \qquad \text{IV (11)}$$

and also form a normal, orthogonal set.

Using the values of the energy E_i, as calcu-

lated in the preceding parts of Section IV, together with the normalization condition, we may use the wave equation to derive the values of the coefficients.

C. Transitions

From the calculated wave functions and matrix elements in the F, m representation, we may compute the matrix elements corresponding to transitions in our system. To do this, we recall that the matrix elements of the oscillating perturbation (in the F, m representation) allow transitions with the selection rule $\Delta F = \pm 1$, $\Delta m = \pm 1$. If we assume small perturbation, the transition probability between states will be proportional to the square of the matrix element. These are found to be

$$P(i, m; j, m\pm 1) = (\Psi_{i,m} | \mathcal{H}' | \Psi_{j,m\pm 1})^2$$
$$= \tfrac{1}{8}\mu_0^2 g_I^2 H_x'^2 (1-\epsilon)^2 \{(a_i b_j + b_i c_j)(1 \mp z) + (c_i b_j + b_i a_j)(1 \pm z)\}^2, \quad \text{IV (12)}$$

where

$$i \neq j; \quad i, j = 1, 2, 3.$$

From these and from the expressions for W, the shape function $D \times P$ can be calculated in any specific case.

V. Discussion

As a result of the calculations contained in this paper, it appears possible that a molecular beam experiment can yield valuable information concerning nuclear electric quadrupole moments. We have shown in Section II that a determination of the (constant) energy difference between subsidiary minima, in a strong magnetic field, yields the quantity e^2qQ. The fact that such minima have been observed for the resonance of Li^7 in LiF (Fig. 1) leads to the expectation that the experimental conditions for their observation may be favorable.

In Fig. 1, the position of the subsidiary minima is difficult to determine. However, for a rough estimate, we shall consider these to be at 18.70 and 19.05, on the scale of the abscissa. This separation corresponds to a field difference[27] of 47 gauss—about 10 times the natural width of the line. Hence, with improved resolving power, it may be expected that the subsidiary minima will be well resolved.

For the temperature at which the LiF beam was formed (1100°K), the most probable value of J is about 16. This is sufficiently greater than $\frac{3}{2}$, the spin of Li^7, so that we may consider the approximation developed in this paper to apply. According to this approximation (see Fig. 5) the ratio of the field difference between minima to the field value at the central resonance is given by

$$\frac{\Delta H}{H} = 2x = \tfrac{1}{2}\frac{e^2qQ}{\mu_0 g_I H}. \quad \text{V (1)}$$

From this, the value of e^2qQ for Li^7 is calculated to be equal to 1×10^{-21} erg. Although the value of the quadrupole moment Q cannot be determined until q is calculated, the above figure may be compared with that found for deuterium in HD and D_2.[5] This was about 0.3×10^{-21} erg and corresponded, in the case of D, to a quadrupole moment of 2.7×10^{-27} cm^2.

The zero-field spectrum, if it could be observed, would give a direct and simple measurement of qQ. However, the experimentally necessary introduction of a small magnetic field leads to complications. For magnitudes of the field much less than the quadrupole interaction (Section III), the lines observed would not be very broad; a determination of their centers of gravity would be sufficient to yield the information we require. However, when the field is of the same order as the quadrupole interaction (about 50 gauss in LiF and Na_2, 100 gauss in K_2)[8] the spectrum becomes complicated with flat, broad, uninterpretable minima. It is hoped that there may soon be presented an opportunity to apply these calculations to the experimental determination of nuclear electric quadrupole moments.

The authors wish to acknowledge their indebtedness to Professor I. I. Rabi, who first suggested this problem, to Professor Edward Teller, for his continued and inspiring interest and discussions, and to the members of the Molecular Beam Laboratory for their help in the preparation and criticism of this manuscript.

[27] The experiment was performed by keeping the frequency of the perturbing oscillator constant and varying the homogeneous magnetic field through the resonance.

PHYSICAL REVIEW VOLUME 67, NUMBERS 1 AND 2 JANUARY 1 AND 15, 1945

Gamma-Rays from Beryllium Caused by Proton Bombardment

W. J. HUSHLEY*
Department of Physics, University of Wisconsin, Madison, Wisconsin
(Received October 23, 1944)

In bombarding thin beryllium targets with protons of energy 0.30 Mev to 3.0 Mev, gamma-ray resonances were observed at proton energies 0.975, 1.06, 1.13, 1.36, and 2.52 Mev and a neutron resonance at 2.52 Mev. For 1.04-Mev protons the value obtained for the gamma-ray energy was 7.5 Mev which indicates a radiative capture process. At the 2.52-Mev resonance the measured value of the energy of the gamma-rays was about 3.0 Mev. The most probable explanation of the observed resonance at 2.52 Mev appears to be that it is a resonance for the capture of a proton to form B^{10*} which later disintegrates into (B^9+n^1) and also into $(Li^{6*}+He^4)$ where Li^{6*} emits 3-Mev gamma-radiation in returning to the ground state.

INTRODUCTION

GAMMA-RAYS from beryllium caused by proton bombardment have been observed by several investigators. Crane, Delsasso, Fowler, and Lauritsen[1] observed gamma-rays from a thick beryllium target for proton energies 0.45 Mev to 0.80 Mev. They detected no resonances but found the energies of four gamma-ray lines to be 2.2, 3.7, 4.8, and 6.0 Mev. Hafstad and Tuve[2] found no resonances for proton energies 0.40 to 0.90 Mev. Herb, Kerst, and McKibben[3] extended the work to 1.6 Mev and obtained a broad resonance at approximately 1.0 Mev. Curran, Dee, and Petržilka[4] examined the excitation curve with proton energies of 0.20 Mev to 1.0 Mev for thin beryllium targets of various thicknesses. They reported resonance peaks at 0.35 Mev and at 0.67 Mev. Measurements of absorption of the gamma-radiation by the same investigators showed that for proton energies of 0.40 Mev to 0.80 Mev the gamma-radiation was caused chiefly by the radiative capture process.

In the present investigation. the excitation curve was studied for a thick beryllium target for proton energies 0.90 Mev to 1.5 Mev and for thin beryllium targets in the range 0.30 Mev to 3.0 Mev. Measurements of gamma-ray energies were made at each of two resonances.

EXPERIMENTAL

Thin beryllium targets were made by evaporating beryllium metal within an evacuated brass chamber. The beryllium was heated by placing it in a molybdenum or tantalum boat which was brought to white heat for a fraction of a minute by passing a current of forty to fifty amperes through the boat. Some difficulty in evaporating beryllium is encountered in this method if a V-shaped ribbon is used for a boat since the beryllium forms a low melting point alloy with molybdenum and tantalum so that the ribbon melts before the beryllium evaporates. The boats used were made by taking a ribbon of molybdenum or tantalum metal about 8 mm wide and 5 cm long and rolling it into a cylinder about 3 mm in diameter and 5 cm long. The ends were then pinched so that the cylinder forms a boat which encloses the beryllium completely except for a slot about a millimeter wide along the top. Although the beryllium alloyed with the tantalum or molybdenum, two or three evaporations could be carried out with the same boat before the reaction penetrated the boat so as to make holes in it. The beryllium was evaporated onto a sheet of molybdenum or tantalum target-backing from a boat of the same material.

The protons were accelerated by the Wisconsin concentric-electrode electrostatic generator[5] and the intensity of the gamma-rays was measured by

* Now at the National Research Council of Canada, Ottawa, Canada.

[1] H. R. Crane, L. A. Delsasso, W. A. Fowler, and C. C. Lauritsen, Phys. Rev. **47**, 782 (1935).

[2] L. R. Hafstad and M. A. Tuve, Phys. Rev. **48**, 306 (1935).

[3] R. G. Herb, D. W. Kerst, and J. L. McKibben, Phys. Rev. **51**, 691 (1937).

[4] S. C. Curran, P. I. Dee, and V. Petržilka, Proc. Roy. Soc. **A169**, 269 (1938).

[5] R. G. Herb, C. M. Turner, C. M. Hudson, and R. E. Warren, Phys. Rev. **58**, 579 (1940).

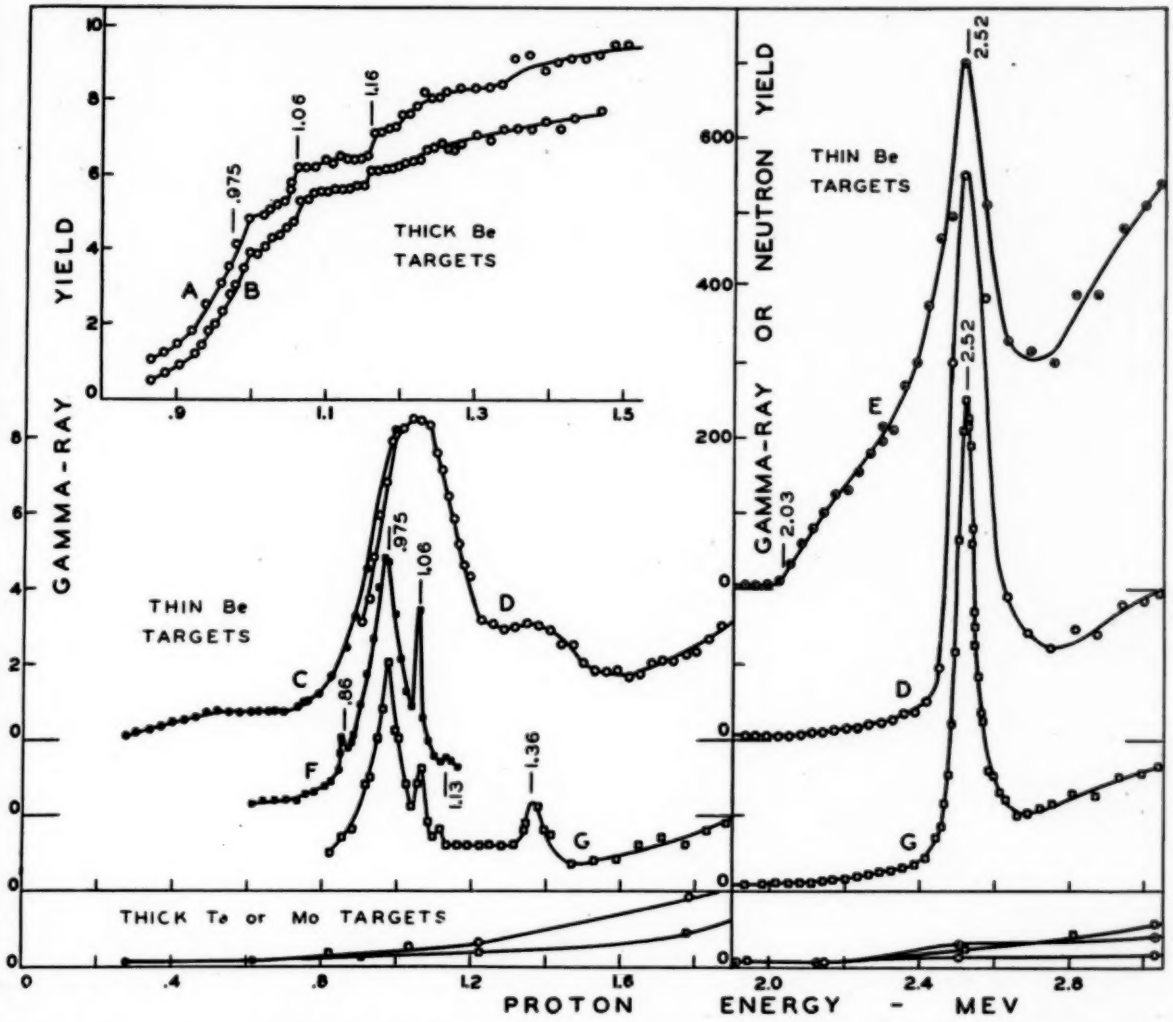

FIG. 1. Gamma-ray and neutron intensities from beryllium as a function of the energy of the bombarding protons. Curve *E* represents the neutron yield; the remaining curves represent gamma-ray yields. Above the proton energy 1.9 Mev the gamma-ray intensity scale is reduced by a factor of fifty. The background, taken on tantalum and molybdenum targets, is shown at the bottom of the figure by points corresponding to the upper curves.

G-M counters with a target chamber and counter arrangement similar to that used by Plain, Herb, Hudson, and Warren.[6]

PROTON ENERGY SCALE

The proton energy scale for the thin target curves was calibrated against the 2.03-Mev Be(p, n) threshold by running a neutron yield curve simultaneously with the gamma-ray yield. This value of the threshold had been reported by Haxby, Shoupp, Stephens, and Wells[7] and had also been measured in this laboratory[8] by comparing it to the 0.440-Mev Li(p, γ) resonance. For the thick target curves the generator voltage was calibrated against the 0.862-Mev F(p, γ) resonance which had previously been compared with the 0.440-Mev Li(p, γ) resonance.

An absolute measurement of the Li(p, n) threshold has been made recently by Hanson and Benedict[8] which, if correct, would revise the proton energy scale. Based on this new determination the Be(p, n) threshold would be at 2.06 Mev instead of the accepted 2.03 Mev. In this

[6] G. P. Plain, R. G. Herb, C. M. Hudson, and R. E. Warren, Phys. Rev. **57**, 187 (1940).
[7] R. O. Haxby, W. E. Shoupp, W. E. Stephens, and W. H. Wells, Phys. Rev. **58**, 1035 (1940).
[8] A. O. Hanson and D. L. Benedict, Phys. Rev. **65**, 33 (1944).

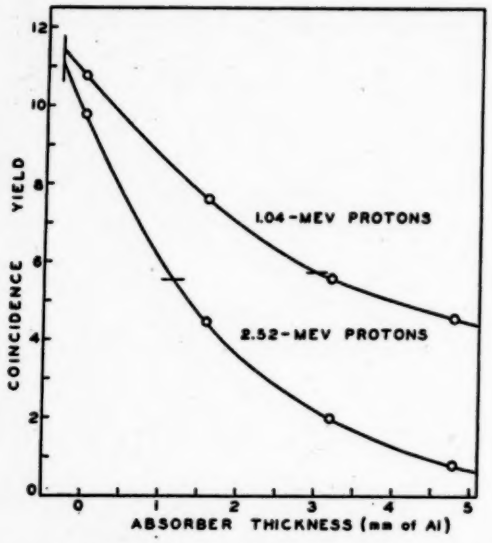

FIG. 2. Absorption curves for secondary electrons caused by gamma-rays from beryllium for 1.04-Mev and 2.52-Mev bombarding protons. The curves are extrapolated back, 0.30 mm, to correct for the absorption by the glass walls of the counters. The short horizontal lines indicate the thickness of aluminum which reduced the yield to one-half.

revised scale all values of proton energies would be raised by 1.5 percent above the previously accepted values which have been used in this report.

EXCITATION CURVES

The gamma-ray yield as a function of the energy of the bombarding protons is shown in Fig. 1 with the yield in arbitrary units. The thick target curves *A* and *B* show resonances at approximately 0.975, 1.06, and 1.16 Mev. Curves *C* and *D* show the gamma-ray yield from a thin beryllium target on molybdenum backing, the molecular beam being used for *C* and the atomic beam for *D*. Curve *E* shows the neutron yield obtained simultaneously with the gamma-ray yield *D*. Curves *F* and *G* show the gamma-ray yield from a thin beryllium target on tantalum backing, the molecular beam being used for *F*, the atomic for *G*. The background yield was taken on a molybdenum target for curves *C*, *D*, and *E* and on a tantalum target for *F* and *G*, and is shown by the corresponding points at the bottom of Fig. 1. Above the proton energy 1.9 Mev, the gamma-ray intensity scale is reduced by a factor of fifty. The thin target yields show resonance peaks at proton energies 0.975, 1.06, 1.36, 2.52, and possibly at 0.86 and 1.13 Mev.

The possibility that the hydrogen-filled G-M counters may have been counting neutrons was tested by placing four cm of paraffin between the target and the counter. The count was reduced by less than one percent showing that neutrons do not make any substantial contribution to the measured gamma-ray yield.

ENERGY OF GAMMA-RAYS

The energy of the gamma-rays was measured by obtaining the coincidence yield of two G-M counters as a function of the thickness of aluminum absorbers placed between the counters. Figure 2 shows the results of the absorption measurements of the secondary electrons caused by the gamma-rays. The abscissa scale gives the thickness of aluminum absorber. To correct for the absorption by the glass walls of the counters the curves are extrapolated back, 0.30 mm, to the short vertical line. This correction figure had been determined by Plain, Herb, Hudson, and Warren.[6] The thickness of aluminum absorber which reduces the coincidence yield to half its vlaue for no absorber is used as a measure of the gamma-ray energy and is shown by short horizontal lines in Fig. 2. The values are 3.3 mm Al for 1.04-Mev protons and 1.5 mm Al for 2.52-Mev protons.

The counters had been calibrated previously[6] by using the 6.2-Mev gamma-rays from fluorine and the 17.5-Mev gamma-rays from lithium giving half-value thicknesses of 2.8 and 7.3 mm Al, respectively. Figure 3 shows the resulting calibration curve. If we assume that the radiation is monochromatic, the energy of the gamma-rays

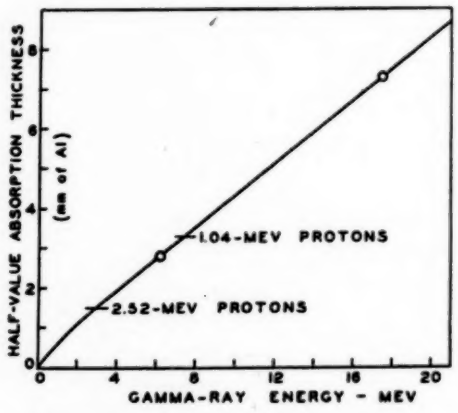

FIG. 3. Calibration curve showing half-value absorption thickness as a function of gamma-ray energy.

from beryllium is found to be 7.5 Mev for 1.04-Mev protons and about 3.0 Mev for 2.52-Mev protons.

Placing 3-mm lead between the target and the counter did not reduce the intensity of the 7.5-Mev radiation appreciably, showing it has no large soft component.

DISCUSSION

Several resonance maxima appear in the excitation curve of Fig. 1 although the group at 1 Mev may not be completely resolved. The maxima at 0.35 Mev and 0.67 Mev reported by Curran, Dee, and Petržilka[4] were not observed.

A summary of the results of the absorption measurements is given in Table I where the values in brackets are obtained if the new proton energy scale is used. The reaction energy given in the table assumes a radiative capture process, i.e.,

$$Be^9+H^1\rightarrow B^{10}+h\nu. \qquad (1)$$

This reaction has 6.56 Mev of available energy plus the resonance energy of the protons. For 1.04-Mev protons the total energy available is 6.56 plus 9/10 of 1.04 or 7.50 Mev. This agreement between the gamma-ray energy and the total energy available shows that the reaction is resonance capture with a single transition to the ground state.

The reaction at the 2.52-Mev resonance is more difficult to interpret. In a radiative capture reaction the available energy would be 6.56 plus 9/10 of 2.52 or 8.83 Mev, whereas the energy of the radiation is about 3.0 Mev. The intensity of the radiation was roughly fifty times greater than the intensity at the 0.975-Mev resonance for the thin target G and about one hundred times greater for the thin target D. For the latter target the neutron yield, which also shows a resonance at 2.52 Mev, was estimated roughly to be of the same magnitude as the gamma-ray yield. This suggests that the neutrons and the gamma-rays are produced in the same reaction.

Some other possible reactions are given below. In calculating the reaction energies the following atomic mass values given by Haxby, Shoupp, Stephens, and Wells[7] are used; $Be^9=9.01484$ m.u., $B^9=9.01600$ m.u., $(n^1-H^1)=0.000806$ m.u. Other mass values are taken from Barkas.[9]

A neutron producing reaction is

$$Be^9+H^1\rightarrow B^9+n^1+Q_2, \qquad (2)$$

where the reaction energy Q_2 is -1.83 Mev. However, B^9 is unstable and may return to Be^9 by emitting a positron or capturing a K electron or it may disintegrate into Be^8 plus H^1. In the first case

$$B^9\rightarrow Be^9+e^+E_+,$$

where the maximum positron energy E_+ is 0.06 Mev. For K-electron capture, reaction (2) above is followed by

$$B^9+e^-\rightarrow Be^9+Q_2',$$

with an energy evolution Q_2' of $+1.08$ Mev. In the third case

$$B^9\rightarrow Be^8+H^1+Q_2'',$$

where Q_2'' is $+0.10$ Mev. If in place of the latter the non-capture disintegration

$$Be^9+H^1\rightarrow Be^8+n^1+H^1+Q_2''$$

takes place, then Q_2'' is -1.73 Mev.

TABLE I. Gamma-ray energies.

Proton energy (Mev)	Half-value (mm of Al)	Gamma-ray energy (Mev)	Reaction energy available (Mev)
1.04 (1.05$_8$)	3.3	7.5	7.50 (7.51)
2.52 (2.56)	1.7	3.0	8.83 (8.86)

Theoretical considerations[10] show that a particle producing process is much more probable than a radiative capture process and since this resonance is above the Be(p, n) threshold it would be expected that the (p, n) reaction would be the most probable. The observed gamma-radiation would have to come from an excited residual nucleus in the Be(p, n) reaction but consideration of the energy evolution in the above three cases of reaction (2) shows that 3.0-Mev gamma-rays are energetically impossible for 2.52-Mev incident protons. It seems certain, then, that the 3.0-Mev gamma-rays and the neutrons are not produced in the same reaction.

[9] W. H. Barkas, Phys. Rev. **55**, 691 (1939).

[10] H. A. Bethe, Rev. Mod. Phys. 9, 69 (1937).

Two other processes have been observed by numerous investigators for low energy protons. They are

$$Be^9+H^1\rightarrow Be^8+H^2+Q_3 \quad (3)$$

and

$$Be^9+H^1\rightarrow Li^6+He^4+Q_4, \quad (4)$$

where $Q_3=+0.44$ Mev and $Q_4=+2.03$ Mev if Be^8 and Li^6 are left in the ground state.

Among other factors the probability of a reaction depends on the energy evolution and on the height of the potential barrier to the particle emitted. The probability is greatest for a high energy evolution and for a low potential barrier. The potential barrier is zero for neutrons and higher for alpha-particles than it is for deuterons. It would be expected that reactions (2), (3), and (4) given above are almost equally probable since in each case the energy evolution compensates for the height of the potential barrier. Skaggs[11] has observed that for 0.262-Mev protons the α-particles and the deuterons are emitted in almost equal numbers. It is necessary, then, to examine whether 3.0-Mev gamma-radiation is energetically possible from an excited state of one of the product nuclei of reaction (3) or (4).

In the reaction

$$Li^7+H^1\rightarrow Be^8+Q,$$

Delsasso, Fowler, and Lauritsen[12] observed 17-Mev and 14-Mev gamma-radiation but no radiation between 2 and 10 Mev. This was considered experimental evidence that Be^8 has an excitation level at about 3.0 Mev but the transition from this state to the ground state by gamma-radiation is forbidden. Rather, the Be^8, in the 3-Mev excited state, disintegrates into two alpha-particles with the excitation energy going into the kinetic energy of the alpha-particles. This interpretation has been confirmed experimentally and theoretically more recently by Wheeler[13] and several others who place the excitation level at 2.8 Mev. Furthermore, if the value of the gamma-ray energy measured here is correct the radiation cannot occur in reaction (3) because of energy considerations.

Assuming that the α-particle has no stable excited state, it appears probable that the observed 3.0-Mev gamma-radiation is caused by an excited state of Li^6 in the Be(p, α) reaction. This reaction has 2.03 Mev of available energy plus the energy of the incident protons so that it is energetically possible to have the Li^6 excited up to about 4 Mev. This could be confirmed by determining the energy of the α-particles emitted in the reaction. One would expect α-particles of about 6.2-mm range from the reaction in which Li^{6*} is formed as well as 17.3-mm alphas corresponding to the formation of unexcited Li^6. These values are calculated from the energy-momentum relations given by Livingston and Bethe.[14]

An alternative explanation of the gamma-rays is to assume that radiative capture with cascade emission is as probable as a neutron producing reaction. That is, B^{10}, excited to 8.83 Mev, would return to the ground state in, say, three steps. The known excitation levels of B^{10} are at 0.55, 2.15, 3.45, and 7.50 Mev so that the 3.0-Mev measured value of the radiation would represent the average effect of several different γ-ray lines.

The phenomenon at the 2.52-Mev resonance may then be interpreted as a resonance for the capture of a proton forming B^{10*} which later disintegrates in one of several ways, such as

$$\begin{aligned} B^{10*}&\rightarrow B^{10}+h\nu_1+h\nu_2+h\nu_3 \\ &\rightarrow Li^{6*}+He^4\rightarrow Li^6+He^4+h\nu \\ &\rightarrow B^9+n^1. \end{aligned}$$

It is expected that the last two are the most probable of the three mentioned.

It would have been desirable to repeat the excitation curve using thinner targets and to make more extensive absorption measurements, but the work was cut short before this could be done.

The author is greatly indebted to Dr. A. O. Hanson for advice and help in the experimental work and to the Wisconsin Alumni Research Foundation for financial assistance.

[11] L. S. Skaggs, Phys. Rev. **56**, 24 (1939).
[12] L. A. Delssaso, W. A. Fowler, and C. C. Lauritsen, Phys. Rev. **51**, 391 (1937).
[13] J. A. Wheeler, Phys. Rev. **59**, 16 (1941) and **59**, 27 (1941).
[14] M. S. Livingston and H. A. Bethe, Rev. Mod. Phys. **9**, 245 (1937).

PHYSICAL REVIEW VOLUME 67, NUMBERS 1 AND 2 JANUARY 1 AND 15, 1945

Electric Circuit Models of the Schrödinger Equation

GABRIEL KRON
General Electric Company, Schenectady, New York
(May 25, 1944)

Equivalent circuits are developed to represent the Schrödinger amplitude equation for one, two, and three independent variables in orthogonal curvilinear coordinate systems. The networks allow the assumption of any arbitrary potential energy and may be solved, within any desired degree of accuracy, either by an a.c. network analyzer, or by numerical and analytical circuit methods. It is shown that by varying the impressed frequency on a network of inductors and capacitors (or by keeping the frequency constant and varying the capacitors), it is possible to find by measurements the eigenvalues, eigenfunctions, and the statistical mean of various operators belonging to the system represented. The electrical model may, of course, be replaced by an analogous mechanical model containing moving masses and springs. At first the network for the one-dimensional wave equation for a single particle in Cartesian coordinates is developed in detail, then the general case. A companion paper contains results of a study made on an a.c. network analyzer of one-dimensional problems: a potential well, a double barrier, the harmonic oscillator, and the rigid rotator. The curves show good agreement, within the accuracy of the instruments, with the known eigenvalues, eigenfunctions, and "tunnel" effects.

THE ONE-DIMENSIONAL SCHRÖDINGER EQUATION

IN Cartesian coordinates, the equation is

$$-\frac{\hbar^2}{2m}\frac{\partial^2\psi}{\partial x^2}+(V-E)\psi=0.$$

Three types of equivalent circuits may be established.

1. The circuit contains positive and negative resistors and in each state the currents and voltages are constant in time. The state is changed by varying the resistances, corresponding to a change in eigenvalue (energy level).

2. Although negative resistances are available for use with a network analyzer, in practice it is more convenient to use a second type of circuit, in which the positive and negative resistors are replaced by inductors and capacitors and the d.c. currents and voltages are replaced by a.c. currents and voltages of *fixed* frequency. The use of the second type of interpretation is equivalent to multiplying the wave equation by $i=\sqrt{-1}$.

In the diagrams to follow, unless otherwise stated, the inductors (whose reactance at the fixed frequency is denoted by X_L) may also be viewed as positive resistances of value X_L and the capacitors (whose reactance is denoted by $-X_c$) as negative resistances of value $-X_c$.

3. The third type of circuit contains inductors and capacitors and in each state the currents and voltages are sinusoidal in time. The state is changed by varying the frequency of the impressed voltage.

The basic network concepts will be introduced in detail in connection with the first type of circuit (with additional comments on the second type of interpretation). The third type of model, although it offers attractive analogies, will be only cursorily treated.

REPRESENTATION OF ENERGY OPERATORS

If the wave equation is multiplied by Δx and the operator $p=-ih\partial/\partial x$ is introduced, the equa-

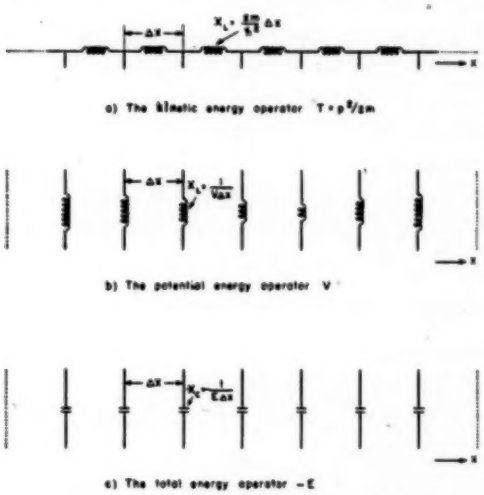

FIG. 1. Representation of energy operators by admittances.

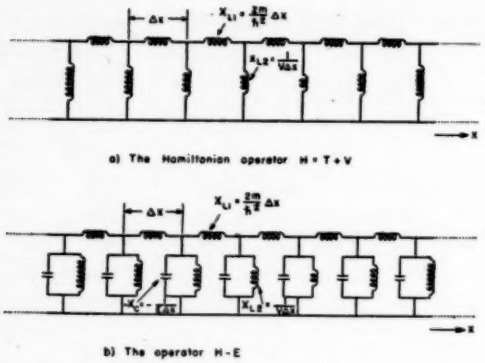

FIG. 2. Representation of the *sum* of operators by an interconnection.

tion becomes

$$H\Delta x\psi - E\Delta x\psi = 0,$$

where

$$H = \frac{p^2}{2m} + V = T + V.$$

The three energy operators will be represented in the following manner: 1. The kinetic energy operator $T = p^2/2m$ is represented (Fig. 1a) by a set of equal positive resistors (or inductive coils) in *series* extending from $-\infty$ to $+\infty$. The impedance of each coil is $(2m/\hbar^2)\Delta x$. 2. The potential energy operator V is represented (Fig. 1b) by a set of isolated positive resistors (inductive coils). The admittance of each coil is $V\Delta x$. These values vary from point to point. 3. The total energy operator $-E$ is represented (Fig. 1c) by a set of isolated equal negative resistors (capacitors). The admittance of each coil is the unknown quantity $E\Delta x$.

The sum of the two operators T and V forming the Hamiltonian operator H is represented by the interconnected network of Fig. 2a. That is, a *summation* of energy operators is represented electrically by an *interconnection* of the component networks.

Finally, the sum of the Hamiltonian H and the total energy $-E$ operators is the resultant network of Fig. 2b extending from $-\infty$ to $+\infty$.

OPERATION ON THE WAVE FUNCTION ψ

The wave function ψ will be assumed to be represented (Fig. 3) by the differences of potential[1] appearing between the junctions of the three types of coils and the ground connection (impedanceless wire). The function ψ varies along x, but is constant in time. An eigenfunction ψ' of H depends on the time as follows: $\psi' = \psi \exp[-i(E/\hbar)t.]$

The differences of potentials appearing between two junctions are $\Delta\psi = (\partial\psi/\partial x)\Delta x + \cdots$ where higher order terms in the Taylor series development are neglected.

The result of the operation $\alpha\psi$ or $\beta\Delta\psi$ (where α and β are operators) is represented by *currents* flowing in the respective component networks, as shown in Fig. 3. In particular: 1. The currents flowing in the capacitors are $E\Delta x\psi$. 2. The currents flowing in the vertical inductors are $V\Delta x\psi$. 3. The currents flowing in the horizontal inductors are $\beta\Delta\psi = (\hbar^2/2m)(\partial\psi/\partial x)$. 4. The currents flowing out of the horizontal inductors at their junctions are $\Delta(\beta\Delta\psi) = (\hbar^2/2m)(\partial^2\psi/\partial x^2)\Delta x$, representing $(-T\Delta x\psi)$.

Since $E\Delta x\psi$ represents the currents flowing in the capacitors and $H\Delta x\psi = (T+V)\Delta x\psi$ those in the inductors, the equation $H\Delta x\psi = E\Delta x\psi$ simply states Kirchhoff's second law, that at each of the junctions of four coils the currents flowing into the positive resistors (inductors) are equal to the currents coming from the negative resistors (capacitors).

Both the voltages and currents appear as standing waves. When the space distribution of ψ is such that it attenuates, the network may be terminated at any point by an equivalent impedance. When ψ does not attenuate the circuit may be terminated by a short circuit at any point of zero voltage, or by an open circuit at any point of zero current. These points are easily determined on the a.c. network analyzer by trial.

It should be noted that the equivalent circuit introduces an indeterminacy between quantities measured in the vertical coils and those in the horizontal coils. If, for instance, the vertical voltage ψ is known at a certain value of x, say x_0, then the horizontal current $(\hbar^2/2m)(\partial\psi/\partial x)$ is not

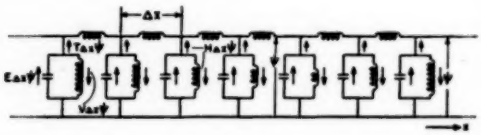

FIG. 3. Representation of ψ by voltages and $\alpha\psi$ by currents.

[1] It is possible to establish in one dimension a dual network in which ψ is represented by a current instead of a voltage. However, in two and three dimensions the dual networks require ideal transformers.

known at that particular x_0, only at some indeterminate value between x_0 and $x_0+\Delta x/2$ or $x_0-\Delta x/2$.

EIGENVALUES AND EIGENFUNCTIONS

Let it be assumed as an example that the V function is a potential well (Fig. 4a). Then in the network the corresponding positive resistances assume either a constant or a zero value as shown in Fig. 4b. In practice it is sufficient to extend the network to, say, twice the width of the potential well on either side.

Let now a d.c. (or a.c.) generator be inserted anywhere in the network parallel with one of the negative resistances (inductors), as shown. If the values of all the negative resistances $-E\Delta x$ (capacitors) are simultaneously varied by the same amount, it will be found that the current (reactive current) in the generator varies and at some value of $E\Delta x$ becomes zero.

It should be noted that while a current (reactive current) flows in the generator the circuit does not satisfy the differential equation, since at *one* point in the network (where the generator is connected) the currents do not add up to zero (as required by the equation) but to the generator current. That is, while a current flows in the generator, the voltages ψ do not represent solutions of the differential equation. Hence, only those network conditions are of interest in which the generator current is zero.

Now a value E of the negative resistances, at which the generator current becomes zero, represents a state at which the circuit is self-supporting and has a continuous existence of its own without the presence of the generator, as the negative resistances just supply the energy consumed by the positive resistances. (If the circuit contains inductors and capacitors, the circuit is a resonant circuit and it oscillates at its basic frequency.) E is then an eigenvalue E_n, while the voltage distribution across the capacitors (Fig. 4c) gives the corresponding eigenfunction ψ_n.

When the generator current is positive the circuit draws energy from the source, and when the current is negative the circuit pumps back energy into the source. At zero generator current the circuit neither gives nor takes energy, and theoretically the generator may be removed. All values of E at which the current crosses the axes and becomes zero are eigenvalues of the equation and the corresponding voltage distribution curves are eigenfunctions. When the energy level E overflows the well, the discrete spectrum of eigenvalues changes into a continuous spectrum and the generator current is zero at all greater values of E.

When the energy E changes sign, the negative resistances become positive resistances and at no value of $-E$ may the circuit be self-supporting (as it contains only positive resistances). That is, the equation has no negative eigenvalues.

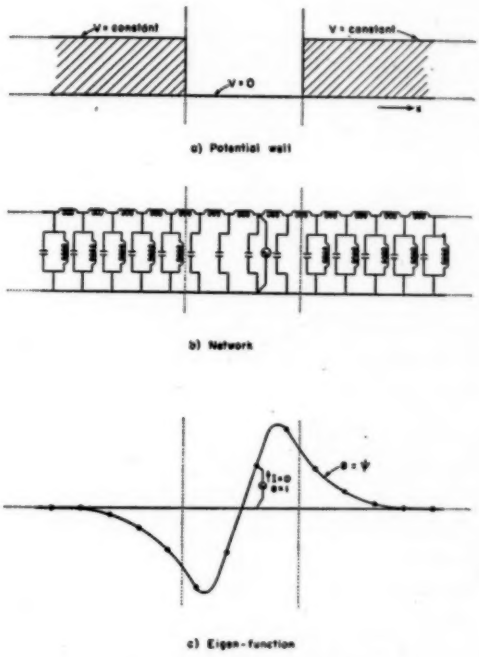

FIG. 4. Measurement of ψ.

THE STATISTICAL MEAN OF OPERATORS

To bring the measurements at the different energy levels to the same base, it is necessary to normalize the measured ψ values so that the new values of ψ satisfy the equation

$$\int_{-\infty}^{+\infty} \psi^*\psi dx = 1.$$

The measured ψ functions are normalized by plotting the square of ψ. If the area under the curve is $1/N^2$, all values of ψ are multiplied by N. Then $N\psi$ is the normalized ψ. (Actually N may contain an arbitrary phase $\epsilon^{i\gamma}$.)

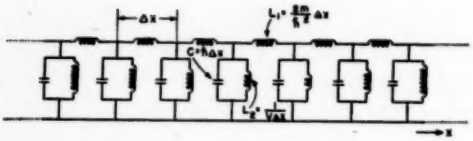

FIG. 5. The variable-frequency model.

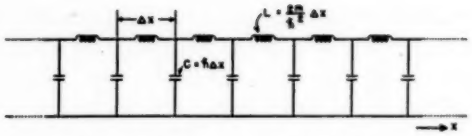

FIG. 6. Model of a free particle.

The statistical mean of an operator α for a state ψ is defined as

$$\mathrm{av}_\psi \alpha = \int_{-\infty}^{+\infty} \psi^* \alpha \psi dx.$$

Since $(\alpha \Delta x)\psi$ is a current (reactive current) flowing through an admittance, $\psi^*(\alpha \Delta x)\psi$ is the power (reactive power) in a single admittance. Hence the total power in a complete set of similar admittances, namely,

$$\text{Power} = \sum_{-\infty}^{+\infty} e^* i = \sum e^* y e = \sum \psi^* \alpha \psi \Delta x,$$

represents the statistical mean of the corresponding energy operator. That is: 1. The total power in all the vertical negative resistors is the average value of E. (That is, E itself, since ψ is an eigenfunction of H). 2. The total power in all the *vertical* resistors is the average value of the potential energy V. 3. The total power in all the *horizontal* resistors is the same as the total power in the vertical units, representing the average of the kinetic energy $T = p^2/2m$.

That is, the total power in all positive resistors is the same as the total power in all the negative resistors, or

$$\mathrm{av}_\psi H = \mathrm{av}_\psi \frac{p^2}{2m} + \mathrm{av}_\psi V = \mathrm{av}_\psi E = E.$$

THE THIRD MODEL

Let the wave equation be divided by $i\omega_c$, where $\omega_c = \sqrt{\omega} = (E/\hbar)^{\frac{1}{2}}$, and multiplied by Δx:

$$-\frac{1}{i\omega_c}\frac{\hbar^2}{2m}\frac{1}{\Delta x}\frac{\partial^2 \psi}{\partial x^2}\Delta x^2 + \left(\frac{V \Delta x}{i\omega_c} + \hbar i \omega_c \Delta x\right)\psi = 0,$$

or

$$\frac{\Delta x}{i\omega_c} H\psi + i\omega_c \hbar \Delta x \psi = 0, \quad \frac{\Delta x}{i\omega_c}(H - E)\psi = 0.$$

In the present case:

1. The kinetic energy operator T is represented (Fig. 5) by a set of equal inductors in series, whose inductance L_1 is $(2m/\hbar^2)\Delta x$. 2. The potential energy operator V is represented by a set of unequal coils in parallel, whose inductance L_2 is $1/V\Delta x$. 3. The total energy operator $-E$ is represented by a set of equal capacitors in parallel whose capacitance is now $\hbar \Delta x$. (In the second model the capacitance was the unknown $E\Delta x$.)

The operand ψ is again represented by voltages and the result of the operation $\alpha\psi$ by the same currents as in the first model. Their variation in time now is sinusoidal, with $2\pi f_c = \omega_c$.

Instead of varying the magnitude of the capacitors, now the frequency of the generator is varied, thereby varying the admittance of the capacitors, $\hbar\omega_c = E$ (and those of the inductors). Again when the generator current becomes zero the circuit is oscillatory and self-supporting and the network represents a stationary solution of the equation. The corresponding eigenvalue is $E = \hbar\omega = \hbar(\omega_c)^2$, rather than $\hbar\omega_c$, because of the simultaneous variation of the reactance of the inductive coils. The eigenfunctions ψ of the model and of the equation are, however, identical.

As the currents in the horizontal inductors are $(\hbar^2/2mi\omega_c)\partial\psi/\partial x$, the results of an operation on ψ by the *momentum* operator $p = (h/i)\partial/\partial x$ are these currents divided by $\hbar/2m\omega_c$. Hence, in the third model the momentum operator p may be represented by a set of equal horizontal coils with inductance $L = \Delta x/\hbar\omega_c$.

One slight disadvantage of this third model is that as the energy E changes sign, the reactance of the capacitor $j\omega_c\hbar$ cannot change signs. Since in most cases no eigenvalues exist in the negative energy range, this disadvantage is of little consequence. Of course, the second model with fixed frequency and variable capacitors works in all cases, since the capacitors simply become inductors when E changes sign.

THE FREE PARTICLE IN ONE DIMENSION

An interesting special case occurs when the potential V is zero everywhere. The one-dimensional equivalent circuit of such a free particle is a conventional transmission line extending to infinity in both directions (Fig. 6) in which the series inductance is $2m\Delta x/\hbar^2$ and the shunt capacitor is $\hbar\Delta x$.

It is well known that such a transmission line may maintain a standing wave at any frequency ω_c between zero and infinity drawing no current from the generator. That is, the positive energy values form a continuous spectrum. If the transmission line is considered as the second type of model with variable capacitors, then at negative energy values E the capacitors also become inductors and the line cannot maintain a standing wave. The corresponding free particle also has no eigenvalue at the negative energy levels.

MODELS ALONG CURVILINEAR AXES

The three-dimensional Schrödinger equation for a single particle is

$$-\frac{\hbar^2}{2m}\nabla^2\psi+(V-E)\psi=0,$$

where ∇^2 is the Laplacian operator in curvilinear coordinates.

In order to establish a physical model for it, it is necessary to change it to a tensor density equation.[2] The above equation in orthogonal curvilinear coordinates may be changed to a tensor density form by multiplying it by $h_1h_2h_3=\sqrt{g}$ giving

$$-\frac{\hbar^2}{2m}\left[\frac{\partial}{\partial u^1}\frac{h_2h_3}{h_1}\frac{\partial\psi}{\partial u^1}+\frac{\partial}{\partial u^2}\frac{h_3h_1}{h_2}\frac{\partial\psi}{\partial u^2}+\frac{\partial}{\partial u^3}\frac{h_1h_2}{h_3}\frac{\partial\psi}{\partial u^3}\right]+\sqrt{g}\,(V-E)\psi=0.$$

If the equation is multiplied through by $\Delta u^1\Delta u^2\Delta u^3$, it represents the surface integral of grad ψ around the six faces of a cube of space with volume $h_1h_2h_3\Delta u^1\Delta u^2\Delta u^3$. The width Δu^q may be arbitrary and different in the three directions.

The corresponding equivalent circuit is shown in Fig. 7. For a free particle ($V=0$) it represents a generalization of the conventional one-dimensional transmission line to three dimensions.

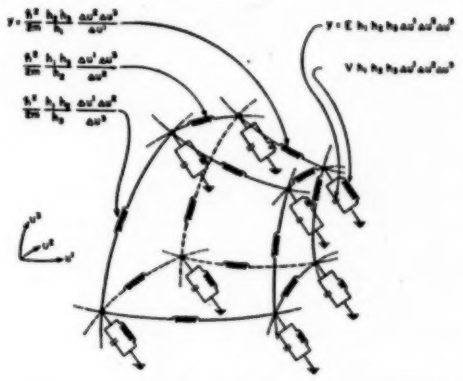

FIG. 7. Model of the Schrödinger equation with three independent variables.

[2] G. Kron, Proc. I. R. E. 32, 289–299 (May, 1944).

PHYSICAL REVIEW VOLUME 67, NUMBERS 1 AND 2 JANUARY 1 AND 15, 1945

A.C. Network Analyzer Study of the Schrödinger Equation

G. K. CARTER† AND GABRIEL KRON††
General Electric Company, Schenectady, New York

(Received May 25, 1944)

Utilizing the type of circuit described by Kron tests were carried out on the a.c. network analyzer. The tests reported include only one-dimensional circuits. Measurements were made of eigenvalues and eigenfunctions for the particular cases of the linear oscillator, the rectangular potential well, the double rectangular barrier, the single barrier, and the rigid rotator. These tests show the circuit representation to be valid and to be adaptable to solution on the network analyzer.

ALTERNATING CURRENT NETWORK ANALYZER

THE alternating current network analyzer[1] consists of a set of adjustable inductance, resistance, and capacitance units, each connected to a pair of flexible cords and plugs. Connections between units to form any desired network are made by inserting the plugs in adjacent jacks in a jack panel. As many units as desired can be connected to a common point. Alternating current electric power is supplied by a motor-generator set to individual generator units so that several different voltages, independently adjustable in both phase and magnitude, can be inserted in different parts of the network. A centrally located set of instruments (voltmeter, ammeter, wattmeter, and varmeter) can be connected to any unit or circuit by a set of key switches.

METHOD OF TEST

The circuit used is that of Fig. 3 of the companion paper,[2] repeated here as Fig. 1 for convenience. The circuit was extended, not from minus to plus infinity, but to the limit of the circuit elements available.

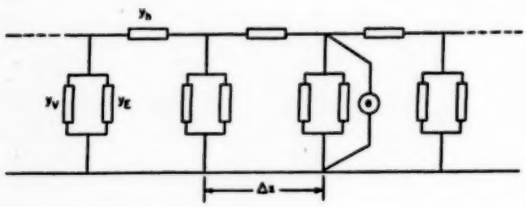

FIG. 1. Equivalent circuit used.

Discrete energy levels are characterized in the circuit usually by a standing voltage wave which attenuates to zero outside of some special region.

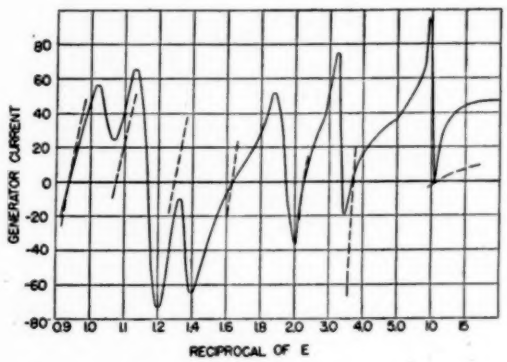

FIG. 2. Generator current as a function of energy levels of Fig. 3.

For this type of wave, the circuit should be terminated in an equivalent impedance. Since no attempt was made to do this, such levels should show an error which increases with the voltage remaining at the end of the line. On the other hand, the continuous energy levels in general exhibit a standing wave which is a space sinusoid of constant amplitude extending to infinity in at least one direction. Hence, at the end of a finite length of line, such a wave must have a loop if the line is open-circuited, a node if it is short-circuited, or other space phase for other types of termination. Since only one length of line and one type of termination (open circuit) were used in these tests, only particular levels and only one wave at each level were actually measured.

For the line elements, inductors and capacitors were used, the former being arbitrarily denoted

† Analytical Division, Central Station Engineering Divisions.
†† Consulting Engineer.
[1] H. P. Kuehni and R. G. Lorraine, Trans. A.I.E.E. **57**, 67 (1938).
[2] G. Kron, Phys. Rev. **67**, 39 (1945).

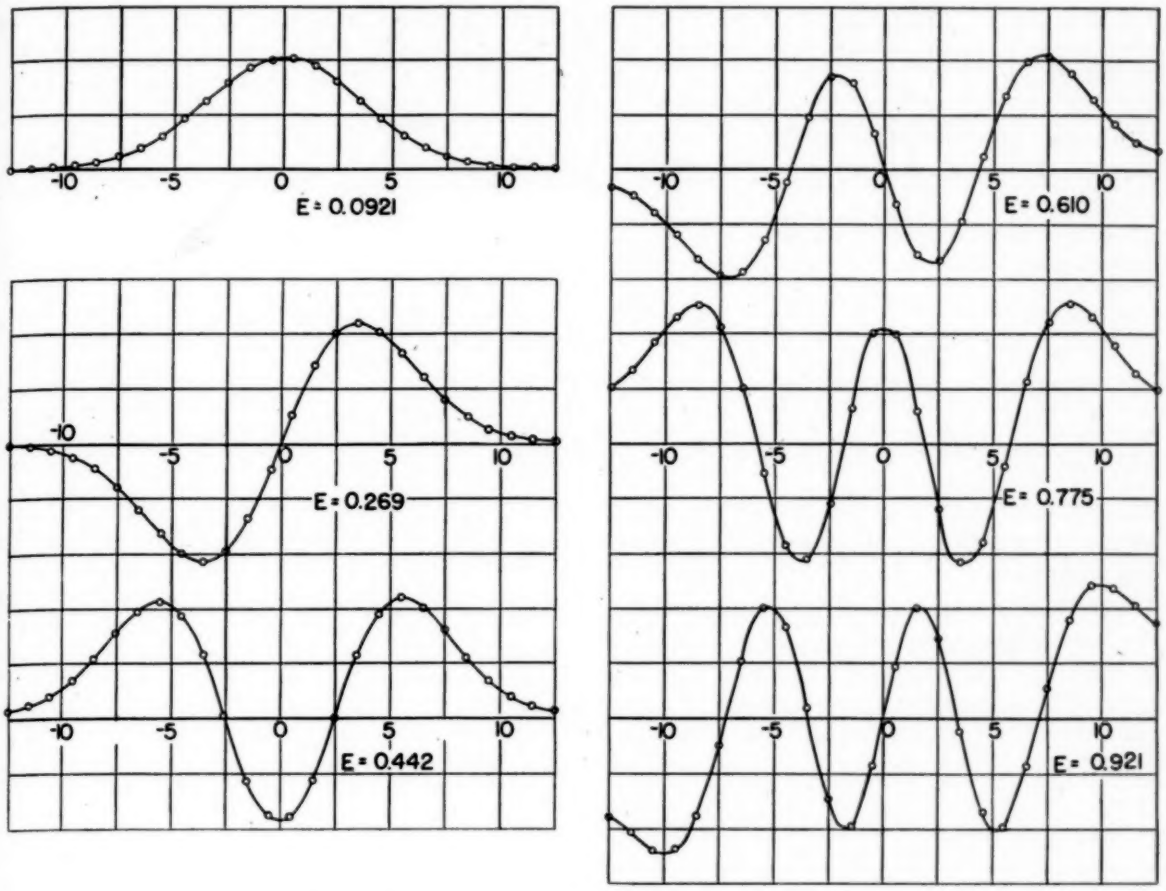

FIG. 3. Eigenfunctions of the linear harmonic oscillator.

as negative admittance units. Curves of generator reactive current *versus* energy level E (admittance y_E) were measured for several generator locations along the line; from these the eigenvalues (values of y_E for zero reactive current) could be determined and the corresponding eigenfunctions (voltage distributions) measured.

Since qualitative, rather than quantitative, results were the prime objective at this time, no special measures were taken to set admittance values closer than the nearest step on the analyzer units.

LINEAR HARMONIC OSCILLATOR

Taking Δx as unit distance,[3] we represent the linear oscillator[4] by $y_A = \hbar^2/2m = 1.10$ and by $y_V = V = 0.00704x^2$. The resulting generator reactive current as a function of energy level $y_E = E$ is shown in Fig. 2. Ideally, the current curve shown in Fig. 2 should always slope upward toward the right (increasing values of $1/E$), passing successively through zero, positive infinity, and negative infinity; the zero points then represent conditions in which the circuit should maintain its oscillations even without the external driving force. Practically, the presence of resistance in the network forces the current to pass through additional zero points in going from large plus values to large minus values; but these additional zeros are readily recognized because the curve has the negative slope in passing through them, and they can therefore be ignored. The solid line is for one generator position; the dotted lines are check curves for other generator positions. Those eigenvalues at which the solid curve tries to reach zero but does not succeed correspond to eigenfunctions such that this

[3] See Appendix for discussion of scale factors.
[4] V. Rojansky, *Introductory Quantum Mechanics* (Prentice-Hall, Inc., New York, 1942).

TABLE I.

Measured eigenvalues	0.0921; 0.269; 0.442; 0.610; 0.775; 0.921
Calculated eigenvalues	0.0880; 0.264; 0.440; 0.616; 0.792; 0.968

TABLE II.

Measured eigenvalues	0.0593; 0.216; 0.465; 0.800
Calculated eigenvalues	0.0552; 0.220; 0.486; 0.832

TABLE III.

Measured l	4.14; 5.12; 6.10; 7.13; 8.12; 9.13
Theoretical l	4 ; 5 ; 6 ; 7 ; 8 ; 9

generator position is near a node of the eigenfunction; it is not practical to supply the circuit losses from such a point.

Figure 3 shows the measured eigenfunctions up to an energy level almost as great as the value of V at the end of the line ($V=1.10$). The measured eigenvalues compare with the calculated values as in Table I. The maximum discrepancy is only about 5 percent. At the lowest value, the discrepancy is largely caused by the approximate representation of the small values of V; while at the highest value, the line termination is probably responsible. While the eigenfunctions have not been normalized for comparison, it can be seen that these too are in good qualitative agreement with the known forms for such functions.*

POTENTIAL WELL

The second case is that of a rectangular potential well. Taking again $\hbar^2/2m=1.10$ and Δx as unit distance, we represent the well by $V=0$ from -6 to $+6$ and by $V_0=1.10$ outside this region. One of the eigenfunctions and eigenvalues in the discrete energy spectrum $E<V_0$, is shown in Fig. 4. Comparison of the measured with the calculated eigenvalues is given in Table II. The lowest figure in this case was not quite at zero current but represented the maximum inductance of the board units; the highest again is subject to some correction because of improper termination. Nevertheless, the agreement is very satisfactory. Again, though not normalized, the eigenfunctions show good agreement with the calculated shapes.*

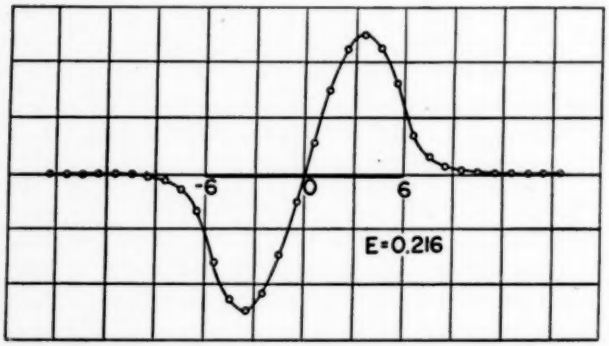

FIG. 4. An eigenfunction of the rectangular potential well in the discrete spectrum.

Figure 5 shows a measured eigenfunction in the continuous spectrum, $E>V_0$. This is, of course, only the particular function corresponding to a loop of the wave at each end of the existing line. For the same energy level, infinitely many other functions are theoretically possible; and a finite number of these, depending upon the number of circuit units per wave-length and the number of units available, could be obtained on the analyzer by simply shifting the nodes in space. Similar statements are true for any energy level $E>V_0$, of course. The figure is given here to show the performance of the circuit and the analyzer in the continuous spectrum region.

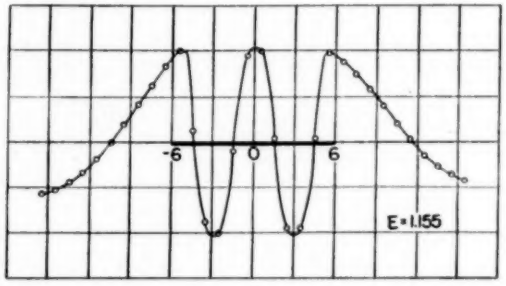

FIG. 5. An eigenfunction of the rectangular potential well in the continuous spectrum.

DOUBLE BARRIER

The double rectangular barrier was represented by $V_0=1.10$ between $+5$ and $+10$ and between -5 and -10, with $V=0$ elsewhere; Δx is again unit distance, and $\hbar^2/2m=1.10$. Figure 6 gives six measured eigenfunctions corresponding to nodes at the ends of the line. The three curves on the

* Reference 4, p. 24.

*Reference 4, p. 156.

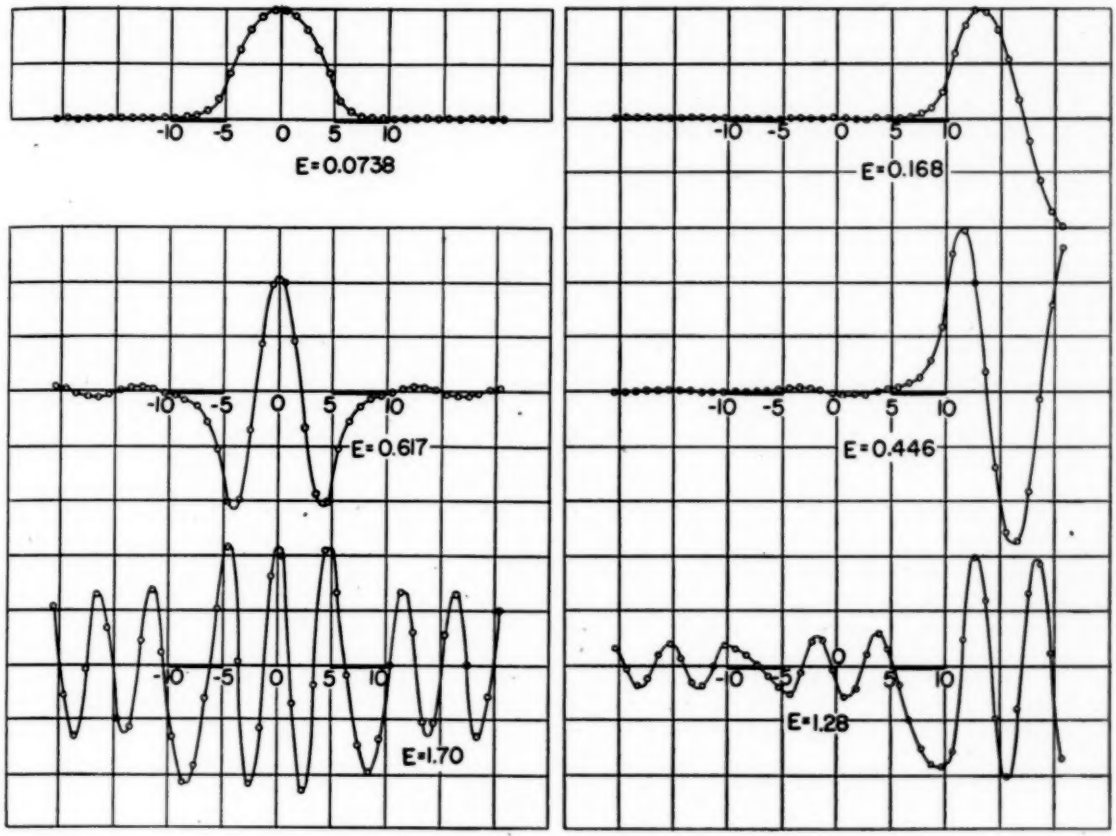

FIG. 6. Eigenfunctions for double rectangular potential barrier.

left represent virtual binding.* The three on the right apparently represent a penetration phenomenon, related to the next section. The function which is large on the outside of both barriers and small between was not obtained in this series of tests, because only one generator was used to supply resistance losses, and these are not readily transmitted through the low voltage region. The curves shown are again but individuals out of infinite families at every energy level.

RECTANGULAR BARRIER

The final test in this group was the single rectangular barrier represented by $V=0$ for $x<0$, $V_0=1.10$ between 0 and 3, and $V_1=0.40$ for $x>3$; as before, Δx is unity and $\hbar^2/2m=1.10$. Figure 7 shows some of the eigenfunctions measured. The three on the left represent penetration from the left, so to speak, at energy levels below V_1, between V_1 and V_0, and above V_0; the three curves on the right, penetration from the right at levels above V_1.

RIGID ROTATOR

Legendre's equation, which arises in the problem of the rigid rotator,* can be written in the form

$$-\frac{d}{dx}(1-x^2)\frac{d\theta}{dx}+\left[\frac{m^2}{1-x^2}-l(l+1)\right]\theta=0.$$

This is of the form of the Schrödinger equation, where $\hbar^2/2m$ is replaced by $(1-x^2)$, V by $m^2/(1-x^2)$ and E by $l(l+1)$; the range of x here is from -1 to $+1$. Tests on this equation were carried out only for $m=0$; one of the resulting measured θ functions with the corresponding value of l is shown in Fig. 8. Comparison with the theoretical values of l, in Table III, shows very good agreement in the range measured. The measured functions have not been normalized;

* Reference 4, p. 225.

* Reference 4, p. 437.

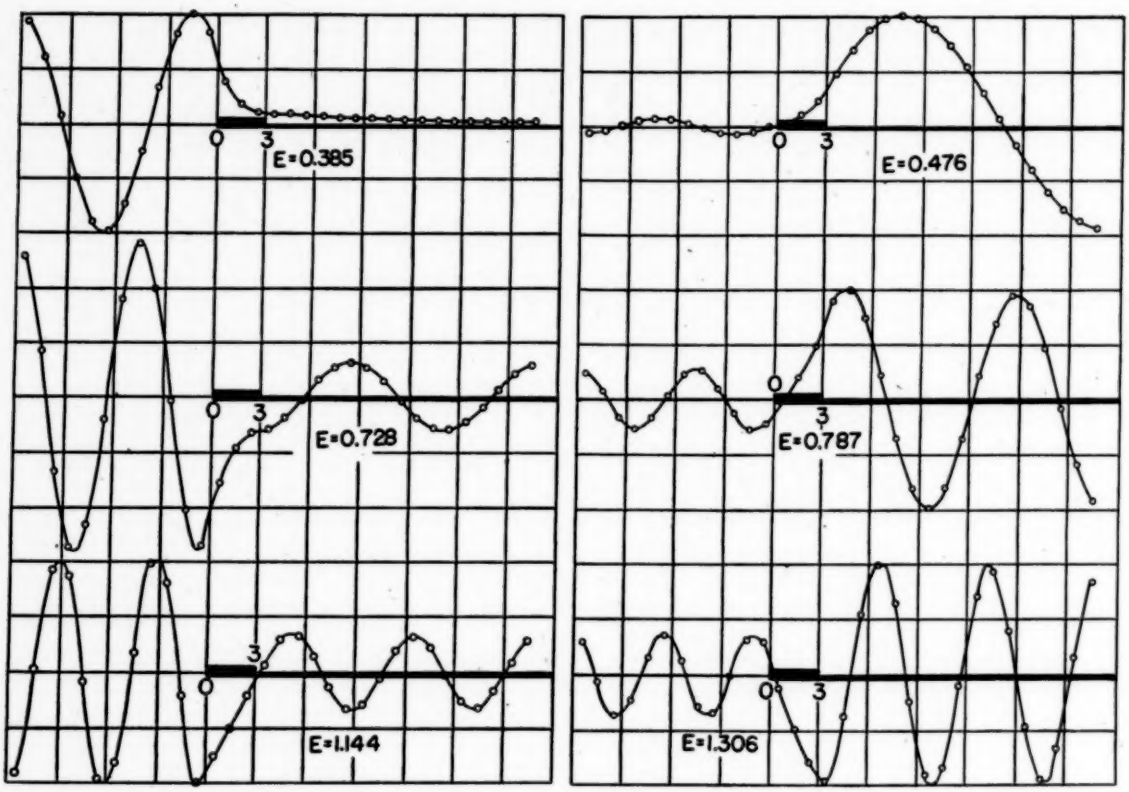

FIG. 7. Eigenfunctions for rectangular barrier between potential levels: Left of barrier $V=0$; barrier height $V_0=1.0$; right of barrier $V_1=0.40$.

but calculated end points, indicated by the dotted end extensions, line up very well with the measured curves.

SUMMARY

The tests reported here demonstrate the applicability of the electric circuit equivalent for determining eigenvalues and eigenfunctions of one-dimensional equations of the Schrödinger type. At the same time, they indicate that it is practical to use for this purpose existing a.c. network analyzers. Experience in these tests leads also to the conclusion that the equivalent circuit together with a small acquaintance with transmission line theory goes far in aiding the visualization of the characteristics to be expected of the solutions.

The significance of the equivalent-circuit method of studying characteristic values is that it is just as simple to study cases which are not readily solved analytically as it is to study the idealized cases given here.

ACKNOWLEDGMENT

The writers are indebted to C. Concordia, F. J. Maginniss, and H. A. Peterson of the Analytical Division, Central Station Engineering Divisions, General Electric Company, for helpful discussion and suggestions.

APPENDIX—SCALE FACTORS

The equation represented in most of these tests is Schrödinger's equation

$$-\frac{\hbar^2}{2m}\frac{d^2\psi}{dx^2}+[V(x)-E]\psi=0.$$

The equation represented by the circuit of Fig. 1 corresponds to

$$-\frac{d}{dx}y_k\frac{de}{dx}(\Delta x)^2+[y_V-y_E]e=0.$$

When the two equations represent the same

system, they give the proportions

$$\frac{\hbar^2/2m}{y_h(\Delta x)^2}=\frac{V(x)}{y_V}=\frac{E}{y_E}=K,$$

where K is the scale factor between the energy level E and the admittance in the equivalent circuit. In Figs. 3–7, the unit of horizontal distance has been taken as Δx; the physical distance represented by this unit is determined by the equation

$$(\Delta x)^2=\frac{\hbar^2/2m}{Ky_h}=\frac{\hbar^2/2m}{V(x)}\cdot\frac{y_V}{y_h}.$$

In the case of the potential well, for example,

$$y_{V_0}=y_h, \quad (\Delta x)^2=\frac{\hbar^2/2m}{V_0}.$$

The half-width of the well is

$$a=6\Delta x$$

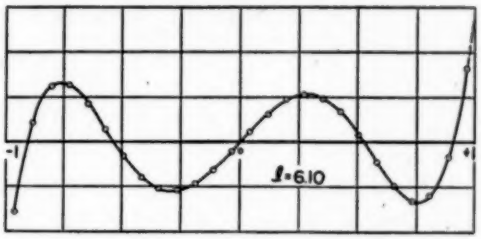

FIG. 8. An eigenfunction of the rigid rotator.

so that

$$(\Delta x)^2=\frac{a^2}{36}=\frac{\hbar^2/2m}{V_0},$$

and

$$\frac{a^2V_0}{\hbar^2/2m}=36,$$

which is the case of Exercise 3.* Other proportions for the well are obtained either by changing the number of Δx units in a or by changing the ratio of y_{V_0} to y_h.

* Reference 4, p. 155.

The Energy Spectrum of the Primary Cosmic Radiation

SHUICHI KUSAKA
Smith College, Northampton, Massachusetts
(Received October 11, 1944)

FROM results of the experiments carried out in India, in Mexico, and the United States, Millikan, Neher, and Pickering[1] have put forward the hypothesis that the primary cosmic rays are electrons* whose energy arises from the complete transformation of the rest mass of atoms such as carbon, nitrogen, oxygen, and silicon which are abundant in interstellar space. Since the high altitude experiments of Schein, Jesse, and Wollan[2] indicate that the primary cosmic rays are not shower producing and hence are probably protons, we have made a comparison with the experimental results of Millikan and his colleagues and theoretical calculations based on the assumption that the distribution in number of the primaries is proportional to the inverse cube of the energy. The choice of the inverse cube is because of the fact that the secondary particle, both the hard and the soft components, is known to have approximately this energy distribution.

The main experimental results obtained by Millikan *et al.* are the variations with magnetic latitude of the energy brought in by cosmic rays arriving vertically, and the total energy brought in from all directions. It has been pointed out by these experimenters that the former is proportional to the area under the curve in which the rate of vertical coincidence is plotted against altitude expressed in an equivalent height of water; and that the latter is proportional to the area under similar curves in which the ordinate is the rate of ion production in an ionization chamber.

With our assumption of the energy spectrum and with the geomagnetic theory of cosmic radiation developed by Lemaitre and Vallarta,[3] it is a simple matter to calculate the latitude variation of the vertical intensity which is inversely proportional to the minimum energy of arrival in the vertical direction, which has been done by these authors.[4] The calculation of the total intensity involves the integration of the product of the distribution in energy and the solid angle subtended by the main cone. The latter was obtained from the computations of Koenig[5] and the integration was carried out graphically.

The results of the calculations and the experimental results of Millikan *et al.* are plotted in the accompanying figures. Since only the relative values are obtainable in both the theoretical calculations and the observations, the theoretical values are normalized to give 100 at the equator; and the relative values of the experimental results are adjusted to give best agreement with the theoretical curve. For the experimental points, the statistical error was estimated to be about 3 percent and this is shown on the graphs. Figures 1 and 2 show that, for the results on the vertical

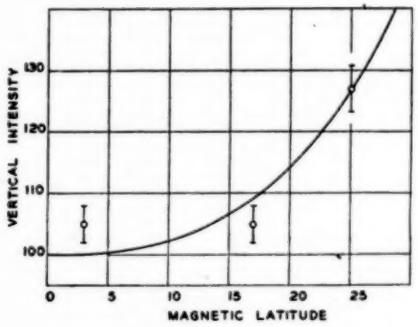

FIG. 1. Vertical intensity as a function of magnetic latitude. The experimental points are for Bangalore (mag. lat. 3° N), Agra (mag. lat. 17° N), and Peshawar (mag. lat. 25° N).

[1] Millikan, Neher, and Pickering, Phys. Rev. **61**, 397 (1942); H. V. Neher and W. H. Pickering, Phys. Rev. **61**, 407 (1942); Millikan, Neher, and Pickering, Phys. Rev. **63**, 234 (1943).

* *Note added in proof:* It has recently been pointed out by Warren [D. T. Warren, Phys. Rev. **66**, 156 (1944)] that the atom annihilation hypothesis is quite independent of the nature of the primary particles, so that they may be protons as well as electrons.

[2] Schein, Jesse, and Wollan, Phys. Rev. **59**, 615 (1941).

[3] G. Lemaitre and M. S. Vallarta, Phys. Rev. **50**, 493 (1936).

[4] In transforming the energy of the particles from störmer units to electron volts, it is necessary to take definite values for the charge and mass of the primary particles. We have here assumed them to be protons, but it does not make any essential difference if we take them to be electrons.

[5] H. P. Koenig, Phys. Rev. **58**, 385 (1940).

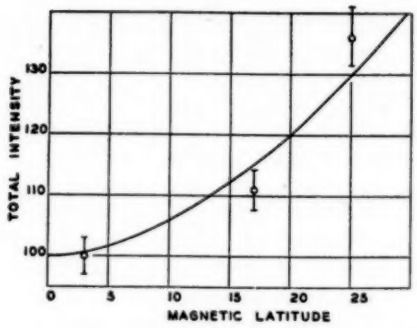

FIG. 2. Total intensity as a function of magnetic latitude. The experimental points are for the same positions as in Fig. 1.

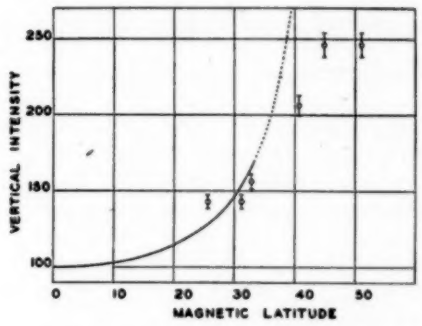

FIG. 3. Vertical intensity as a function of magnetic latitude. The experimental points are for Acapulco (mag. lat. 25.6° N), Valles (mag. lat. 31.1° N), Victoria (mag. lat. 32.8° N), Pasadena (mag. lat. 40.7° N), St. George (mag. lat. 44.8° N), and Pocatello (mag. lat. 51.0° N).

and total intensity that were obtained in India, the agreement is within the experimental error. From Fig. 3 we see the values obtained in Mexico and in the United States. The points for Acapulco (magnetic latitude 25.6°), Valles (mag. lat. 31.1°), and Victoria (mag. lat. 32.8°) do not agree as well, seeming to be just barely within the limits of statistical error. The points for Pasadena (mag. lat. 40.7°), St. George (mag. lat. 44.8°), and Pocatello (mag. lat. 51.0°) are completely off the theoretical curve. This divergence is probably caused by the fact that the spectrum of the primaries no longer follows the inverse cube law for energies of the order of 5 Bev, which is necessary for the vertical arrival of the primaries at Pasadena.

Another point which has been put forward as evidence of the discontinuous nature of the primary spectrum is that the observed vertical intensity at Acapulco, Mexico (mag. lat. 25.6°) is 8.3 percent lower than that at Peshawar, India (mag. lat. 24.8°). On the atom annihilation hypothesis, the intensities at both places should be the same, while the continuous distribution hypothesis holds that the intensity at Acapulco should be higher. The observed sea level longitude effect gives a maximum intensity off of the South American coast and a minimum west of the Malay Peninsula with amplitude variation of about 4 percent. However, it is to be noted that the theoretical calculations of Vallarta[6] give a maximum off of the west coast and a minimum in the Pacific Ocean. From the theoretical standpoint, there should be no difference in intensity at Acapulco and Peshawar because of the longitude since they are both just about midpoint between the longitudes at which the maximum and minimum intensities occur. It seems more reasonable to take the theoretical result rather than the observed sea level longitude effect since the discrepancy in phase possibly may be caused by local surface effects which do not influence the cosmic rays arriving at the top of the atmosphere. The fact that Acapulco is 0.8 degree farther north than Peshawar should make the intensity about 2.0 percent higher at Acapulco; but this percentage is within the statistical error.

Thus, generally, we may conclude that the agreement between the theoretical calculations and the experimental results is within the experimental error if the distribution is taken to be a curve which follows the inverse cube law for high energies and which flattens out on the low energy side at about 6 Bev. This interpretation, then, is offered as a possible alternate to the atom annihilation hypothesis derived from the experimental results of Millikan and his colleagues.

[6] M. S. Vallarta, Phys. Rev. **47**, 647 (1935).

Letters to the Editor

PROMPT publication of brief reports of important discoveries in physics may be secured by addressing them to this department. The closing date for this department is the third of the month. Because of the late closing date for the section no proof can be shown to authors. The Board of Editors does not hold itself responsible for the opinions expressed by the correspondents. Communications should not in general exceed 600 words in length.

Evidence for the Artificial Production of a New Neutral Radiation

GERHART GROETZINGER, P. GERALD KRUGER, AND LLOYD SMITH
The Nuclear Radiations Laboratory, Department of Physics, University of Illinois, Urbana, Illinois

January 3, 1945

PROMPTED by indications, found by one of us, of a new non-ionizing radiation produced by a cyclotron, which manifested itself by the appearance of high energy electrons, we have performed a series of experiments to establish its existence definitely.

Since gamma-rays and neutrons (which are produced in large numbers in a cyclotron) may also give rise to electrons of several million volts energy, it was necessary to devise methods of detection which could distinguish between these various radiations.

Two Geiger-Mueller counters were set up at a distance of four meters from the target of the cyclotron and almost in direct line with the deuteron beam hitting the target. The axes of the counters were five cm apart, the line joining them being perpendicular to the direction of the deuteron beam. The counters had a wall thickness so that only electrons of energies higher than 2 Mev have an appreciable chance to trip both counters in coincidence. The cyclotron was completely enclosed by water tanks of 120-cm thickness. The tanks on the side facing the counters contained a saturated solution of boric acid. A lead house of 19-cm minimum thickness surrounded the counters on all sides. In addition, this cubical lead house was surrounded on the sides by 0.5-mm sheets of cadmium and by boric acid solution in water, at least 23 cm thick. The top and bottom of the house were shielded by Cd sheets and 16 cm of paraffin.

With this arrangement we recorded the number of coincidences and simultaneously the total number of 10.5-Mev deuterons striking the target of the cyclotron. The beam current was of the order of 30–50 microamperes and the number of coincidence counts about twice background. Table I shows the results for Mn and W targets.

In order to establish how many of the coincidences were caused by fast and slow neutrons, the water cans and Cd shields between the counters and the target were removed. This should have increased the neutron intensity by a factor of 100 inside the lead house, but no measurable effect on the counting rate was observed. Even the 1500 lb. of boric acid which were dissolved in the 120-cm thick water tanks did not affect the counting rate in the case of the W target. This experiment, and further work to be described in a more complete report which will appear later, show that the observed counting rates are not the result of neutrons.

The following experiments were performed to determine to what extent these coincidences could be caused by gamma-rays. Removing 9.5 cm of lead from the top and sides of the lead house increased the counting rate by a factor of 25 in the case of the W target, and by a factor of 22 for the Mn target. Since for gamma-rays of maximum penetrating power in lead this factor should be 80, it is concluded that a radiation more penetrating than gamma-rays exists. In the case of the Mn target, an additional layer of lead, 9.5 cm thick, placed between the target and the counters reduced the counting rate only by a factor of 4. In this connection it should be mentioned that separate experiments showed that the counting rate was not affected by removing 9.5 cm of lead from the other three sides of the house, indicating that all of the coincidences are caused by radiation arriving from the direction of the cyclotron.

Second, the counter telescope was turned through 90 degrees, so that the line joining the axes of the counters was parallel to the deuteron beam. Under these conditions, the counting rate was unchanged for lead thicknesses of 19 cm and 28.5 cm, while it was increased by a factor of 2.5 for the 9.5-cm thickness. This increase in the latter case indicates that most of the radiation penetrating 9.5 cm of lead still consists of gamma-rays coming from the cyclotron; the isotropism of the electrons recorded in the former cases indicates that a different radiation is producing them. Other measurements indicated that the energies of these last-mentioned electrons are higher than 5 Mev.

TABLE I. Coincidences per deuteron ($\times 10^{17}$).

Target material	Neutron shields	Lead absorber thickness 9.5 cm	19 cm	28.5 cm
W	in	37.7±1.2	1.5±0.2	
W	out		1.5±0.4	
Mn	in	46.0±1.7	2.1±0.3	0.53±0.28
Mn	out		2.2±0.6	

Similar experiments were performed with P, Sb, and NaCl targets and it was found that the yield does not change appreciably with target material.

From these data it appears that the radiation here observed is more penetrating than neutrons in water or gamma-rays in lead. Therefore it seems likely that the radiation consists of neutral particles of low mass (low mass mesotrons). In this case the observed electrons would be decay electrons which are emitted after the mesotrons are slowed down or stopped. It is believed that there is evidence for charged mesotrons of low mass in cosmic radiation.[1]

[1] Marcel Schein (private communication).

Absorption of 2.8-Mev Gamma-Rays in Lead

GERHART GROETZINGER AND LLOYD SMITH
Department of Physics, University of Illinois, Urbana, Illinois
January 3, 1945

IN a recent paper[1] an absorption coefficient of 0.405 cm^{-1} for 2.85-Mev gamma-rays in lead was reported. This value, taken together with the result of a similar measurement in copper, was interpreted as indicating an "insufficiency" in the Klein-Nishina formula for this energy, since the absorption coefficient predicted by the theory (which also takes into account absorption caused by the photoelectric effect and pair production) is 0.46 cm^{-1}.[2] On the other hand, complete agreement was found at 1.30 and 1.14 Mev. The discrepancy of more than 10 percent at 2.85 Mev is the more striking since the theory has been confirmed at higher and lower energies by many workers.

The reported low absorption coefficients were obtained by measuring the ionization produced by the gamma-rays of radioactive Na after passing through various thicknesses of lead and copper. Since this radiation is assumed to contain both 1.38- and 2.85-Mev gamma-rays,[3] the absorption coefficient of the high energy component had to be deduced from the absorption of the mixture.

To provide further information on this matter we have measured the absorption of Na gamma-rays in lead by an arrangement which, for two reasons, practically excluded the effect of the low energy component. First, we used a minimum absorber thickness of 9.5 cm, so that the ratio of the high energy to the low energy quanta is raised to 3:1 according to the theory[2] or even higher according to the above-mentioned paper;[1] second, we recorded the gamma-radiation with a twofold Geiger-Mueller counter arrangement of high resolving power, the counter walls being of such a thickness that only electrons of energies greater than 2 Mev had an appreciable chance of penetrating both counters and being recorded.

On account of a strong activity in the room in which the experiment was performed[4] the counters were surrounded on all sides by at least 19 cm of lead, except for an opening on the side facing the Na source in which lead was placed to make up a number of absorber thicknesses between 9.5 and 19 cm. The source was placed 40 cm from the first counter, a position which allowed a suitable counting rate even at the greatest thickness. The effect of the imperfect geometry of this arrangement was overcome by pointing the counter telescope toward the source, causing it to be insensitive to radiation proceeding in any other direction than straight from the source. This directional effect occurs because most of the electrons which are produced by 2.8-Mev gamma-rays and which have sufficient energy to penetrate both counters are Compton electrons emitted in a forward direction. This was proved by turning the counter telescope through 90°, which reduced the counting rate by a factor of 3.

Using lead absorber thicknesses of 9.50, 12.13, 14.60, and 19.0 cm we found an absorption coefficient of 0.467 ± 0.009 cm^{-1}. The absorption curve is of pure exponential form, indicating that the 1.98-Mev radiation was indeed eliminated by the method used. The result thus substantiates the present theory.

[1] J. M. Cork and R. W. Pidd, Phys. Rev. 66, 227 (1944).
[2] W. Heitler, *The Quantum Theory of Radiation* (Clarendon Press, Oxford, 1936).
[3] Actually experiments by P. Gerald Kruger and W. E. Ogle indicate that there are four gamma-ray lines between 2.6 and 2.9 Mev. Since in this region the absorption coefficient varies very slowly with energy, this fact is of minor importance for absorption measurements (private communication).
[4] The arrangement was primarily set up for a different purpose.

The Nuclear Isomerism of Gold

MARCELLUS L. WIEDENBECK
Department of Physics, University of Notre Dame, Notre Dame, Indiana
November 27, 1944

STRONG activity has been observed when gold is irradiated with high energy x-rays. This activity has been observed when self-quenching counters, having gold cathodes, have been irradiated directly; and it can also be detected when a gold sheet is irradiated and quickly placed before a counter with a thin (1.5 mil) aluminum window.

This activity is attributed to a metastable state of stable $_{79}Au^{197}$ produced by line absorption in the following reaction: $_{79}Au^{197} + \gamma \rightarrow {}_{79}Au^{197*}$.

The period, evaluated from a decay curve extending over one minute, has been found to be 7.5 ± 0.5 second and the energy of the metastable level, which has been evaluated from the measurement of the energy of the conversion electron by absorption in aluminum foils, is 250 kev.

Since the spin of gold in the ground state is 3/2, the spin of Au* is probably 9/2 or 11/2.

It is of interest to note that gold, along with platinum[1] and mercury,[2] form a triad similar to the one formed by silver, cadmium, and indium.

A detailed study of the energy levels which combine with the metastable state is in progress and will be reported in the near future.

[1] Sherr, Bainbridge, and Anderson, Phys. Rev. 59, 400 (1941).
[2] G. Friedlander and C. S. Wu, Phys. Rev. 63, 227 (1943); McMillan, Kamen, and Ruben, Phys. Rev. 52, 375 (1937); Pool, Cork, and Thornton, Phys. Rev. 52, 239 (1937).

Gamma-Ray Absorption

J. M. CORK
University of Michigan, Ann Arbor, Michigan
December 23, 1944

IN a recent paper[1] the linear absorption coefficient for certain gamma-rays in lead and copper was reported. Attention was given particularly to the 2.75-Mev radiation from sodium (24), showing an apparent discrepancy between observed and computed values of the absorption coefficients in lead and copper. To examine more conclusively the behavior of the other radiations mentioned, namely, that from zinc (65) and from cobalt(60), much stronger sources of these gamma-rays were studied.

A sample of radio-cobalt of 32 millicuries equivalent intensity was kindly lent by Professor R. D. Evans of the Massachusetts Institute of Technology and a sample of zinc was bombarded as a probe in the cyclotron in this

TABLE I. Linear absorption coefficients in cm^{-1}.

Absorber	1.14 Mev	1.30 Mev
Iron	0.426 cm^{-1}	0.400 cm^{-1}
Copper	0.460	0.440
Lead	0.678	0.610

laboratory for many hours. With these very strong samples it was possible to make observations through much thicker layers of the absorber than had been done before and hence more accurately determine the absorption coefficients. These values together with the absorption coefficients for iron are collected in Table I.

The same values are shown graphically, along with the curves computed[2] by Heitler, in Fig. 1. There is some

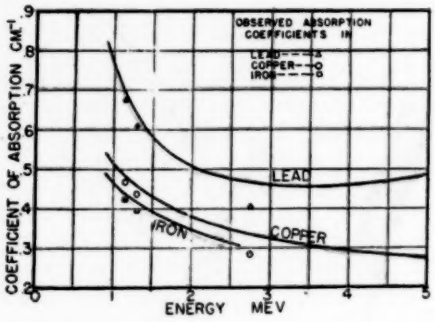

FIG. 1. Absorption coefficients, observed and computed (Heitler).

uncertainty in the energy of the cobalt radiation as it has been reported[3] to be complex, with energies 1.1 and 1.33 Mev. The value of the absorption coefficient recorded is that after passing through 9 cm of lead, and hence 1.3 Mev is used. The assumption of a lower value for the energy would have increased the observed discrepancy.

It is apparent that in every case the experimental points are below the computed Heitler curves, leading to a conclusion similar to that expressed in the previous paper, namely, an inadequacy in the Klein-Nishina formula at high energies.

[1] J. M. Cork and R. W. Pidd, Phys. Rev. 66, 227 (1944).
[2] W. Heitler, *The Quantum Theory of Radiation* (Clarendon Press, Oxford, 1936).
[3] M. Deutsch and L. G. Elliott, Phys. Rev. 62, 558 (1942); C. E. Mandeville and H. W. Fulbright, Phys. Rev. 64, 265 (1943).

A New Method for Determining Thresholds in γ-n Processes

MARCELLUS L. WIEDENBECK AND C. J. MARHOEFER
Department of Physics, University of Notre Dame, Notre Dame, Indiana
October 20, 1944

AN exact determination of the threshold energy of photo-disintegration is of importance in nuclear physics and is especially useful in determining the relative masses of various nuclei. Up to this time, only two elements have been quantitatively studied in this connection, namely, beryllium and deuterium. However, it seems probable that many more will be studied in the near future, and a discussion of the methods previously used and of the new method developed in this laboratory thus seems justified.

The earliest method used[1] consisted in irradiating a sample of beryllium or deuterium with the γ-rays from natural sources, ThC″, etc., the energy of which is known, and observing the energy of the proton liberated from the process, ${}_1D^2+\gamma\rightarrow{}_1H^1+{}_0n^1$. The threshold energy was then the energy of the γ-ray minus twice the energy of the proton. The values obtained for the threshold determined in this manner vary from 2.16 to 2.26 Mev. More recent experiments indicate that the threshold for deuterium is 2.18 Mev and that of beryllium is 1.63 Mev.

With the introduction of various devices to produce high energy electrons, it became possible to vary easily the maximum energy of the x-rays and thus to study the cross section for disintegration as a function of the accelerating potential. In general, by this method the emitted neutrons were slowed down with paraffin and then detected by means of the activity produced in silver or rhodium. The activity obtained from such an arrangement is proportional to the total cross section for the process and when plotted against the accelerating voltage, all other quantities kept constant, gives a curve[2] of the form $A=K(V-V_t)^p$ where K and p are experimental constants and V_t is the threshold potential. Such a curve for deuterium is plotted in Fig. 1 (broken curve). The value of the threshold can be obtained by extrapolating this curve to zero activity.

The method described above has the disadvantage that the value chosen as the threshold depends only upon the few experimental points near the threshold where the activity is low. For a higher degree of accuracy, it is imperative that several points be obtained very close to the threshold.

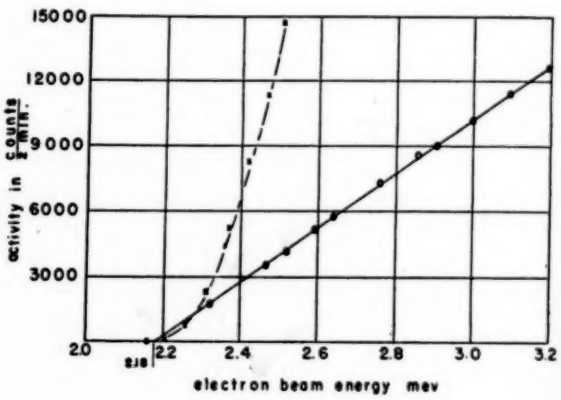

FIG. 1. Neutron counting rate *versus* accelerating potential. Broken curve, drawn from experimental points marked as crosses, obtained by interposing paraffin between deuterium samples and detector. Solid curve obtained without the use of paraffin.

The present method makes use of the resonance absorption of neutrons by rhodium or silver. It is well known, from theory[3] and from experiments on the excitation of nuclei by x-rays,[4,5] that the intensity of any isochromat in

the thick target continuous x-ray spectrum increases linearly with applied electron accelerating potential greater than the energy of the isochromat. Therefore, in a γ-

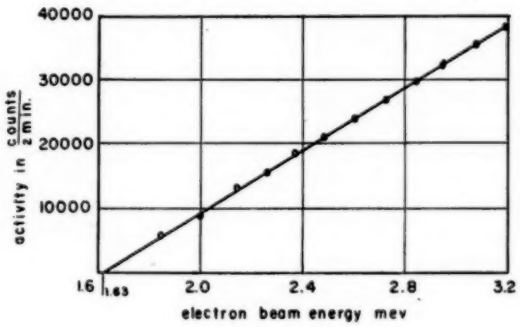

FIG. 2. Neutron counting rate *versus* accelerating potential for disintegration of beryllium. The curve was obtained without the use of paraffin.

n process, the number of neutrons of a given energy should also be linear with the applied voltage V, when

$$V \geq V_t + \frac{A}{A-1} V_n$$

(V_t being the threshold potential; A, the atomic weight of the nucleus being disintegrated; and V_n, the energy of the neutron being considered).

If no paraffin or other hydrogen-containing materials is present to slow down the emitted neutrons, the detector will be sensitive to essentially only one such neutron "line" of energy equal to the resonance energy of the detector and will not be affected by the faster neutrons. Thus the activity *vs.* accelerating potential curve should give a straight line intersecting the abscissa at the threshold potential.

This conclusion was tested with both deuterium and beryllium. The detector used was an argon-ether filled counter with a rhodium cathode. Small samples of deuterium and beryllium were bombarded for two minutes by the x-rays produced by a beam current of 100 microamperes striking a thick gold target. The activity was taken as the number of counts above background obtained during the two minutes after the irradiation was stopped.

The activity is plotted (solid curves in Fig. 1 and Fig. 2) from the threshold to 3.2 Mev as a function of the applied potential. It is seen that in both cases a straight line is obtained, which when extrapolated to zero activity, gives the threshold for the process, namely, 1.630 ± 0.006 for beryllium and 2.185 ± 0.006 for deuterium.

Thus, the threshold can be determined from a linear curve drawn through many points separated by very considerable distances. By this method the thresholds can be determined with a high degree of accuracy.

[1] J. Chadwich and M. Goldhaber, Proc. Roy. Soc. 151, 479 (1935). N. Feather, Nature 136, 468 (1935).
[2] F. E. Myers and L. C. Van Atta, Phys. Rev. 61, 19 (1942).
[3] E. Guth, Phys. Rev. 59, 325 (1941).
[4] B. Waldman and M. Wiedenbeck, Bull. Am. Phys. Soc. 17, Nos. 4, 5 (1942).
[5] M. Wiedenbeck, Bull. Am. Phys. Soc. 19, Nos. 3, 5 (1944).

Showers of Penetrating Particles

O. SALA AND G. WATAGHIN
Department of Physics, University of São Paulo, São Paulo, Brazil
November 24, 1944

COMPARATIVE studies of showers of penetrating particles at various altitudes with different materials were begun in July and August, 1944, in Campos de Jordão (Brasil) at an altitude of 1750 m and latitude 23°, and in São Paulo (altitude 750 m and latitude 23° 5′).

The multivibrator circuit,[1] elaborated by M. D. de Souza Santos, was adopted in connection with counters of fast type (alcohol-argon mixture). The resolving time of the coincidence set used was $\sim 6 \times 10^{-6}$ sec. The rate of chance 4-fold coincidences in all experiments was negligible. The efficiency was tested before and after the experiments and was >97 percent. The arrangements XV and XVI are indicated in Fig. 1. They are of the type used in previous experiments in order to observe showers of penetrating particles.[2]

Fourfold coincidences were observed between counters fully surrounded by lead of thicknesses not smaller than 10 cm Pb and separated also by 10 cm of lead.

In the experiment XVI the arrangement of counters and lead was the same as the experiment XV, and only an absorber of water was added. A total amount of about 750

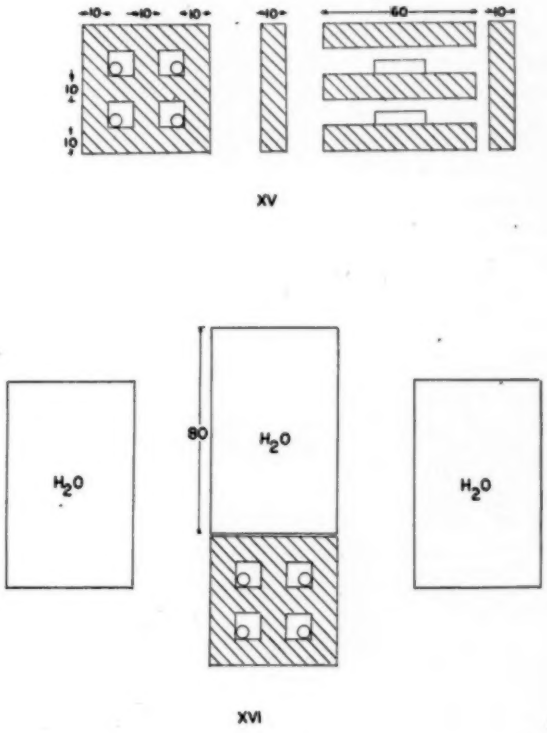

FIG. 1.

liters of water was used forming a layer of 80-cm thickness. The preliminary results are given in Table I.

Although the number of observed 4-fold coincidences is very reduced it seems to us that the results can be considered as an indication of an increase of 23 percent in the frequency of penetrating showers, because of the additional layer of water. Indeed the observed increase is more than 3 times the standard error. Obviously this layer functions as an absorber and as a source of secondary radiation. Our observations seem to indicate that groups of particles penetrating more than 30 cm of Pb are produced in a layer of water of only 80 cm.

TABLE I. Number of 4-fold coincidences in arrangements XV and XVI.

	arrang.	4-fold coinc.	time min.	freq. 10^3 min.$^{-1}$
S. Paulo	XV	73	36300	2.0±0.3
C. de Jordão	XV	155	21830	7.1±0.5
C. de Jordão	XVI	290	32440	8.9±0.5

Recently V. Regener[3] and Schein, Iona, and Tabin[4] observed production of particles in paraffin. Jánossy and Rochester[5] observed production of groups of penetrating secondaries in lead. Evidence on production of groups of penetrating particles in heavy materials was obtained also in cloud-chamber photographs.[6]

The comparison of frequencies in the arrangement XV at two altitudes (1750–750) gives an increase by a factor ~3.5. Thus the shower producing radiation is rapidly absorbed in a layer of 1000 m of air (at an atmospheric pressure ~66 cm Hg, the absorbing mass being ~100 g/cm²). This finding and the fact that shower producing radiation generates showers of penetrating particles in layer of water ~80 g/cm² seems to indicate that this radiation could not be responsible for showers of penetrating particles under clay in a depth of 50 m water equivalent[7] (observed in S. Paulo). It seems possible that there exist several types of showers of penetrating particles produced by different kinds of rays. Further studies are in progress.

[1] M. D. de Souza Santos, An. Acad. Bras. de Ciências 12, 183 (1940).
[2] Wataghin, de Souza Santos, and Pompeia, Phys. Rev. 57, 61 (1940); 57, 339 (1940); 59, 902 (1941).
[3] V. H. Regener, Phys. Rev. 64, 250 (1943).
[4] Schein, Iona, and Tabin, Phys. Rev. 64, 253 (1943).
[5] L. Jánossy and G. D. Rochester, Nature 150, 633 (1942).
[6] E. O. Wollan, Symposium sobre Raios Cosmicos, Acad. Bras. de Ciências, 123 (1941). D. Hughes, *ibid.* 67 (1941). W. E. Hazen, Phys. Rev. 65, 67 (1944).
[7] Symposium sobre Raios Cosmicos, Acad. Bras. de Ciências, 155 (1941).

The Two-Body Problem in Birkhoff's and Einstein's Theories

CARLETON W. BERENDA
Physics Department, Massachusetts State College, Amherst, Massachusetts
November 17, 1944

IN a recent article by the late G. Birkhoff and others,[1] a new general theory of relativity (with a flat space-time) was further advanced.[2] The authors contend, in support of their theory, that it provides a solution of the two-body problem while Einstein's theory does not. However, Einstein, Infeld, Hoffmann, and Robertson in 1939 and in 1940[3] submitted a solution of the two-body problem which, to the approximation desired, predicts a rate of advance of periastron per revolution of

$$P_e=(m_1+m_2)\cdot\frac{6\pi}{a(1-e^2)}.$$

Relativistic units of mass (cm) are used.

Birkhoff's theory predicts, to his approximation, a value of

$$P_b=\frac{3m_1^2+7m_1m_2+3m_2^2}{m_1+m_2}\cdot\frac{2\pi}{a(1-e^2)}.$$

This gives

$$\frac{P_b-P_e}{P_e}=\frac{1}{3}\cdot\frac{m_1m_2}{(m_1+m_2)^2},$$

or, for $m_1\backsimeq m_2$ (the optimum test case):

$$P_b-P_e=P_e/12.$$

Hence, the maximum difference obtainable between the two theories certainly falls within the limits of experimental error, and may arise from differences in the approximation methods employed by the two theories. If any preference can be given to Birkhoff's theory, it must be on the ground of simplicity of its general mathematical (geometrical) structure. All other predictions are the same as in Einstein's theory. The special assumption, in Birkhoff's theory, of a "disturbance velocity of matter equal to c" for subatomic particles, seems a reasonable postulate in the light of the equations of retarded potentials in Maxwell's electrodynamics. The assumption of flat (homaloidal) space-time in a gravitational field is as acceptable *per se* as it is in N. Rosen's[4] or in A. N. Whitehead's[5] theory of relativity.

[1] Barajas, Birkhoff, Graef, and Vallarta, Phys. Rev. 66, 138–143 (1944).
[2] Proc. Nat. Acad. Sci. 29, 231 (1943).
[3] Einstein, Infeld, Hoffmann, and Robertson, Ann. Math. [1] 39, 65, 101; [2] 41, 455.
[4] N. Rosen, Phys. Rev. 57, 147–155 (1940).
[5] A. N. Whitehead, *Principle of Relativity*.

Proceedings of the American Physical Society

Meeting at Chicago, December 1 and 2, 1944

THE 263rd meeting of the American Physical Society was held in the Museum of Science and Industry at Chicago on Friday and Saturday, the first and second of December, 1944. The registration came to one hundred and twenty-six. President Dempster assumed the functions of the Local Committee; the gratitude of the Society is due him for the arrangements and to the Museum of Science and Industry for the excellent facilities which they put at our disposal without charge.

The meeting was distinguished by a symposium of fourteen invited papers on spectroscopy. The Secretary acknowledges with thanks the aid of R. S. Mulliken, H. H. Nielsen, and O. Struve in seeking and finding speakers able in these difficult times to illustrate so many of the facets of spectroscopy, and expresses the thanks of the Society to the speakers themselves. Their names and the titles of their papers are appended to these minutes. At one of the sessions opportunity was provided for the planning of the proposed Division of Spectroscopy, and many and valuable were the opinions and the suggestions which were received.

Twenty-six contributed papers were submitted for the meetings; the abstracts are printed hereinafter.

The dinner of the Society was held at the Windermere West Hotel on Friday evening with an attendance of almost one hundred. The after-dinner speakers were P. Klopsteg, J. Franck, R. S. Mulliken, and H. H. Nielsen, Mr. Klopsteg speaking of the scientific institutions of Australia and the other three on the topic of the Division of Spectroscopy.

The Council met on Friday afternoon, and elected to Fellowship two candidates and to Membership the unprecedented number of no fewer than one hundred and eighty-two candidates; their names follow. The Council further appointed an Organizing Committee for the Division of Spectroscopy composed of K. K. Darrow, G. R. Harrison, R. S. Mulliken, and three more to be selected by those three. The Council further authorized, in response to numerous petitions, the formation of a Division of Chemical Physics in the Society, and appointed as its Organizing Committee the following: O. Beeck, F. G. Brickwedde, K. K. Darrow, J. E. Mayer, R. S. Mulliken, and O. K. Rice.

The Society has lost through death the Fellows and Members here listed: John M. Adams, H. A. Clark, Milo A. Durand, Sir Ralph Fowler, and F. W. Stallmann.

Advanced from Membership to Fellowship: M. L. Huggins.

Elected to Fellowship: W. T. Szymanowski.

Elected to Membership: A. R. Anderson, D. L. Anderson, D. E. Andrews, Jr., John Angus, D. A. Baldwin, T. F. Ball, N. H. Barbre, J. S. Barlow, Stanley Bashkin, J. R. Beatty, Richard Bellman, A. L. Bennett, Theodore Berlin, Marietta Blau, S. D. Bloom, J. C. Boonshaft, I. B. Born, John Bowman, L. L. Boyarsky, I. R. Brenholdt, W. G. Brock, C. J. Burbank, E. A. Burrill, F. X. Byrnes, Leon Camp, R. R. Carhart, C. W. Christensen, R. J. Christensen, H. H. Q. Chun, W. H. Clohessy, B. L. Cohen, R. E. Corby, N. H. Coy, W. S. Cramer, Lawrence Cranberg, J. A. Crawford, L. L. Cruise, O. R. Cruzon, J. R. Curry, H. W. Curtis, Jack Dainty, E. B. Dale, S. L. Dart, J. R. Davis, E. S. Dayhoff, W. B. Denny, P. M. Doty, W. W. Drake, L. F. Drummeter, G. E. Dewell, B. G. Eaton, C. J. Engle, L. C. Erich, W. F. Fairbank, Abraham Fineman, M. D. Fiske, E. R. Fitzgerald, Harold Fleisher, E. P. Fricke, M. M. Freundlich, J. A. Galvin, W. C. Geer, M. I. Goldberg, Oscar Goldman, J. E. Goldman, P. C. Goldmark, L. S. Goodman, Kathryn Greene, Jack Greenfield, R. M. Hadley, W. C. Hall, E. A. Hamacher, W. A. Hargreaves, S. P. Harris, C. W. Harrison, J. R. Holmes, Leroy Hughbanks, H. W. Hunter, E. C. Y. Inn, B. A. Jacobsohn, A. T. Jaques, D. G. Jelatis, R. R. Johns, H. C. Johnson, Christian Johnston, J. F. Kane, Rockwell Kent III, M. J. Klein, R. W. Koza, Arnold Kramish, G. L. Krieger, F. W. Kuether, W. A. Ladd, J. R. Laugham, Martha H. Lawson, Boris Leaf, Irvin Levin, Harold Levine, J. W. Lewis, W. F. Libby, P. J. Loatman,

M. J. Lun, W. B. Lurie, W. F. Main, E. A. Marx, J. E. Mayer, W. S. McAfee, F. T. McClure, W. J. McGonnagle, E. S. McKee, K. A. McMurtrio, Edward Melkonian, R. P. Miller, William Miller, D. J. Montgomery, J. R. Morgan, F. S. Mortimer, Nathan Most, H. R. Molton, R. E. Mueser, H. M. Muncheryan, J. D. Orndoff, Eleanor Oshry, Alfred Owyang, Murray Peshkin, R. P. Peterson, R. L. Platzman, R. V. Pound, W. W. Pratt, William Primak, Wilfrid Rall, D. H. Ransom, R. R. Rau, W. C. Redman, R. B. Reddy, G. W. Renner, R. C. Reed, F. G. Rest, D. P. Riley, H. L. Ritter, F. L. Roth, Paul Rudnick, Stanley Ruthberg, D. S. Sakon, A. L. Schawlow, R. E. Schofield, A. H. Sharbaugh, M. J. Sheehy, W. A. Sisson, V. D. Snyder, K. H. Sommermeyer, Anthony Sperduto, R. E. Stephens, D. W. Stewart, J. L. Stewart, W. G. Stroud, Mrs. George Sutton, Preston Taulbee, E. A. Taylor, R. W. Treharne, P. S. Turner, Douglas Venable, G. C. Wallick, H. F. Webster, R. A. Weiss, A. M. Weitzenhoffer, G. F. Welch, R. M. Whaley, D. H. Wilkinson, F. H. Willis, J. M. Willson, W. F. Witzig, Victor Wouk, Dorothy Wrinch, K. K. Wyckoff, Sidney Visner, T. F. Young, L. W. Zabel, M. G. Zabetakis, Henry Zatzkis, Paul Zilczer, Kurt Zuber.

KARL K. DARROW, *Secretary*

SYMPOSIUM ON SPECTROSCOPY

Address of Welcome by K. K. DARROW.

Forbidden Lines in the Laboratory: the Past and the Future. S. MROZOWSKI, *University of Chicago.*

Partial Selection Rule for Sensitized Fluorescence. J. G. WINANS, *University of Wisconsin.*

Some Features of the Spectroscopy of the Atmosphere. O. R. WULF, *University of Chicago.*

Double-Bond Absorption in the Vacuum Ultraviolet. J. R. PLATT, *Northwestern University.*

The Near Ultraviolet Absorption of Pyridine Vapor. H. SPONER, *Duke University.*

Spectroscopic Properties of Chlorophyl and Porphyrines. E. RABINOWITSCH, *Massachusetts Institute of Technology.*

Measurements of Line Width in the Infra-Red Spectra of CO_2, N_2O, and NH_3. A ADEL AND E. F. BARKER, *University of Michigan.*

The Infra-Red Absorption Spectrum of Deutero-Methyl Chloride. A. H. NIELSEN, *University of Tennessee,* AND H. H. NIELSEN, *Ohio State University.*

Degenerate Modes of Vibration and Perturbations in Polyatomic Molecules. W. H. SHAFFER, *Ohio State University.*

Absorption Spectra of the Planets. N. BOBROVNIKOFF, *Perkins Observatory.*

Progress in the Interpretation of Stellar Spectra. O. STRUVE, *Yerkes Observatory.*

The Lines of Hydrogen and Oxygen in Stellar Atmospheres. S. CHANDRASEKHAR, *Yerkes Observatory.*

Physical Problems Related to the Hydrogen and Helium Lines in Stellar Spectra. M. K. KROGDAHL, *Yerkes Observatory.*

The Absorption Laws for Gases in the Infra-Red. J. R. NIELSEN, *University of Oklahoma,* V. THORNTON AND E. BROCKDALE, *Phillips Petroleum Company.*

ABSTRACTS OF CONTRIBUTED PAPERS

E1. A Simple Counting System for Alpha-Ray Spectra. S. ROSENBLUM AND W. Y. CHANG, *Princeton University.*—When several tungsten wires are stretched parallel in front of a brass plate, it is found that each wire answers alpha-particles very well but is not affected by strong beta- or gamma-rays. Hence each wire behaves as an alpha-ray counter. The voltage of the plate relative to each wire is about negative 3000 v, when the distance of each wire from the plate is 1.5 mm, the operation taking place in air of atmospheric pressure. The conditions of reliable operation have been carefully examined and well defined. If a capacity of about 500 cm is connected across each counter, the power output of even a single power tube is high enough to operate a mechanical counter. Removal of the capacity needs an amplifier of the multivibrator type to actuate a Cenco high voltage impulse counter, but reduces the resolving time of each counter considerably. The interference between the different counters can be eliminated by erecting aluminium walls between any two adjacent wires. When the system of counters is made airtight and each wire is properly coupled to an amplifier of the above type, they can be used in a deflection chamber under the action of the magnetic field to determine the alpha-ray spectra. The counter voltage should be well stabilized. The distribution form of the Po alpha-particles determined by these counters agrees well with that obtained from the photographic line (see the other abstract by W. Y. C.).

E2. A Study of the Alpha-Ray Spectra by the Cyclotron Magnet. W. Y. CHANG, *Princeton University.*—An alpha-ray magnet spectrograph has been constructed, consisting of the Princeton cyclotron magnet and a Plexiglas deflection chamber, in which the alpha-particles can be bent into a semicircle of 75-cm maximum diameter. A balance has been devised to measure the magnetic field, which is sensitive to about 1 in 10,000. A non-linear deflection coil has been used to indicate the variation of the field and can also be employed to control directly the magnetic field by

allowing a light spot reflected from the mirror of the coil to fall on to a twin photo-cell, which then regulates the current of the generator exciting field. Three methods of detection have been used according to the different strengths of the sources. They are, namely, the ordinary photographic method, the counting method, and the method of photographic tracks. The counters, specially developed for this purpose, consist of eight tungsten wires stretched in front of a brass plate and are described in another abstract. By using the track method a source of one microcurie or smaller can be detected. The forms of the energy distribution of the Po alpha-particles have been determined, respectively, by these three methods and agree fairly well with one another. The half-width is smaller than $\frac{1}{3}$ mm, i.e., about 0.01 Mev. Hence according to the dimensions of the chamber, two lines separated by 0.01 Mev can be resolved. The intensities a few mm away from the maximum are practically zero, being quite different from the results of Roy Ringo.*

* Roy Ringo, Phys. Rev. **58**, 942 (1940).

E3. The Nuclear Excitation of Silver. MARCELLUS L. WIEDENBECK, *University of Notre Dame.*—The excitation of silver[1] has been studied in the region from the threshold for the process to 3.3 Mev. The thick target x-ray[2] excitation curve was obtained by the direct bombardment of an argon (90 percent)-ether (10 percent) counter with a silver cathode. This curve shows sharp increases in slope when the maximum energy of the x-rays reaches a new energy level. These levels indicate that the threshold for the process $Ag+\gamma \rightarrow Ag^*$ is 1.18 ± 0.03 Mev and higher activation levels were also found at 1.59, 1.95, 2.32, 2.76, and 3.13 Mev, respectively. The decay period of the metastable state was obtained from a curve extending over 6 half-lives and was found to be 40.4 ± 0.2 sec. The excitation was also obtained by direct electron bombardment of silver in the process $Ag+e_{v_1} \rightarrow Ag^*+e_{v_2}$.

[1] Alvarez, Helmholtz, and Nelson, Phys. Rev. **57**, 600 (1940).
[2] J. R. Feldmeier and G. B. Collins, Phys. Rev. **59**, 937 (1941).

E4. A "Fast" Gamma-Ray Transition. ROSALYN S. YALOW AND M. GOLDHABER, *University of Illinois.*—We have continued the investigation of the "fast" gamma-ray transition, first detected by O'Neal and Scharff-Goldhaber[1] through the presence of a "tellurium-like" satellite among the Sb x-rays emitted in the decay of Te^{121}. This decay leads to two excited states of Sb^{121}, of 0.23-Mev and 0.61-Mev energy. These energies, determined by absorption of the gamma-rays in several elements, are in good agreement with the energies found by Hales and Jordan[2] for the internal conversion electrons from Te^{121}. By studying the coincidences between the x-ray satellite and the internal conversion electrons we could show that the transition from the 0.23-Mev level to the ground state is the "fast" transition, taking place before the K-electron captured by Te^{121} is replaced. Its internal conversion coefficient is surprisingly large, >0.5, though one K-electron is missing! The mean lifetime of this state is $<2\times10^{-17}$ sec. and the corresponding half-width >30 ev. The transition from the 0.61-Mev level to the ground state is "slow," and its half-width <1 ev.

[1] R. D. O'Neal and G. Scharff-Goldhaber, Phys. Rev. **62**, 83 (1942).
[2] E. B. Hales and E. B. Jordan, Phys. Rev. **64**, 202 (1943).

E5. Attempt to Detect Nuclear Resonance Absorption of Gamma-Rays. GERTRUDE SCHARFF-GOLDHABER, M. GOLDHABER, AND ROSALYN S. YALOW, *University of Illinois.*—Since past attempts to discover nuclear resonance absorption with ThC″ gamma-rays were unsuccessful, it seemed of interest to search for resonance absorption with a gamma-ray which appeared to be particularly suited for such an experiment: the 0.23-Mev gamma-ray[1] emitted from an anomalously wide level of Sb^{121}, resulting from the decay of Te^{121}. However, we were unable to detect a nuclear absorption of this gamma-ray in Sb; if present it is <3 percent of the atomic absorption and at least a hundred times smaller than expected. A search was therefore made for a low lying excited state of Sb^{121}, but no gamma-rays above 10 kev were found. If the 0.23-Mev transition leads to the ground state of Sb^{121}, a new factor must be responsible for a shift of the gamma-ray line from the resonance position. As this "fast" gamma-ray is emitted with one K-electron missing, while it would have to be absorbed in a neutral Sb^{121} atom, it may be that the interaction of the nucleus with the "hole in the K-shell" leads to a considerable shift of the nuclear level from its "normal" position.

[1] See preceding abstract by R. S. Yalow and M. Goldhaber.

E6. Radiation Widths of Highly Excited Nuclei. M. GOLDHABER, *University of Illinois.*—Recent evidence for a wide low energy level in a medium weight nucleus (Sb^{121}) appears to be difficult to reconcile—within the framework of the compound nucleus theory—with the sharp states found for resonance capture of slow neutrons. In that theory the existence of sharp resonance states, ~9 Mev above the ground state, is ascribed to the "slowness" of gamma-ray transitions, as observed for some heavy radioactive nuclei. For medium weight nuclei it may be necessary to treat the sharp "initial capture state" formally as a particular state of the combination Z^M+n rather than as one of the many states of the highly excited compound nucleus Z^{M+1}. If such a view were taken many experimental results would have to be reinterpreted. In particular, the empirical rule that sharp resonance states are predominantly found for nuclei of odd mass number, may take on new significance. For an odd M nucleus the magnetic interaction with a neutron is comparable in magnitude to the energies found for neutron resonance. For even M nuclei this interaction is usually absent. This correlation suggests that the influence of the magnetic forces on the position and width of the "initial capture state" may be important.

E7. Effect of Nuclear Electric Quadrupole Moment on the Energy Levels of a Diatomic Molecule in a Magnetic Field. BERNARD T. FELD AND WILLIS E. LAMB, *Pupin Physics Laboratories, Columbia University.*—In molecular beam experiments[1] performed on diatomic molecules of zero electronic spin, effects were observed which seemed to indi-

cate an electrical interaction between the nucleus and the rest of the molecule. It was suggested that these effects are caused by an interaction between a nuclear electrical quadrupole moment and the electric field of the molecule. We have calculated the energy level system and expected molecular beam resonance spectrum for heteronuclear molecules in which one nucleus has quadrupole moment and the other zero spin. The calculations were carried out, by the use of perturbation theory, for nuclear spins 1 through 9/2 in weak and strong magnetic fields. It is shown that the observed effects could be owing to a nuclear electric quadrupole moment. Analysis of unpublished data on resonances in LiF give for Li^7 the value $qQ=1\times10^{-21}$ erg (Q is the nuclear electric quadrupole moment; q, a quantity, depending on the distribution of charge in the molecule, which must be independently calculated). This may be compared with 0.3×10^{-21} erg for D in HD and D_2.[2]

[1] Kusch, Millman, and Rabi, Phys. Rev. 55, 1176 (1939).
[2] Kellogg, Rabi, Ramsey, and Zacharias, Phys. Rev. 57, 677 (1940).

E8. Neutron-Proton Scattering and the Meson Theory of Nuclear Forces. J. M. JAUCH, *Palmer Physical Laboratory, Princeton University.*—The ratio $R=\sigma(\pi)/\sigma(\pi/2)$ of the scattering cross section for 14-Mev neutrons on protons has been calculated assuming for the interaction the expression which results from the charge symmetrical meson theory with two kinds of mesons of masses κ and $\mu(\mu>\kappa)$. The previously determined values for the coupling constant and the mass ratio μ/κ[1] are used. The value of the ratio R is essentially determined by the sign of the interaction in P states. The sign is such as to give repulsive forces for the charge symmetrical theory. Numerical calculations have been carried out to an accuracy for R of $\sim1\%$ for all states of angular momentum ≤2. The effect of the higher states can be estimated with an approximation method and is found to be negligible. The result is $R=1.11$. This value is at variance with the recently determined[2] ratio of 0.52 ± 0.03 for the same energy. This discrepancy supported by other similar calculations[3] is a strong argument against any charge symmetrical meson theory.

[1] J. M. Jauch and Ning Hu, Phys. Rev. 65, 289 (1944).
[2] E. Amaldi *et al.*, Naturwiss. 30, 582 (1942).
[3] L. Hulthén, Arkiv f. Mat. Astronom. o. Fysik 29, No. 33 (1943); B. Ferreti, Nuovo Cimento [XXI] 1, 25 (1943); J. Schwinger and W. Rarita, Phys. Rev. 59, 556 (1941).

E9. The Influence of the Recoil of Heavy Particles on the Nuclear Potential Energy. J. LEITE LOPES, *Princeton University.*—An attempt to improve the value of the quadrupole moment of the deuteron in Schwinger's mixed meson theory of nuclear forces[1] was made by taking into account the recoil of the nucleons during the emission and absorption of mesons. The interaction energy operator of the system proton-neutron was calculated by perturbation theory and represented by an integral operator in momentum space. In the pseudoscalar and vector symmetrical theories the tensor force has a singularity of the type $1/r^4$ in configuration space; in Schwinger's mixture it has a singularity of the form $1/r^3$. This singularity still remains if relativistic terms are considered, even if recoil is neglected. An evaluation of the quadrupole moment of the deuteron is therefore only possible with a cut-off procedure and this would make unimportant the relativistic and recoil contributions as well as the mixed theory itself.

[1] J. M. Jauch and Ning Hu, Phys. Rev. 65, 289 (1944).

E10. The Adaptation of the Cauchois Spectrograph to Artificial Radioactive Sources. J. E. EDWARDS, M. L. POOL, AND F. C. BLAKE, *Ohio State University.*—To identify x-rays emitted by an artificial radioactive source it is usually necessary to distinguish x-ray wave-lengths characteristic of two neighboring elements. The feeble x-rays from such sources can be photographed with a curved crystal spectrograph. Quartz and mica crystals have been used in the transmission (Cauchois) type curved crystal spectrograph to photograph characteristic $K\alpha$ and $K\beta$ x-ray lines from radioactive sources. Quartz crystals adapted to this type of spectrograph by DuMond and Watson were found to be most efficient for the longer wave-length range of the instrument from about 0.7A to 1.9A. Mica crystals proved to be more efficient for shorter wave-lengths from about 0.36A to 1A. Spectrographs with curvatures of 8″ and 15″ were used with both mica and quartz crystals. Broad sources resulting from chemical separations may be used in this type spectrograph. Line sharpness is decreased by the broad source but the $K\alpha$ lines of two neighboring elements are easily identified. The characteristic silver x-rays associated with the decay of 6.7-hour $Cd^{107,109}$ were photographed with a mica spectrograph. The nickel x-rays associated with the decay of Cu^{64} have been identified by use of a quartz spectrograph.

E11. Radioactive Zirconium and Columbium. M. L. POOL AND J. E. EDWARDS, *Ohio State University.*—Extended observations on the decay of Zr^{93} and Cb^{93} show a genetical relationship between these two isotopes. Zr^{93} is characterized by a half-life of 67.8 days, a gamma-ray of 0.85 Mev, a strong β-ray of 0.29 Mev, and a weak one of 0.8 Mev. The ratio of the intensities is approximately 8. Cb^{93} is characterized by a half-life of 38.7 days, a gamma-ray of 0.78 Mev, and soft electrons of 0.140 Mev. The gamma-radiation from Zr^{93} rises in intensity with time after a chemical separation of the Cb^{93}; the β-radiation, however, decreases. Cb x-rays have been observed by absorption and also by photography in a curved crystal spectrograph. The ratio of the number of x-rays to that of γ-rays is approximately $\frac{1}{4}$. A new reaction Y^{89} (α, n) Cb^{92} gives Cb^{92} very strongly. The half-life is 10.1 days. A gamma-ray of 1.1 Mev is emitted. X-rays have been established by absorption measurements and are about as intense as the γ-rays. By the spectrograph these x-rays are shown to be those of Zr.

E12. Progress in the Determination of the Number of Artificially Produced Radioactive Atoms. J. D. KURBATOV AND M. H. KURBATOV, *Ohio State University.*—A determination of the number of atoms obtained by some means of activation requires the development of a method for

quantities less than 10^{-8} gram. A possible solution of this problem has been tested using the adsorption phenomena of divalent ions on different hydrous oxides. The method consists in obtaining adsorption isotherms for known minute quantities of divalent ions under conditions such that the exponent in the activated adsorption equation is considerably below unity; then an unknown initial quantity can be found from the adsorption ratio. The adsorption constants have been evaluated for radium since a technique is known for its accurate determination in quantities of less than 10^{-8} gram. The investigations have been extended to obtain the adsorption isotherms of minute quantities of barium and strontium using the radioactive tracers Ba^{133} and Sr^{89}. However, it has been found experimentally that with conventional quantities of adsorbent, that is more than 10 mg, the exponent in the adsorption equation became unity for quantities of Ra, Ba, and Sr below 10^{-6} gram and the fraction of ions adsorbed was constant. Thus, to evaluate minute quantities of Ra, Ba, and Sr it appears necessary to use the adsorbents, ferric hydrous oxide or manganic oxide (IV), in quantities less than 10^{-4} g.

F1. The Hardy Coefficient for Instrument Oil. S. BLOOMENTHAL, *Automatic Electric Company.*—The method of inclination, ascribed to W. B. Hardy, appears to be the most straightforward of many ways for comparing lubricants. The coefficient of static friction μ for glass on glass was measured by the inclination method on an apparatus which functions automatically. A number of instrument oils, suggested as possible substitutes for genuine porpoise jaw oil, which is unobtainable at the present time, were tried. Addition of only 1 percent glyceryl monoricinoleate to a pure lubricating fluid caused a decrease in μ from 0.26 to 0.13 because of boundary layer formation. The disclosure on last August 15 by G. E. Barker of the composition of a non-spreading synthetic instrument oil, made available to the public by the Elgin National Watch Company, is noteworthy in this connection. This oil contains a stable aralkyl ether with an aliphatic chain of at least five carbon atoms and a benzene nucleus connected to the ether oxygen atom. μ for M56A Elgin Watch Oil was found to be 0.17 when 100 grams total load is used. This compares with $\mu=0.26$ for a light oil derived entirely from petroleum.

F2. Equations of State and Phase Changes in Films on Liquids and Solids. WILLIAM D. HARKINS AND GEORGE JURA, *University of Chicago and Universal Oil Products Company.*—Oil films on water seem not to be stable unless they are monomolecular but adsorbed films on solids may be monomolecular but more generally are multimolecular in the sense that they may attain thicknesses *equivalent* to from five to ten or even more molecular layers. Monolayers on water exhibit three condensed and three non-condensed phases, or six in all. The relation between film pressure (π) and molecular area (σ) is linear ($\pi=b-a\sigma$, equivalent to $\log p/p_0=B-A/v^2$) for any condensed phase, but for liquid intermediate or expanded films or for gaseous films the equations are more complicated. At sufficiently low temperatures films adsorbed on solids are often condensed at the higher vapor pressures, but gaseous at very low pressures. At higher corresponding temperatures either liquid expanded or liquid intermediate phases may occur. Phase changes which are first order in three dimensions usually become second order in two dimensions, though in the latter the condensation of a vapor may be either first or second order.

F3. The Effect of the Subphase upon the Properties of Physically Adsorbed Films. GEORGE JURA AND WILLIAM D. HARKINS, *University of Chicago and Universal Oil Products Company.*—Almost all theoretical approaches to the problem of the physical adsorption of gases on the surfaces of solids have assumed a negligible interaction between the solid and the film. Recent careful experimental work shows that this is incorrect. A few effects which show this are listed. (1) When the effective cross-sectional area of nitrogen on 100 solids is calculated it is found that three maxima are obtained at 14.0, 15.2, and 16.2A². It is found that in some cases at least there is a relation between the area exhibited and the composition or the crystal structure of the solid. (2) The film of propyl alcohol on barium sulphate is monomolecular, but polymolecular on anatase (titanium dioxide) and quartz. The thickness of the film is related to the lattice constants of the solids. (3) The transition from a gaseous to an intermediate film is first order at 1000A² per molecule for one solid while for another of the same crystal structure and particle size, the transition is found to be second order at 50A² per molecule.

F4. Molecular Weights of Proteins as Determined by Light Scattering. W. HELLER AND H. B. KLEVENS, *Chemistry Department, University of Chicago.*—Molecular weights can be determined by light scattering by using either the theoretical principle of Mie[1]—light scattering is considered as an effect of material units—or the principle of Einstein[2]—light scattering is considered as an effect of fluctuations in concentration. Debye's recent equation based on the latter principle[3] could be verified on suspensions of polymers and on protein solutions by using a spectrophotometric-interferometric method (18-cm layer). The symmetry of radiation was tested by means of Tyndall spectra.[4] Aqueous solutions of egg albumin gave, for example, the following data (p_H: 4.65–4.68):

Immediately after preparation (4°C)	47,000±1500
24 hours later (4°C)	64,000±2000
72 hours later (4°C)	81,000±3000.

The ultracentrifugal and osmotic pressure data (literature) are 40,500–44,000 and 42,000–45,100, respectively. Similar agreement between light scattering and ultracentrifugal data was found for serum-albumin. It is apparent that the method is extremely sensitive towards aggregation (denaturation) of proteins. Symmetrically radiating polymer suspensions gave an agreement within 10 percent with ultramicroscopic data of H. Oppenheimer.

[1] Mie, Ann. d. Physik **25**, 377 (1908).
[2] A. Einstein, Ann. d. Physik **33**, 1275 (1910).
[3] P. Debye, J. App. Phys. **15**, 338 (1944).
[4] W. Heller and E. Vassy, Phys. Rev. **63**, 65 (1943).

F5. Diode Modulation. G. H. FETT AND A. D. BAILEY, *Department of Electrical Engineering, University of Illinois.*—It is shown analytically that a perfect diode in series with a pure resistance load is capable of producing frequency components required in amplitude modulation either when the effect of the diode is considered as a series of pulses analysed by means of Fourier series, or when the diode is considered as a synchronous commutator. The end result is identical in either case. The experimental verification of the mathematical result is given for a pure resistance load, and it is shown that if account is taken of the resistance of the diode the agreement is good. It is also shown that the maximum modulated output takes place when the load resistance is about equal to the diode resistance. The problem of the parallel resonant circuit load is discussed, and it is shown that the diode under these conditions behaves like a variable effective resistance, the magnitude of which is controlled by the magnitude and sign of the modulating signal in series with the carrier. When the Q of the load is high, complete modulation is obtained with about half of the signal voltage required with a resistance load.

F6. The Multiple Production of Mesotrons in Paraffin at High Altitudes. W. G. STROUD AND MARCEL SCHEIN, *University of Chicago.*—By modifications of a technique used in previous balloon flights,[1] more information regarding the production of mesotrons in the stratosphere has been obtained. The number of mesotron showers, involving three or more particles, under three and six cm of paraffin, have been measured and compared with the curve for the mesotron intensity as a function of atmospheric pressure. The results show that at altitudes between 13 and 16.5 km 10 percent of the recorded penetrating particles are accompanied by mesotron showers of at least three particles below the paraffin. The angular divergence of these showers is between 9 and 20 degrees. Showers of penetrating particles were also detected below 6 cm of paraffin plus an additional 8 cm of lead. It was found that in the above-mentioned altitude range more than 20 percent of the penetrating particles are accompanied by mesotron showers below the paraffin plus lead. Many of these showers were in coincidence with those below the paraffin only which demonstrates that a large fraction of the particles generated in the paraffin are able to penetrate 8 cm of lead.

[1] M. Schein, W. P. Jesse, and E. O. Wollan, Phys. Rev. **59**, 615 (1941); M. Schein, M. Iona, Jr., and J. Tabin, Phys. Rev. **64**, 253 (1943).

F7. Investigation of Bursts Observed in Two Thin-Walled Ionization Chambers. KONRAD L. KINGSHILL (introduced by Marcel Schein) AND LLOYD G. LEWIS, *University of Chicago.*—Coincidences in time between bursts of ionization occurring in each of two thin-walled ionization chambers were measured at Chicago. The apparatus used here was the same as that used at Echo Lake, Colorado (elevation 3100 meters). The cumulative size-frequency distribution curve for all bursts recorded in each chamber is essentially in agreement with the data obtained by previous investigators. The altitude comparison was made with the data obtained at Echo Lake. The ratio of burst rates found at Echo Lake and at Chicago for bursts caused by 50 or more cosmic-ray particles was approximately 10:1. This is in general agreement with Geiger-Mueller counter coincidence measurements. For bursts caused by more than 150 particles the corresponding ratio is 200:1. Since burst coincidence rates measured in two ionization chambers showed a similar altitude effect when the chambers were separated by a distance of 1 meter, it can be assumed that both the large single bursts and the coincidence bursts are caused by the same type of atmospheric shower. The rate of occurrence of burst coincidences was found to be very small in comparison to the rate for bursts occuring in a single chamber. This demonstrates that most of the atmospheric showers must have a very small lateral width of their region of high particle density. Provided that the cascade theory of showers is valid for electron energies higher than 10^{13} ev, it can be concluded that sea-level showers exhibiting such narrow high density regions (of 1-meter extension) cannot originate from primary electrons.

F8. Investigation of Extensive Atmospheric Showers in the Stratosphere. P. AUGER, A. ROGOZINSKI, AND MARCEL SCHEIN, *University of Chicago.*—To measure the frequency of extensive atmospheric showers at high altitudes a counter apparatus of large linear dimensions (10 meter) was constructed and sent to the stratosphere. The essential part of the apparatus consisted of six large Geiger-Mueller counters (area 125 cm²) arranged in a horizontal plane. The maximum separation between counters was 7 meters. Another set of 4 small counters (area 15 cm²), separated by 50-cm distance, was placed in the middle between the large counters. Six different combinations of threefold coincidences were registered simultaneously. The coincidence circuits had a resolving time of 2×10^{-6} second and therefore chance coincidences could be neglected. The results show that from sea level to an altitude of 15 km the shower rate increases by a factor of 4 for showers of 2-m average spread and by a factor of 30 for showers of 50-cm average spread. It was also found that in the high altitude no coincidences occurred between the set of small counters and any of the large ones which was frequently the case at sea level. This demonstrates that at 15-km altitude the air showers consist of a very narrow and dense bundle of particles. According to the cascade theory these showers must be in the initial stages of their development.

G1. A Method for Obtaining Depolarization Factors of Raman Lines. FORREST F. CLEVELAND, *Illinois Institute of Technology.*—In many cases it is possible to determine the structure of a molecule by interpreting the Raman and infra-red spectra with the aid of the group theory selection rules for two or more assumed structures. To do this, one must know how many lines are depolarized (depolarization factor $=\rho=6/7$) and how many lines are polarized ($\rho<6/7$). This requires very precise values of those depolarization factors whose values are near 6/7 in order to decide whether these lines are polarized or depolarized. Consequently, the method previously used has been revised with a view toward more precise results. A 90° split-field, Polaroid disk

is placed in contact with the window of the Raman tube, with the dividing line horizontal, and is sharply focused on the slit of the spectrograph. A single exposure is made. Calibration marks corresponding to known relative intensities are placed upon each plate by use of a ground-glass screen and a small incandescent lamp. One-minute exposures are used for the calibration marks and correction for failure of the reciprocity law is made by use of information obtained in preliminary experiments. Intensities are obtained by use of a Gaertner microdensitometer. Results thus obtained for CCl_4 will be compared with data obtained by Reitz.

G2. Raman Spectrum of Dimethyldiacetylene. ARNOLD G. MEISTER AND FORREST F. CLEVELAND, *Illinois Institute of Technology*.—Raman frequencies, relative intensities, and depolarization factors were obtained for dimethyldiacetylene. The relative intensities and the depolarization factors were obtained with the use of a Gaertner microdensitometer. A tentative assignment was made of all the observed Raman frequencies assuming that the molecule has the symmetry D'_{3h}. The chain frequencies were established by comparison with Wu and Shen's[1] analysis of the vibrational spectrum of diacetylene. Crawford's[2] analysis of the dimethylacetylene Raman spectrum was used in determining the methyl group frequencies. Three cases of Fermi resonance were observed, but there were also two cases where only a single line was observed in spite of the fact that the frequency and symmetry conditions for resonance were satisfied. The carbon-carbon triple-bond frequency which appears at 2183 cm^{-1} for diacetylene is shifted considerably, appearing at 2264 cm^{-1} for dimethyldiacetylene.

[1] T. Y. Wu, *Vibrational Spectra and Structure of Polyatomic Molecules* (National University of Peking, Kunming, China, 1939), p. 259.
[2] B. L. Crawford, Jr., J. Chem. Phys. 7, 555 (1939).

G3. A Difficulty in Analysis of Some ClO_2 Bands. J. B. COON, *Department of Physics, Indiana University*.—The rotational structure of the violet absorption spectrum of ClO_2 cannot be explained in terms of energy levels of a rigid, approximately symmetrical top. If these levels are used, an additional term linear in K is needed. The spectrum can, however, be explained using the levels*

$$F=\frac{B+C}{2}[L(L+1)-K^2]+Ak^2.$$

Replacing k by K gives levels of a rigid, approximately symmetrical top. Here the symbol A refers to the quasi-symmetry axis of the approximately prolate top model. L, K, and k refer, respectively, to the total angular momentum excluding spin, component of this along the axis, and the component of the angular momentum of molecular rotation along the axis. Though k is not integral, it is assumed that any change in k is integral. $\nu=F'-F''(\Delta L=\Delta K=\Delta k=0)$ was fitted to the observed Qq branches. Within a given band it was found that $2\Delta A$ is constant. Using constants of the spectrum, k was calculated and $k-K$ was found to be a positive constant within a given band, 1.68 for (000←000) band.

* H. Sponer and E. Teller, Rev. Mod. Phys. 13, 75 (1941).

G4. New Evidence for the Magnetic Current. FELIX EHRENHAFT, *New York, New York*.—In a homogeneous electric field through which flows a constant electric current, a single magnetic pole circulates. If the single magnetic pole also bears an electric charge, this movement is a spiral (electrodynamics). Observation discloses that in a constant vertical homogeneous magnetic field, single test bodies move in a spiral path in gases as well as in liquids with velocities that are measurable in the dark field of the microscope. These velocities are of the order of 10^{10}–10^{12} smaller than the velocity of light, showing that they bear electric as well as magnetic charges (magnetodynamics). If they bear a magnetic charge alone, their movement is polar.* New experiments will be demonstrated in gases where the permanent magnet is used. Covering the vertical magnetodes of the electromagnet with glass caps, the opposing faces of which are fitted with platinum surfaces, one obtains in the space between the caps vertical homogeneous fields where the electric and magnetic force lines are parallel to one another. When the two fields are in action simultaneously a circulation of the liquid can be observed with the microscope and a twisting of the stream of electrically evolved gas bubbles rising from the lower platinum surface occurs. The direction of twist as well as the direction of circulation follows the rule of Ampere. New facts about magnetolytic processes will be given.

* F. Ehrenhaft, Nature 154, 426 (1944).

G5. Magnetic Saturation of Microscopic Particles. BROTHER GABRIEL KANE, *Manhattan College*.—Microscopic particles of nickel have been observed to move in the direction of the lines of force in a vertical homogeneous magnetic field when illuminated by a strong beam of light.[1] The velocity of the particles is a function of the field strength. The direction of motion reverses with a reversal of the magnetic field. For low field intensities, the velocity is directly proportional to the field strength. For higher intensities, the velocity either approaches a limiting value or reaches a maximum with increasing field and then decreases. Increase of field strength may even reverse the sense of direction of the motion. All of these motions can be accounted for if it is assumed that the force acting on a particle is qH, where q is the magnetic charge and H the effective field strength. The value of H is determined from the equation $H=H'-NI$ used for the macroscopic state. H' is the applied field, N the demagnetizing factor, and I the intensity of magnetization. N is a function of the field strength.[2]

[1] F. Ehrenhaft, Ann. de physique 13, 151 (1940); Phys. Rev. 57, 562 (1940); J. Frank. Inst. 230, 381 (1940).
[2] Shuddemagen, Phys. Rev. 31, 165 (1910).

G6. The Rotation of Electrolytes under the Influence of a Magnetic Field. CHARLES B. REYNOLDS, *Federal Communications Commission, New York, New York*.—The rotation of solutions of $CuSO_4$, H_2SO_4, and $FeCl_3$ under the

influence of a magnetic field has been reported.[1] The author has repeated this experiment using many additional electrolytes of ferro-, para-, and diamagnetic materials, organic and inorganic in nature. The experiments performed to determine whether or not the motions could be explained by the Lorentz force, $F=q(v\times H/c)$, or in terms of some other well-known theory, will be described. It will be shown that the rotations are not explained by the Lorentz force, concentration gradient, or pure electrochemical action. A satisfactory explanation can be shown if the existence of a magnetic current is assumed.

[1] F. Ehrenhaft, Bull. Am. Phys. Soc. 19, 3, 10 (June 23, 1944).

Proceedings of the American Physical Society

Meeting at Pasadena, California, December 16, 1944

THE 264th meeting of the American Physical Society was held at the California Institute of Technology, Pasadena, California, on Saturday, December 16, 1944. The attendance varied from 90 to 125, the largest at any Pacific Coast meeting since the start of the war. Thus the trend of increasing numbers, started a year ago, continues in evidence. The audience was, however, almost exclusively from Southern California. Nearly 50 members and guests had luncheon together in Dabney Hall, the shift from the Athenaeum having been forced by war conditions.

The morning session opened at 9:30 A.M. and adjourned at 12:30 P.M. It was devoted to three invited papers, *viz:*

The Conceptual Content of the Quantum Theory, PAUL S. EPSTEIN, *California Institute of Technology.*

The Logical Foundations of Quantum Mechanics, HANS REICHENBACH, *University of California at Los Angeles.*

The 1944 Values of the Physical Constants of the Quantum Theory, RAYMOND T. BIRGE, *University of California.*

The afternoon session opened at 2 P.M. and adjourned at 4:30 P.M. Abstracts follow of the twelve contributed papers presented at that session. Number 10 was read by title.

R. T. BIRGE
Local Secretary for the Pacific Coast

Abstracts of Contributed Papers

1. A Possible Cause of the Variability with Time of the Incoming Cosmic Rays at High Latitudes. ROBERT A. MILLIKAN, H. VICTOR NEHER, AND WILLIAM H. PICKERING, *California Institute of Technology.*—(1) We present new evidence that a new band of rays which we interpret as helium annihilation rays comes in vertically at about the predicted latitude. (2) We present a discussion of the possible composite character of the so-called silicon annihilation band and of the so-called oxygen annihilation band. (3) We bring forward an explanation of a possible cause of our observed variability in the incoming cosmic rays at high latitudes. (4) We make a new and more accurate determination of the value of the field sensitive and the non-field sensitive components of the incoming cosmic rays.

2. Some Recent Investigations on Hydrodynamic Stability. C. C. LIN, *Guggenheim Laboratory, California Institute of Technology* (Introduced by R. A. Millikan).—Recent investigations of the stability of two-dimensional parallel flows bring out that the physical mechanism underlying hydrodynamic stability in an incompressible fluid can be understood in terms of vorticity transfer.[1] In particular, the condition of vanishing curvature of the velocity profile in Rayleigh's criterion is identified with an extremum of vorticity distribution, and the physical picture describing the associated instability has been worked out in some detail. Conditions similar to Rayleigh's criterion have now been obtained for curved and axially symmetrical flows, and these can also be interpreted in a similar manner. Investigations of the stability in a compressible fluid are being carried out with the collaboration of L. Lees.

[1] Proc. Nat. Acad. Sci. (October, 1944).

3. Pressure Flow of a Turbulent Fluid between Two Parallel Infinite Planes. P. Y. CHOU, *Guggenheim Laboratory, California Institute of Technology* (Introduced by R. A. Millikan).—This investigation is based upon a general theory developed by the author: "On velocity correlations and the solutions of the equations of turbulent fluctuation."[1] Two solutions of the problem are given. The first is the

consequence of the equations of mean motion and of double correlation, while, in the second solution, all the equations of mean motion and of double and triple correlations are utilized. It is shown that the first solution holds good only in the central portion of the channel, while the second covers the entire channel except the immediate vicinity of the channel wall. The behavior of the mean squares of turbulent fluctuations is discussed qualitatively. The present calculation also indicates that the velocity defect $(U_c - U)/U_c$, which is independent of the Reynolds number of the mean flow, according to von Karman,[2] may also be independent of the magnitudes of the turbulent velocity fluctuation, after the flow has reached its steady turbulent state.

[1] To appear in the *Quarterly of Applied Mathematics* (April, 1945).
[2] Th. von Karman, Proc. Fourth Internat. Congress App. Mech. 1934), p. 69.

4. Frequency Elimination in Spirotron Systems for Accelerating Ions and Electrons. L. E. DODD, *University of California at Los Angeles.*—The spirotron design changes the speed of an electron or ion by components, with relatively low frequency of potential-reversal. It combines the cyclotron and magnetic-electron-microscope principles. Further modification eliminates frequency by using constant potential. This is getting back somewhat to former designs before the advent of the cyclotron. However, a difference is that here smaller diameter magnetic fields are permitted. Multiple electrode pairs, oppositely arranged on the surface of a cone, are replaced by a single pair of long straight electrodes, of the same general character as before, parallel to the magnetic field. The particle moves on the surfaces of a sequence of right-cylindrical helixes. These, with successive changes of radii, are joined together by a single straight line—the axis of the one electrode pair—parallel to the axes of all cylinders, but located in the surface of each, this common line and the cylinder axes being confined to the same plane. The particle travels a whole revolution between accelerations, instead of a half-revolution as in the cyclotron. Its path during this time is on one of the cylinders. Constant potential avoids frequency difficulties from relativistic change of mass at higher velocities.

5. Minimum Conditions Necessary to Achieve the Velocity of Escape. H. S. SEIFERT, *California Institute of Technology.*—The maximum velocity which may be achieved by a rocket directed vertically upward depends upon five basic parameters: (1) The velocity (relative to the rocket) with which mass is ejected; (2) the fraction of the total mass which is finally ejected, or "loading factor;" (3) the initial acceleration; (4) the dependence of acceleration upon time (flight law); (5) the dependence of frictional resistance upon time and velocity. The flight laws of constant acceleration and constant thrust have been considered. Although constant thrust produces higher terminal velocities than constant acceleration, the terminal accelerations produced in an efficient rocket by constant thrust are greater than a human passenger could tolerate. Assuming an initial acceleration of g, an energy loss due to friction equal to the kinetic energy of escape, constant thrust, and a step rocket consisting of three parts of mass ratios 16:4:1, each with a loading factor of 0.9, the attainment of escape velocity would require an ejection velocity over 3000 meters per second.

6. The Relativistic Increase in Ionization of Cosmic-Ray Electrons. WAYNE E. HAZEN, *University of California.*—The preliminary experiments of Corson and Brode[1] have been continued with improved techniques and a stronger magnetic field (4500 gauss). It is believed that uncertainties in condensation efficiency and curvature no longer contribute significantly to the errors. The overlapping of drop images and its variation with track diffuseness probably limit the accuracy of both absolute and comparative ionizations to 10 percent. The minimum ionization, which was obtained from 35 tracks of P^{32} beta-rays with $H\rho > 4500$, is 40 ion pairs per cm in air at N.T.P. The average ionization of 15 cosmic-ray electrons with $H\rho$ of $1\text{–}8\times10^5$ is 53. These figures for ionization are for the ionization produced as a result of all collisions in which the primary electron loses less than ~ 600 ev. Theory predicts an increase of 40 percent, which agrees with the experimental results within the estimated uncertainty.

[1] D. R. Corson and R. B. Brode, Phys. Rev. 53, 773 (1938).

7. The Diffusion Problem and the Theory of Connected Events. DONALD A. DARLING, *California Institute of Technology* (Introduced by R. A. Millikan).—An extension of the one-dimensional random walk to the case where the particles possess inertia leads to a statistical problem in the theory of non-independent, or Markoff, processes. The modification of the "homogeneous random process" in this case is deduced, and the meaning to be attached to random events extended to the continuum is studied. The analogue to the ordinary diffusion equation becomes an integro-differential equation

$$\frac{\partial p(t, x)}{\partial t} = \kappa \frac{\partial^2 p(t, x)}{\partial x^2} \int_0^\infty \Phi(t, y) y^2 dy,$$

where $p(t, x)$ is the probability that the particle (possessing inertia) has a displacement x at a time t, and $\Phi(t, y)$ is a solution to the ordinary diffusion equation. Solutions of the equation are deduced by considering the moments of the probability distribution. Some of the equations used in turbulence and Brownian movement problems are special cases of the integro-differential equation, with a suitable interpretation of the dependence function Φ.

8. Magnesium Ion Source for High Intensity Mass Spectrograph. T. H. PI, *California Institute of Technology* (Introduced by R. A. Millikan).—Magnesium ions were produced by bombarding magnesium vapor by electrons emitted from oxide-coated cathodes. The ions were then focused into a thin sheet by means of an electrostatic lens. This ion sheet was sent into the magnetic lens, which focused the sheet into a small spot where the different isotopes were collected. The ion current obtained at the collector was 120 microamperes with good resolution.

9. The Movement of Bed Particles in a Turbulent Stream. HANS ALBERT EINSTEIN, *California Institute of Technology* (Introduced by R. A. Millikan).—The current theory of suspensions in turbulent streams uses an equilibrium condition between the continuous settling of the particles in the surrounding water and the vertical turbulent exchange of water masses to establish the law for the vertical distribution of sediment concentration. At the bed itself this argument breaks down because here the exchange of liquid approaches zero. However, an exchange of particles between the bed and the moving layers exists, and like all such acts of exchange, is governed by the general rules of probability. The probability of a particle moving out of its position in the bed can be related directly to the probability of the adjoining liquid having a certain velocity. If one introduces the measured probabilities for instantaneous velocities near the bed, the law for the movement of particles out of the bed can be predicted up to some general constants. The law obtained describes very closely the sediment movement in laboratory flumes and natural rivers.

10. The Rydberg Constants and the Value of e/m. CHAO-WANG HSUEH, *California Institute of Technology*.—The wave-lengths of the H-alpha and D-alpha lines were measured with a Fabry-Perot interferometer directly against the primary standard of wave-length, 6438.4696IA. The results of the measurements are: 6562.85337 ± 0.00022IA for H-alpha, and 6561.06811 ± 0.00005IA for D-alpha. Following William's assignment,[1] they are the respective wave-lengths of the strong component-group (145). From the above values, the Rydberg constant for hydrogen R_H, for deuterium R_D, for helium R_{He}, and for infinite mass R_∞, and also the values of e/m and E, the atomic weight of electron, were calculated. They are as follows:

$$R_H = 109{,}677.5795 \pm 0.0037 \text{ cm}^{-1},$$
$$R_D = 109{,}707.4226 \pm 0.0008 \text{ cm}^{-1},$$
$$R_{He} = 109{,}722.2694 \pm 0.0024 \text{ cm}^{-1},$$
$$R_\infty = 109{,}737.3111 \pm 0.0041 \text{ cm}^{-1},$$
$$e/m = (1.75883 \pm 0.00022) \times 10^7 \text{e.m.u./g},$$
$$E = (5.48740 \pm 0.00069) \times 10^{-4}.$$

For convenience, the result for E is also expressed in the following ways: $1/E = 1822.36 \pm 0.23$, number of electrons per unit atomic weight; $H/E = 1837.17 \pm 0.24$, ratio of mass of hydrogen atom to that of electron.

[1] R. C. Williams, Phys. Rev. **54**, 559 (1938).

11. The Turbulent Jet. P. Y. CHOU, *Guggenheim Laboratory, California Institute of Technology* (Introduced by R. A. Millikan).—The first solution of the jet problem based upon the equations of turbulent fluctuation was given by C. C. Lin,[1] who derived the so-called constant "exchange coefficient" from the equations of mean motion and of double correlations by using the values of the triple correlations at the center of the jet. The agreement between theory and experiment of the velocity and temperature distributions for the plane and axial jets is satisfactory. This constant exchange coefficient has been assumed recently by Görtler, based upon physical arguments.[2] Since 1941 the general theory of turbulence has been improved and the jet problem has again been attacked by S. S. Huang,[3] and the solution agrees with Lin's result for the plane and axial jets and with Tollmien's for the half-jet under the momentum transport theory. According to the latest version of the general theory, the constant exchange coefficient still follows as a first approximation from the equations of mean motion and of double correlations, substantiating Lin and Huang's results. It is also shown that these equations provide a basis for the more accurate solutions to the problem.

[1] Science Report of National Tsing Hua University, 1941.
[2] Zeits. f. angew. Math. u. Mech. **22**, 244 (1942).
[3] S. S. Huang, master's thesis, National Tsing Hua University, 1943.

12. Radio Direction Finding at a Wave-Length of 1.8 Meters. W. H. PICKERING, J. DAVID, AND W. F. HORNYAK, *California Institute of Technology*.—The accuracy attainable with an Adcock type antenna has been investigated. Particular attention has been directed to bearing errors due to polarization of the transmitted wave and to nearby objects behaving as parasitic radiators. The antenna consisted of two vertical quarter-wave rods spaced three-quarters of a wave-length. The effects of various types of grounding plane have also been investigated. With favorable conditions an accuracy of 0.2 degree is attainable, but polarization errors may be as large as 10 degrees. For best determination of the null direction, the receiver output is recorded on a paper strip synchronized with the rotation of the antenna.